Ordering Transitions and Localisation Properties of Frustrated Systems

Thomas Pickles
St Hugh's College
University of Oxford

A thesis submitted for the degree of
Doctor of Philosophy

Trinity 2009

To Mum and Dad

Acknowledgements

I would like to convey my extensive and sincere thanks to my supervisor, Professor John Chalker, for providing guidance over the course of this work. I have benefitted hugely from our meetings, as a result of which my frequent befuddlement has become less frequent. I am grateful for lucid and pithy explanations of key concepts. In particular, I have been helped by answers to those questions that I had aspired to ask, but often found myself struggling to frame.

In addition, I am pleased to acknowledge a number of helpful discussions in connection with this work: Roderich Moessner, Fabian Essler, Joe Bhaseen, Peter Holdsworth and Timothy Saunders have all provided useful advice.

I have been lucky to share an office with several affable people, and particularly thank Richard and Iain for keeping me balanced during long periods battling with unruly integrals. Also in this respect, I am indebted to Prachi for her patience and cheer during the writing of this.

A number of friends have made living in Oxford extremely enjoyable: they know who they are. I have learned an immeasurable amount just hanging out, and value this time above everything.

Abstract

In this work we investigate themes related to many-body systems in which multiple ground states are accessible, a condition known as frustration. Frustration can arise in a number of contexts, and we consider the consequences of this situation with some examples from condensed-matter physics.

In some magnetic materials interactions between spins are such that no single spin configuration provides a unique ground state. In the class of frustrated magnets where the number of ground states is extensive, thermal fluctuations are strong even at temperatures significantly below the interaction strength. At such temperatures spins are highly correlated, and small perturbations may have profound consequences.

In this thesis we provide an example of this. By considering classical n-component spins with nearest-neigbour exchange on a frustrated octahedral lattice we show that – in the limit where exchange interactions are large – the system is in a disordered, correlated phase where correlations have the form of a dipole field. This is termed a Coulomb phase. From this phase we induce an ordering transition, lifting the degeneracy with weak, additional short-range interactions. By studying the transition in the solvable limit of $n \to \infty$, we discover that the transition has identical thermodynamics to that of a magnetic system interacting through long-range, dipolar forces. Finally, we provide a more apposite characterisation of the transition, where the high-temperature side of the transition is described through the fluctuations of solenoidal fields, and the ordering corresponds to a condensation of these fields.

In a separate part of the thesis, we investigate the influence of disorder on frustrated lattices. We study a two-dimensional tight-binding model with nearest-neighbour hopping and on-site disorder. Restricting the allowed states to being those from the low-lying manifold of ground states, the disorder feeds through to act as effective disorder in the hopping terms, which decay algebraically with distance. The quasi-long range nature of this effective hopping leads to a situation in which the resultant single-particle eigenstates are critical, and we probe their behaviour numerically with a transfer matrix calculation.

Contents

1 Setting the Scene: From Conventional Phase Transitions to the Coulomb Phase **1**

1.1 A Ferromagnetic–Paramagnetic Transition 2

1.2 The Landau-Ginzburg-Wilson Theory of Phase Transitions 4

1.2.1 Mean-field Approximation 5

1.3 Unusual Disordered Phases 7

1.3.1 Classical Dimer Models 8

1.3.2 Classical Dimer Transitions 11

1.4 Summary 12

2 General Introduction: A Brief Survey of Frustrated Magnets **14**

2.1 Types of Frustration 17

2.1.1 Frustration arising from competition 17

2.1.2 Frustration arising from geometry 18

2.2 Coulomb Phases in Geometrically-Frustrated Antiferromagnets 18

2.2.1 Demonstration of the Mapping from Spin Picture to Flux Picture 20

2.2.2 Hamiltonian in the Flux Picture: A Verification of the Coulomb Phase . 23

2.2.3 The Effect of Fluctuations off Ground-State Manifold 24

2.3 Summary 24

3 Some Approximation Schemes for Investigating Interacting Systems **26**

3.1 Continuum Descriptions as Field Theory 27

3.2 Gaussian Field Theory 28

3.3 Interacting Field Theories 29

3.3.1 Weak-Coupling Expansion 29

3.3.2 Expansion in Number of Field Components 30

3.3.2.1 In a Diagrammatic Representation 32

3.4 Thermodynamics of a Ferromagnet in the Limit of $n \to \infty$ 35

3.4.1 Critical Exponents at the Transtion 38

3.4.1.1 Heat capacity 38

3.4.1.2 Susceptibility . . . 38
3.5 Summary . . . 38

4 Ordering Transitions in Highly-Frustrated Antiferromagnets 40
4.1 Spectrum of the Nearest-Neighbour Interaction Matrix J_{ij} . . . 41
4.1.1 Flat band Eigenvalues of J_{ij} and the Projection Matrix . . . 42
4.2 Further Neighbour Interactions . . . 43
4.2.1 Projected Interaction Matrix $\widetilde{\Delta}_{ij}$ . . . 45
4.3 Large-n Limit of the Transition . . . 47
4.3.1 Critical Exponents . . . 50
4.3.1.1 Heat capacity . . . 51
4.3.1.2 Susceptibility . . . 51
4.3.1.3 Magnetisation . . . 51
4.3.2 Correlation Functions . . . 53
4.3.2.1 At High Temperatures . . . 54
4.3.2.2 Close to the Critical Temperature . . . 55
4.3.2.3 At the Critical Temperature . . . 55
4.3.2.4 At Low Temperatures in the Ordered State . . . 56
4.4 Summary . . . 57

5 Flux Picture of the Transition 58
5.1 Hamiltonian in Flux Picture . . . 59
5.2 Effective Theory of Transition . . . 60
5.2.1 Spin-Length Constraint in Flux Picture . . . 61
5.2.2 Effective Hamiltonian . . . 62
5.3 Summary and Discussion . . . 62

6 Towards a More Complete Understanding of the Ordering Transition 64
6.1 $1/n$ Expansion . . . 65
6.1.1 Interactions . . . 66
6.1.2 Free Energy to $\mathcal{O}(1/n)$ . . . 67
6.1.2.1 Coefficient of B_0^2 to $\mathcal{O}(1/n)$ . . . 67
6.1.2.2 Coefficient of B_0^4 to $\mathcal{O}(1/n)$ . . . 68
6.1.3 Critical Behaviour at $\mathcal{O}(1/n)$ . . . 72
6.2 Local approximation to the free energy . . . 72
6.3 Conclusions . . . 75

7 Effects of Disorder on Frustrated Lattices **76**
7.1 Motivation . . . 76
7.2 Background on Localisation . . . 76
7.2.1 Physical Origin of Quenched Disorder . . . 76
7.2.2 Localisation in Eigenfunctions of Linear Operators . . . 77
7.2.3 Localisation in Tight-Binding Models . . . 77
7.2.4 Characterisation of Localised States . . . 78
7.2.5 Models with Long-Range Hopping . . . 79
7.3 Localisation in Models with Flat Bands . . . 80
7.3.1 Random Perturbations on Eigenstates from a Flat Band . . . 80
7.3.2 Application to spin-waves in GFAFMs . . . 82
7.3.3 Recent developments on flat-band localisation . . . 83
7.4 Transfer Matrix Methods . . . 84
7.4.1 Transfer Matrix for a Tight-Binding Model . . . 85
7.4.2 Numerical Implementation . . . 86
7.4.3 Finite size scaling . . . 87
7.4.3.1 Inverse Participation Ratio . . . 89
7.5 Two-Dimensional Pyrochlore Lattice . . . 89
7.5.1 Exact Results in the absence of Disorder . . . 89
7.5.2 Weak Disorder . . . 92
7.5.2.1 Explicit Form of Transfer Matrices . . . 93
7.6 Numerical Results . . . 97
7.6.1 Dependence of Eigenstates on Energy . . . 98
7.6.2 Dependence of Eigenstates on Disorder Strength . . . 99
7.6.2.1 Smallest Exponent . . . 104
7.6.3 Dependence of Eigenstates on System Width in the Limit of $W \to 0$ . . . 107
7.7 Other evidence . . . 107
7.8 Summary and Discussion . . . 107

8 Summary and Further Work **109**
8.1 Future Research Directions . . . 111

A A Compendium of Integrals for Thermodynamics in the Limit of $n \to \infty$ **112**
A.1 Integrals used in Calculations involving a Conventional Ferromagnet . . . 112
A.1.1 $D^{(F)}_{n\geq 2}(\mu^2, \Lambda)$ . . . 113
A.1.2 $I^{(F)}_2(k, \mu^2, \Lambda)$ . . . 114
A.2 Integrals used in Calculations involving a Highly-Constrained Antiferromagnet . 115
A.2.1 $D_2(s^2, \Lambda)$ . . . 116

A.2.2 $I_2(\mathbf{k}, s, \Lambda)$ . . . 117
A.2.3 $K(\mathbf{q})$ . . . 119
A.2.4 $F_n(s, \Lambda)$ . . . 121

B Useful Results for Correlation Functions in the Highly-Constrained Antiferromagnet **123**
B.1 Correlations in the high-T phase . . . 123
B.2 Correlations at the critical point . . . 125
B.2.1 Parallel to the strain . . . 125
B.2.2 Perpendicular to the strain . . . 125

Bibliography **127**

List of Figures

1.1 Close packed dimers . . . 9
1.2 Flux Picture . . . 10

2.1 Examples of Bipartite Lattices . . . 15
2.2 Examples of Non-Bipartite Lattices . . . 15
2.3 Ground States of the Kagomé Lattice . . . 16
2.4 Ground States of the Square Lattice with Crossings . . . 18
2.5 The Lattice of Corner-Sharing Octahedra . . . 21
2.6 Position of Field Variables . . . 22

3.1 Bare Propagator and Bare Interaction . . . 32
3.2 Dyson Equation . . . 33
3.3 Self Energy . . . 33
3.4 Bethe-Salpeter Equation . . . 34

4.1 Spectrum of Nearest-Neighbour Interaction Matrix . . . 42
4.2 Néel State . . . 44

6.1 First order transition . . . 65
6.2 B_0^2 terms to $\mathcal{O}(1/n)$ . . . 68
6.3 B_0^4 terms to $\mathcal{O}(1/n)$ . . . 69
6.4 Combinatorial Factors . . . 70

7.1 Density of States of Frustrated System without Disorder . . . 80
7.2 Density of States of Frustrated System with Disorder . . . 81
7.3 Representation of Scattering and Transfer Matrices . . . 84
7.4 Two-Dimensional Pyrochlore Lattice . . . 90
7.5 Exact Result: Localisation Lengths in System without Disorder ($\sigma = 10^{-2}$) . . . 91
7.6 Exact Result: Localisation Lengths in System without Disorder ($\sigma = 10^{-6}$) . . . 93
7.7 Transfer Matrix on Two-dimensional Pyrochlore Lattice . . . 95
7.8 Numerical Result: Localisation Lengths of System without Disorder ($\sigma = 10^{-2}$) . 97
7.9 Numerical Result: Energy Dependence of Localisation Lengths . . . 98

7.10 Numerical Result: Energy Dependence of Localisation Lengths (Detailed) 99
7.11 Numerical Result: Disorder Dependence of Localisation Lengths (i) 100
7.12 Numerical Result: Disorder Dependence of Localisation Lengths (ii) 101
7.13 Numerical Result: Disorder Dependence of Localisation Lengths (iii) 102
7.14 Numerical Result: Disorder Dependence of Localisation Lengths (Detailed) . . . 103
7.15 Numerical Result: Disorder Dependence of Longest Localisation Length 104
7.16 Numerical Result: Dependence of Localisation Length on System Width 105
7.17 Numerical Result: Inverse Participation Ratio 106

A.1 Domain of Integration 120

Chapter 1

Setting the Scene: From Conventional Phase Transitions to the Coulomb Phase

At first sight, the characterisation of any interesting phenomenon within condensed-matter physics would seem to be a hopeless venture. Even for modestly sized lumps of matter, trying to construct an understanding of the bulk behaviour of 10^{23} *interacting* particles is an endeavour beyond even the most powerful supercomputer. Yet, remarkably, a detailed picture of all the microscopic principles that must govern that bulk behaviour is rarely the most convenient description. It often turns out that these particles – the microscopic building blocks of all condensed matter – act together in a coherent manner. This permits a description of the system based only on collective properties: a description that might even seem to gloss over many of those microscopic details.

To this end, if, close to a phase transition – a sudden and profound structural change resulting from variations in environmental conditions – the behaviour in the bulk of a material appears insensitive to certain elements of its exact microscopic makeup, we might imagine a theory that includes all of the microscopic details to be overly cumbersome and obscure some of the principal mechanisms at play. Certainly we must conclude that there is some redundancy in keeping all of the details. Indeed, in the study of phase transitions systems that, on the surface, appear to be utterly different in fact share a wealth of similarities when we dig a little deeper.

The interacting agents of a liquid–gas transition ostensibly have little in common with a those at ferromagnetic–paramagnetic transition (van der Waals forces between itinerant molecules compared with magnetic interactions between immobile atoms), but both turn up in the same class of transition in a Landau theory framework[1]. Clearly some grander organising principle controls the properties of these transitions. In fact, we find that it is the *symmetries* inherent to such systems that sets the behaviour in the vicinity of a transtion.

Around a critical point, the response of a system to an external stimulus can be profound. Exactly at the critical point of a liquid–gas transition, the mixture becomes infinitely compressible; exactly at the critical point of a magnetic transition, any infinitesimal external field can drive a complete microscopic reordering. Generally, the response of the order parameter to an applied external field defines a quantity known as susceptibility, and around a transition this diverges with some characteristic exponent γ:

$$\chi \sim |t|^{-\gamma}, \tag{1.1}$$

where t is some control parameter that goes to zero at the transition. The exponent γ is the first exponent that we meet, and a full set of exponents serve as the fingerprint of a transition, placing it within a particular universality class. The susceptibility can be shown to be set by the scale of microscopic fluctuations within a material, and a divergent susceptibility is the hallmark that fluctuations are correlated over all lengthscales within a material: that is that the correlation length ξ becomes infinite. The correlation length can loosely be thought of as a length over which microscopic fluctuations are correlated; beyond the correlation length domains are essentially independent of each other.

1.1 A Ferromagnetic–Paramagnetic Transition

Most of the principles of condensed-matter physics are well understood. Certainly all explanations of condensed-matter phenomena must be consistent with the laws of relativistic quantum mechanics; nevertheless it would be a mistake to presume that knowing these laws rendered the behaviour of interacting systems particularly predictible. To predict which insulators are

[1]For an Ising ferromagnet

likely to exhibit magnetism in the first place, a full quantum-mechanical treatment of a single atom is required: first considering intraatomic interactions, and then including the splitting of the orbital angular momentum through the local crystal field. However, once the behaviour of an array of these magnetic moments is under investigation, it becomes extraneous to include details of how that magnetism arose. In developing an understanding of one piece of physics, it is important to leave out those inessential details which would only serve to cloud the important mechanisms at work.

Let us illustrate this with the prototype for many systems in statistical physics: the nearest-neighbour Heisenberg model[27, 7]. It is sufficient to describe many magnetic materials by writing a purely classical expression for the energy of a microscopic configuration:

$$E = J \sum_{<ij>} \mathbf{S}_i \cdot \mathbf{S}_j, \tag{1.2}$$

where $\mathbf{S}_i$ is a three-component vector lying on the surface of a sphere in spin-space, and the angled brackets indicate a sum over all neighbouring pairs. J is a measure of interaction strength between neighbouring spins, and taking $J < 0$ corresponds to ferromagnetic interactions, which act to align spins; $J > 0$ corresponds to antiferromagnetic interactions, where energy is minimised by making neighbouring pairs of spins antiparallel.

At zero temperature, the favoured spin-configuration is one that minimises the internal energy: in the ground state of a ferromagnet all spins point along some axis in spin-space, $\mathbf{S}_i = S\mathbf{e}_z$ for spins of length S. In this Heisenberg model, all the ground states can be continuously connected (no energy barriers) by rotating all of the spins simultaneously, a so-called global rotation.

Then, at finite temperature, the system has some thermal energy and the spins fluctuate dynamically, increasing the entropy of the system. At low temperatures, configurations of spins will be low-energy ones, qualitatively similar to the ground state. A natural method for investigating the physics would then be to write the configurations in a Taylor series expansion around the minimum-energy configuration to see what influence these dynamic fluctuations have on the ordered phase. In the next section, we will see how to construct a theory that encapsulates these details.

1.2 The Landau-Ginzburg-Wilson Theory of Phase Transitions

We remember that all the statistical physics of a system can be obtained from minimising its free energy. At high temperatures, the dominant contribution to the free energy $F = E - TS$ is obtained by maximising the entropy. Using the example of the Heisenberg ferromagnet, entropy S may be maximised by requiring each spin to fluctuate independently of every other spin. In this way there are no correlations between any spins. Obviously this is at the other extreme from the zero temperature case where, since all spins point in the same direction to minimise internal energy E, the direction of every spin is correlated with every other spin. Furthermore, at zero temperature the macroscopic magnetisation $\mathbf{M} = \sum_i \mathbf{S}_i = NS\mathbf{e}_z$ takes a non-zero value; at infinite temperature the independent spin directions causes the magnetisation to sum to zero. Below some intermediate temperature[2], the total magnetisation will depart from zero. In order to investigate this transition more carefully, we appeal to an argument proposed by Landau[36], and conventionally known as a Landau-Ginzburg-Wilson description.

We may separate the ordered phase from the disordered phase by considering an object known as an order parameter. This has a non-zero expectation value in the ordered phase, and takes a zero expectation value in the disordered phase. In the case of the Heisenberg ferromagnet, this order parameter $\mathbf{m}(\mathbf{x})$ is obtained from a coarse-grained average of the spin magnetic moments in the vicinity of $\mathbf{x}$. Within this coarse-graining framework, fluctuations of $\mathbf{m}(\mathbf{x})$ on lengthscales of order the lattice spacing are disallowed: in obtaining a coarse-grained average these short-wavelength fluctuations have been integrated out.

Near to a phase transition, the correlation length is large in comparison to the region of coarse graining, and so we are entitled to construct a continuum field-theory based on the symmetries of the system. We begin by writing down all terms allowed by the symmetries of the system, and then proceed to explain the physical significance. An effective Hamiltonian is written

$$\beta H[\mathbf{m}(\mathbf{x})] = \int_V d\mathbf{x}\{t\mathbf{m}^2(\mathbf{x}) + r(\nabla\mathbf{m}(\mathbf{x}))^2 + u(\mathbf{m}^2(\mathbf{x}))^2 + \ldots - \mathbf{h}(\mathbf{x})\cdot\mathbf{m}(\mathbf{x})\},$$

where $\mathbf{h}(\mathbf{x})$ is an external magnetic field, and the system occupies a volume V. Gradient terms

[2]In principle this temperature could be zero or infinite. Here we are concerned with finite-temperature phase transitions which, for the short-ranged Heisenberg ferromagnet, requires a dimesion of $d > 2$.

represent an energy penalty paid by configurations which have some spatial variation, and is the leading order gradient term in the Taylor expansion that we touched upon in the previous section. We note that, with $h = 0$, this action is invariant under global rotations of the spins, since any global rotation must leave the energy unchanged. Only with $h \neq 0$ do we have any physical reason for favouring a particular direction in spin-space. The model-dependent parameters $t, u, \ldots$ are, in principle, obtained from integrating out the short-wavelength fluctuations, but since the primary interest is not in the dependence of these parameters on the choice of microscopic model, they are treated as phenomenological.

Within this framework, the partition function is obtained from a functional integration over allowed field configurations

$$\mathcal{Z} = \int D\mathbf{m}(\mathbf{x}) \exp\{-\beta \int_V d\mathbf{x} H[\mathbf{m}(\mathbf{x})]\} = \exp\{-\beta V f\}.$$

Even under this simplified coarse-grained scheme, valid provided we do not expect to discern behaviour at very small lengthscales, a full analytical understanding of the transition is elusive since the integral is, in general, intractable; various approximation schemes exist to get a handle on its behaviour. We defer discussion of these approximation schemes until chapter 3, but pause to employ an approximation to calculate the critical behaviour of the Heisenberg ferromagnet, and comment on its validity.

1.2.1 Mean-field Approximation

Taking the external field to be zero, suppose that the order parameter $\mathbf{m}(\mathbf{x})$ has no spatial variation, so that we write $\mathbf{m}(\mathbf{x}) = \mathbf{m}$, where $\mathbf{m}$ is chosen to minimise the action. This is known as a mean-field approximation, and corresponds to constructing an effective Hamiltonian without any gradient terms. Since correlations between fluctuations are precluded in the mean-field approximation, the action reduces to a free energy, known as a Landau free-energy, the latter given by $f = t\mathbf{m}^2 + u(\mathbf{m}^2)^2 + \ldots$. Around the transition $\mathbf{m}$ is small, and only the lowest order terms in the free energy are important. The equilibrium magnetisation is obtained through minimising the free energy

$$0 = \frac{\partial f}{\partial m_i} = (2t + 4um^2)m_i.$$

The equilibrium value of $\mathbf{m}$ depends on the sign of the parameter t. For $t > 0$ the free energy is minimised by taking $\mathbf{m} = 0$. For $t < 0$ a minimum of the free energy is given by $m = (-t/2u)^{1/2}$, a remarkable result that indicates spontaneous magnetisation develops with a critical exponent of $\beta = 1/2$ within a mean-field analysis. We notice that, for $t < 0$, only the magnitude of the spontaneous magnetisation $\mathbf{m}$ is specified; the direction could equivalently be any direction in three-dimensional spin-space. This result is central to the idea of symmetry breaking in a transition: the symmetry-broken phase, by choosing an arbitrary axis for spontaneous magnetisation, ceases to have the full symmetry of the effective Hamiltonian that describes the system.

In the above analysis, a number of approximations were made without any appeal to physical reasoning. Principal amongst these was the approximation that the order parameter should have no spatial variation. We now consider in what regime such an approximation may be justified.

In a system in which interactions serve to align spins, pertinent questions should be: over what lengthscale do these interactions act; and how many other spins are contained within this radius? If a spin interacts with more of its neighbours, so that the number of interacting pairs increases, the tendancy is for these spins to form coherent regions of aligned spins, since the energy penalty increases with every pair of interacting, but non-aligned, spins. Clearly then we should imagine that long-range interactions, in which spins interact with neighbours over a significant lengthscale, would bring a system more into line with a mean-field description than an equivalent system with short-range interactions. In three-dimensional systems, mean-field theory breaks down sufficiently close to the critical point; however, this critical regime becomes narrower as the range of interactions is made larger. We will explore the applicability of mean-field theory in the remainder of this section.

Perhaps less clear than the observation the interaction range affects the validity of a mean-field description, also the dimensionality of a system also affects whether it is likely to display mean-field type behaviour. To understand this, we outline a criterion developed by Ginzburg[25] for calculating the dimension above which mean-field theory is an accurate description. For mean-field theory to have any physical relevance, the scale of magnetic fluctuations within a correlated volume of the sample must be significantly smaller than the average magnetisation. We write

$$\langle (\delta m)_\xi^2 \rangle \ll m^2,$$

where $(\delta m)_\xi$ is the average fluctuation in m within a d-dimensional volume of space of linear size ξ. The angled brackets denote an average over all correlated regions of the sample. Within a correlated region, the fluctuation in magnetisation is given by

$$(\delta m)_\xi = \frac{1}{\xi^d} \sum_{i \in \xi^d} S_i \ - m,$$

so that

$$\langle (\delta m)_\xi^2 \rangle = \frac{1}{\xi^{2d}} \sum_{ij \in \xi^d} [\langle S_i S_j \rangle - \langle S_i \rangle \langle S_j \rangle] = \frac{1}{\xi^d} \chi,$$

and we have used the result for the susceptibility χ written in terms of the scale of fluctuations within a sample. For mean-field theory to be valid $\chi \ll \xi^d m^2$, and we use the definitions, valid close to a transition,

$$m \sim |t|^\beta; \quad \xi \sim |t|^{-\nu}, \tag{1.3}$$

to write the inequality in terms of these exponents:

$$|t|^{-\gamma + \nu d - 2\beta} \ll 1,$$

so that, for small enough t the strong inequality may be satisfied by taking $d > \frac{2\beta+\gamma}{\nu}$. The previous analysis showed that $\beta = 1/2$ in a mean-field framework. The exponents $\nu = 1/2$ and $\gamma = 1$ are also elementary results of a mean-field analysis. Substituting in these values gives $d > 4$ for mean-field analysis to be valid. This defines an upper critical dimension as $d_c^u = 4$.

1.3 Unusual Disordered Phases

The Heisenberg magnet serves as a useful archetype for transitions within condensed-matter physics. Its high-temperature phase is very conventional, having both rotational and translational symmetry in real space and rotational symmetry in order-parameter (spin) space. In three spatial dimensions, a regime in which mean-field theory is insufficient, the exponents are obtained by including the effects of spatial fluctuations of the order parameter. At large separations, correlations between values of the order parameter are supressed exponentially with a length scale ξ that defines the correlation length, $\langle m_\alpha(\mathbf{x}) m_\beta(0) \rangle \sim \delta_{\alpha\beta} x^{2-d} e^{-x/\xi}$. This form of

correlations was first suggested by Ornstein and Zernike in a discussion of light scattering from a fluid in the vicinity of a liquid–gas transition. The correlation length diverges at the transition, and correlations there take a qualitatively different form. The signature of the ordered phase is that one or more of the symmetries of the disordered phase are broken: in the case of the ferromagnet, the spin alignment along a particular axis corresponds to a breaking of the spin-rotational symmetry.

In a class of systems that have recently attracted the attention of the condensed-matter community, the above description is incomplete. These novel systems exhibit a high-temperature phase that has the full symmetry of the underlying Hamiltonian, but exhibit correlations that decay not exponentially with distance, as in the conventional Heisenberg case, but instead as a power of the distance with an orientational dependence.

Common to all known examples of these unusual disordered phases is the notion of *local constraints*. These constraints place some restrictions on the configurations that the system may take, and drastically alter the form of correlations in the disordered phase. In fact, we will later see that the disordered phase does not exhibit conventional short-ranged, exponentially decaying correlations, but instead takes a qualitatively different quasi-long-range, algebraic form[30, 31, 28]. This is perhaps best illustrated with an example: the arrangements of dimers on a lattice[23].

1.3.1 Classical Dimer Models

A dimer is an object that sits on two nodes and the link between them on a lattice. Suppose that we impose the condition that each and every lattice node should be occupied by a dimer; that is, only complete dimer coverings are permitted as configurations of the system. Let us also assume that all permitted configurations are degenerate, so that only the entropy serves to select states.

In Figure (1.1) we show a small section of a simple cubic lattice with an example arrangement of dimers.

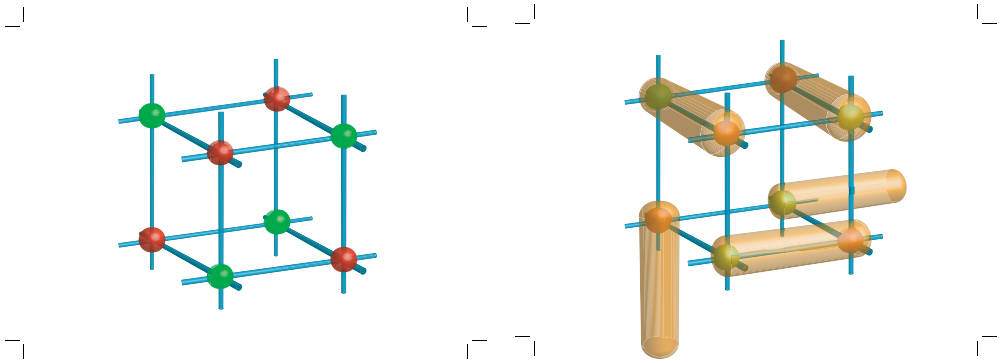

(a) Simple cubic lattice (b) Example dimer configuration

Figure 1.1: Example dimer configuration on a simple-cubic lattice

We begin by mapping this dimer system onto a solenoidal field picture, which will prove to be an extremely useful framework in which to describe these unconventional phases. Work by Huse *et al.* [30] and Henley [28] was pioneering in establishing this mapping, as was earlier work on related problems by Youngblood and Axe[71, 70]. A criterion for it is that the lattice on which the dimers sit must be bipartite: each site of one type, say A, must only be connected to sites of type B, and vice versa. A simple cubic lattice provides a particularly simple example of a bipartite lattice. Once this condition is met, each link i may be ascribed a direction vector $\mathbf{e}_i$ that points from the A site to the B site. A field is then defined according to

$$\mathbf{B}_i = (n_i - z^{-1})\mathbf{e}_i, \tag{1.4}$$

where n_i takes the value of 1 or 0 according to whether the link is occupied or unoccupied by a dimer. Here, z is the coordination number of the lattice which, in the case of the simple cubic, is six. A close-packing condition on the dimers then enforces the requirement that there are no sources of $\mathbf{B}$, that it must have zero lattice divergence at each site. In Figure 1.2 we illustrate this mapping on a square lattice, for which the coordination number $z = 4$. In the upper two diagrams, we show two example dimer configurations, and in the lower two diagrams we show how this translates into the lattice flux picture.

In each of the upper two diagrams of Figure 1.2, a pair of dimers have been highlighted: in the left diagram these staggered dimers cannot be placed in any other configuration without moving other dimers; in the diagram on the right side the aligned pair of dimers may be mutually rotated through $\pi/2$ to generate another allowed configuration. We thus note that states with

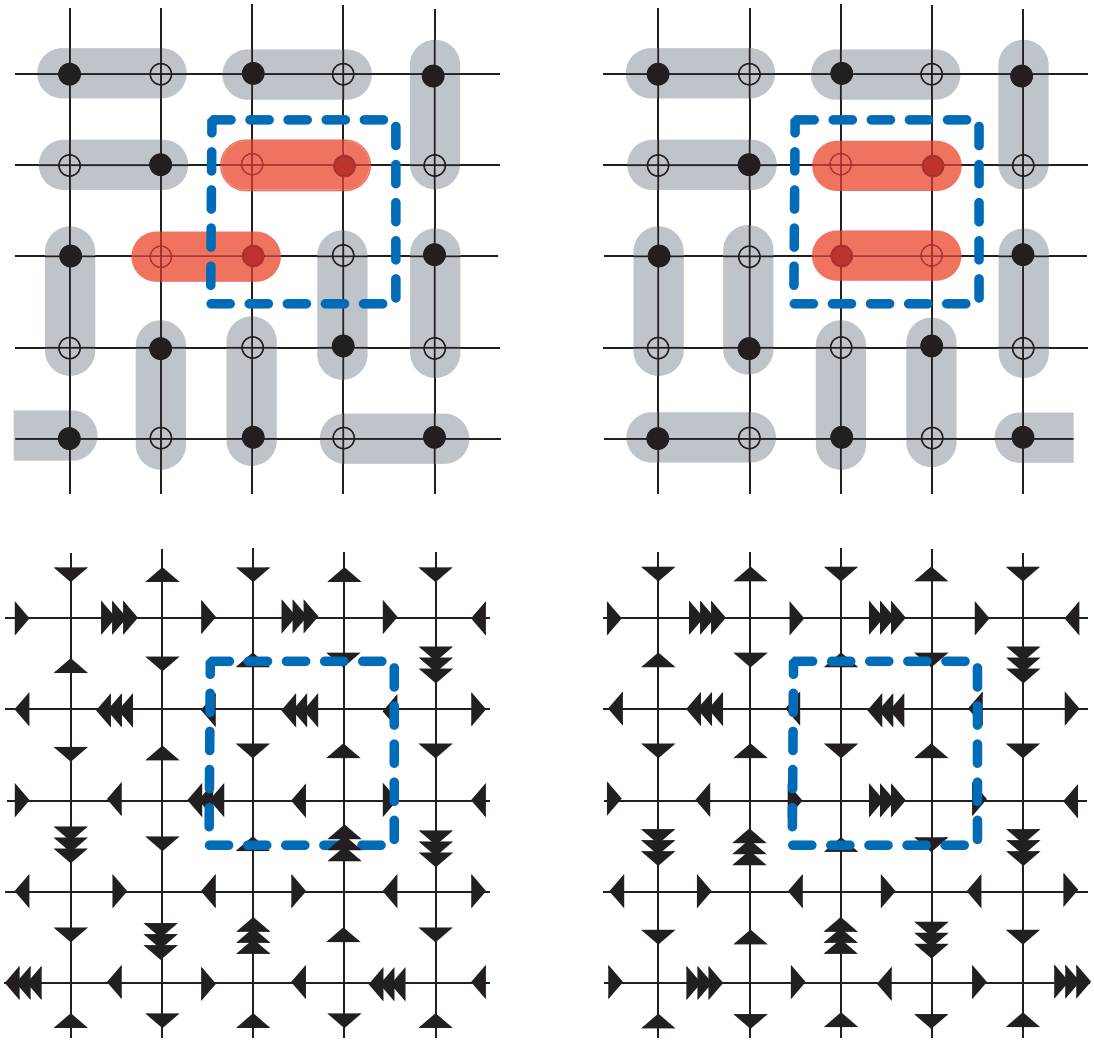

Figure 1.2: Example dimer configurations on a square lattice, and the flux representation

alignment of neighbouring dimers generate a larger degeneracy. We emphasize this by looking at the surface Σ, represented by the dashed line in each of the four diagrams; we call the perpendicular flux through a surface Φ_Σ. Clearly the net flux through any closed surface must be zero by virtue of the divergence theorem. However, in the lower left diagram, through the left suface Σ_{left} there are 4 units of flux exiting so that $\Phi_{\Sigma_{\text{left}}} = +4$, and 4 units of flux entering through the bottom surface Σ_{bottom} so that $\Phi_{\Sigma_{\text{bottom}}} = -4$, with the other two suraces have flux $\Phi = 0$. In the lower right diagram (the case with the larger degeneracy), each separate surface Σ_i has flux $\Phi_{\Sigma_i} = 0$.

These considerations are important in helping to provide a coarse-grained description of such a phase, through introducing a continuum field $\mathbf{B}(\mathbf{r})$. Starting from a lattice model such as that shown in Figure 1.1, the number of microstates is maximised by having a zero continuum field

everywhere. Large values of the field thus correspond to few microstates. An entropic weight on states, having the correct combinatorial properties, is postulated [31, 28] to be

$$\mathcal{P}[\mathbf{B}(\mathbf{r})] = \exp\left\{-\frac{\kappa}{2}\int d\mathbf{r}[\mathbf{B}(\mathbf{r})]^2\right\},$$

where κ is the sole parameter of the theory. Integrating this weight over allowed field configurations generates the partition function. We have seen that local constraints restrict the field $\mathbf{B}(\mathbf{r})$ to be divergence-free, that is $\nabla \cdot \mathbf{B}(\mathbf{r}) = 0$, and we integrate the weight $\mathcal{P}$ only over solenoidal fields. Correlation functions follow immediately from introducing a gauge field $\mathbf{A}(\mathbf{r})$ through $\mathbf{B}(\mathbf{r}) = \nabla \times \mathbf{A}(\mathbf{r})$; this gauge field solves the zero-divergence constraint at the cost of introducing a gauge degree of freedom. In three dimensions we obtain the correlation function

$$\langle B_i(\mathbf{r})B_j(0)\rangle = \frac{1}{4\pi\kappa}\frac{3r_ir_j - r^2\delta_{ij}}{r^5},$$

giving correlations of an algebraically decaying nature, in constrast to the short-range exponential correlations of conventional disordered phases. This algebraic decay means that correlations are quasi-long-range, and identical in functional form to the field of an electric dipole.

For a system of electric charges interacting only through the Coulomb potential, the potential energy stored within the field is proportional to $\int d\mathbf{r}[\mathbf{E}(\mathbf{r})]^2$. In the absence of free charges, at large distances away fom the system, the leading term in a multipole expansion of the potential is dipolar. A partition function for this Coulomb system is obtained through integrating the Boltzmann weight $\exp\{-\kappa\int d\mathbf{r}[\mathbf{E}(\mathbf{r})]^2\}$ over all allowed ($\nabla \cdot \mathbf{E} = 0$) field configurations. Although this partition function has an energetic origin, while that of the dimer system has an entropic origin, they are identical in form. This observation lends these unusual phases the name *Coulomb phases*.

1.3.2 Classical Dimer Transitions

Statistical mechanical systems that exhibit Coulomb phases are attracting a great deal of attention. An interesting question therefore, and central to much of this thesis, concerns the behaviour of ordering transitions out of such phases. Dimer models provide an excellent test bed for investigating this question.

One of the first attempts to understand such a transition was done by Alet and collaborators[4]: by introducing a potential that favours alignment of neighbouring dimers in order to induce a transition, a numerical study of the critical behaviour was performed. Through large-scale simulations, it was shown that this transition was continuous and compatible with a tricritical point. A naive application of the LGW prescription, using the order parameter that distinguishes amongst the six columnar ordered ground states cannot capture the dipolar correlations on the high-temperature side of the transition. In this model, simulations showed that, although the correlations of the Coulomb phase are algebraic with a fixed, integer power of r^{-3}, their scale is set by a temperature dependent prefactor. Close to the critical point, this prefactor vanishes, and the observed correlations become isotropic[49]. In Reference [49], it is argued that critical behaviour is best described by a spin-like degree of freedom possessing $O(3)$ symmetry, with no cubic lattice anisotropies close enough to the critical point.

Candidate field theories are put forward in a recent paper by Chen *et al.*[15], where dimer models are mapped onto a $U(1)$ gauge theory, and through a duality transformation[33] to describe the transition as Higgs confinement driven by monopole condensation. Dimer transitions are currently a very intensive area of research, serving as examples of classical systems that appear to evade a LGW description.

For an example of a system related to the quantum dimer model that displays a transition out of a strongly correlated "spin liquid" state, where quantum effects serve to pick an ordered ground state that is maximally delocalised, see the papers by Bergman *et al.*[11, 10].

1.4 Summary

In this chapter, we have introduced phase transitions as an important and broad subject within physics. We have taken a conventional Heisenberg magnetic system and analysed its critical behaviour in a mean-field framework. We have discussed where a mean-field theory is applicable, and also when fluctuations serve to disrupt a mean-field description. Having described the disordered, paramagnetic phase of a Heisenberg magnet, we turned attention to the disordered phase of a dimer model, where exponentially decaying correlations are absent. We find that the highly-constrained nature of the ground-state manifold feeds through to induce quasi-long-range ordering of dimers, and show that this is a general principle for any system which may

be mapped onto a description in solenoidal fields.

Chapter 2

General Introduction: A Brief Survey of Frustrated Magnets

We note that a number of insulating solids possess permanent magnetic moments at some of their lattice sites. The origin of these permanent moments is a predominantly intraatomic electrostatic effect, resulting in maximisation of the total angular momentum of each atom in an effort to keep the valence electrons localised as far apart as possible in each atom. If these moments are then considered to be independent, there should be no correlation between their orientation in a solid. However, it is empirically observed that moments have a tendency to order at low-temperatures, and so there must be further interactions between them. This ordering is mediated through exchange interactions (again, of electrostatic origin) and long-range dipolar interactions (a magnetostatic property). The strength of magnetic dipolar interactions is typically very weak, on the order of 10^{-4}eV in a typical solid, and so the dominant effect that drives spin alignment is exchange interactions, which have an energy of the order of electrostatic energy differences. The exact strength of these exchange interactions is, however, material-dependent, and interactions may favour spin alignment in the case of a ferromagnet ($J < 0$), or spin anti-alignment in antiferromagnet ($J > 0$). For reasons we will discuss below, antiferromagnets yield a much richer range of possibilities in their behaviour.

Antiferromagnets occur on two distinct types of lattice: bipartite, and non-bipartite. A bipartite lattice (Figure 2.1) may be decomposed into two sublattices, say A and B, where every site A has only B sites as its neighbours, and *vice versa*. In this figure, the different

sublattices are indicated by solid and hollow circles.

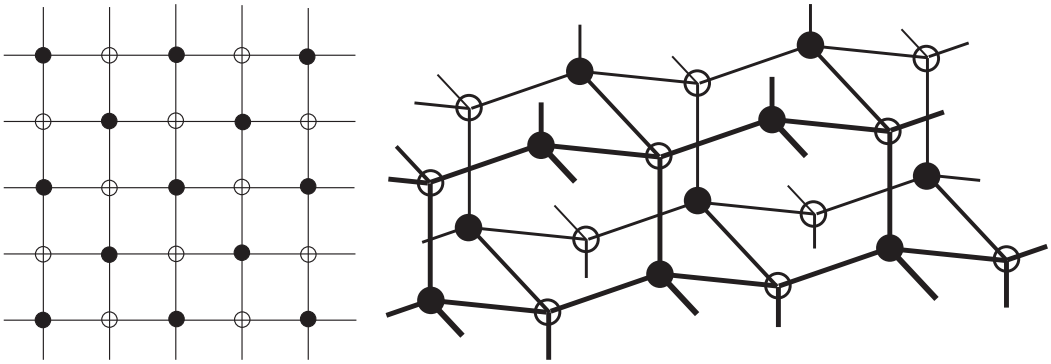

(a) Square lattice (b) Diamond lattice

Figure 2.1: Examples of bipartite lattices: in two dimensions (a) the square lattice, and in three dimensions (b) the diamond lattice.

The decomposition into two sublattices cannot be made in non-bipartite lattices, examples of which are shown in Fig. 2.2.

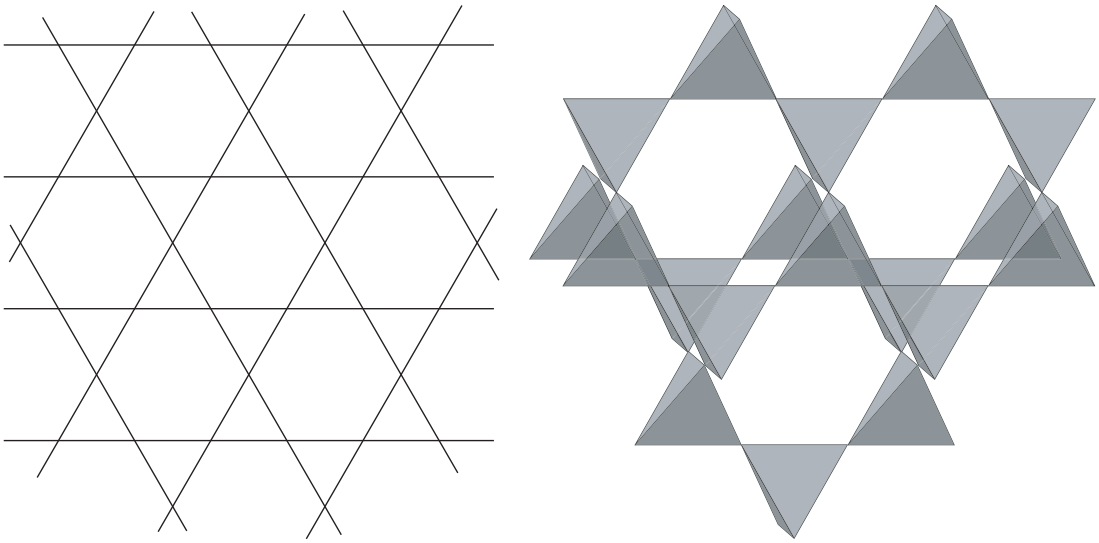

(a) Kagomé lattice (b) Pyrochlore lattice

Figure 2.2: Examples of non-bipartite lattices: in two dimensions (a) the kagomé lattice and in three dimensions (b) the pyrochlore lattice.

For a classical antiferromagnet containing only nearest-neigbour interactions, on a bipartite lattice the ground state is clear: it is possible to construct a state where the quantity $\mathbf{S}_i \cdot \mathbf{S}_j = -S^2$ for all neigbouring pairs by taking the spins on A sites to point in opposite direc-

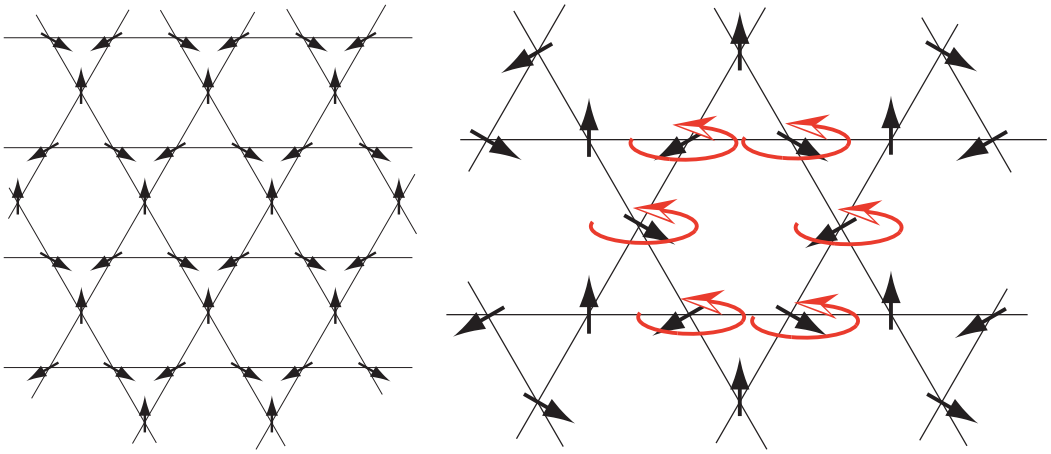

(a) Planar ground state (b) Weathervane mode

Figure 2.3: Ground state configurations for a Heisenberg model on the kagomé lattice. Figure (a) illustrates a planar ground state, and figure (b) a weathervane mode.

tions to spins on B sites. Such a state is known as a Néel state[54], and corresponds to magnetic ordering at a particular wavevector. Néel states provide a unique (up to global spin rotations) minimum energy configuration.

Antiferromagnets built on non-bipartite lattices provide an interesting contrast, since they illustrate a concept known as *frustration*[5]. In a frustrated system, no single configuration corresponds to a unique minimum of the energy: many degenerate ground states exist. For a non-bipartite lattice, the condition $\mathbf{S}_i \cdot \mathbf{S}_j = -S^2$ cannot be met on all antiferromagnetic bonds, since the geometry of the lattice precludes this. Again, to illustrate this concept, we provide the example of a Heisenberg model formulated on the kagomé lattice of Figure 2.2(a). A little thought should convice that a satisfactory ground state is the planar state (Fig. 2.3(a)). To illustrate the huge ground-state degeneracy, we display another ground state in Figure 2.3(b). This ground state supports a *local* mode, known as a weathervane mode, where a *local* rearrangement of spins is possible: in each of the spins around the hexagon highlighted in the figure, spins may simultaneously be freely rotated through arbitrary angle about the axis defined by the six surrounding spins. Since the number of local modes scales with system size, we conclude that the degeneracy of the ground state is an extensive quantity.

At temperatures $T \gg J$, the susceptibility of all antiferromagnets is well-described by Curie's Law, $\chi^{-1} \propto T - \Theta_{CW}$, and allows the definition of a Curie-Weiss temperature Θ_{CW}, which is a measure of the sign and strength of nearest-neighbour interactions. At temperatures of the order

of $|\Theta_{CW}|$, at which an ordering transition would occur in an unfrustrated system, frustrated magnets do not display an ordering transition since strong fluctuations within the ground-state manifold prevent the selection of a unique, ordered state. Only at temperatures much lower than $|\Theta_{CW}|$ is spin ordering sometimes observed, and it is driven by other mechanisms that lift the degeneracy. These mechanisms may take the form of (previously neglected) further-neighbour interactions or be through coupling to the lattice, and accompanied by a structural distortion.

The experimental evidence for frustrated magnets is covered in a classic review by Ramirez[60]. In this paper, a number of strongly-frustrated lattices are studied across a range of temperatures. It was found that magnetic ordering, signalled by a cusp in the susceptibility χ, occurs at a temperature $T_c \ll |\Theta_{CW}|$. The exact value of $f \equiv |\Theta_{CW}|/T_c$ is material-dependent: for commonly studied materials, $ZnCrO_4$ (pyrochlore) it is found $f \sim 30$; in ceramic samples of SCGO (pyrochlore slabs), $f \sim 150$.

2.1 Types of Frustration

2.1.1 Frustration arising from competition

The mechanisms by which frustration is achieved are broadly split into the categories of competition between interactions, or on geometric grounds. Frustration resulting from competition is illustrated in Figure 2.4 on the square lattice with nearest neigbour and second-neighbour interactions[14]. Taking J_1 as the strength of nearest-neighbour interactions (solid lines), and $J_2 = \alpha J_1$ as the strength of next-nearest-neigbour interactions (dashed lines), for $\alpha < 1/2$ the classical ground state for Heisenberg spins has conventional Néel order with two sublattices (Figure 2.4(a)). When $\alpha > 1/2$ the two sublattices each separately exhibit Néel ordering, with the relative directions being offset from each other by $\pi/2$, leading to the four-sublattice state of Figure 2.4(b). At the point $\alpha = 1/2$ the system is frustrated, and any state in which the vector sum of spins in a square plaquette equals zero is a valid ground state; both states described above satisfy this criterion.

This type of frustration, which arises from competition between interactions, is typically not very robust, resulting as it does from a fine-tuning of interaction strengths ($\alpha = 1/2$), and is likely to be a good description for only a very small number of real materials. Indeed, in real materials, quantum corrections to these classical ground states can preferentially select one of

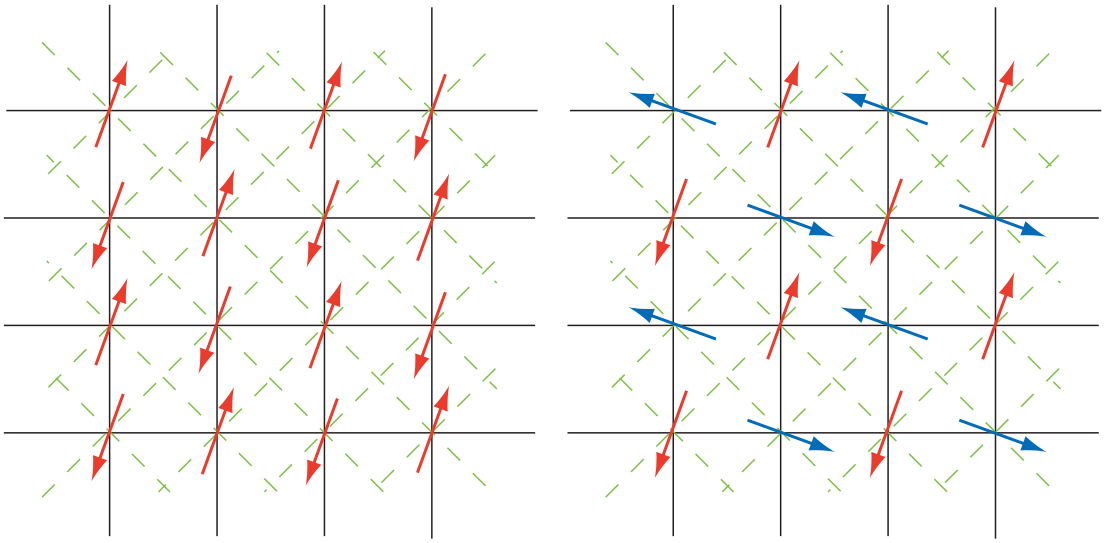

(a) Two sublattice state (b) Four sublattice state

Figure 2.4: Ordering on the square lattice with crossings: (a) two-sublattice state and (b) four-sublattice state.

the ordered states, so the classical description may be too simplistic.

2.1.2 Frustration arising from geometry

We next turn to geometric frustration, which is much more robust against perturbations of the local environment. The origin of geometric frustration has been touched upon above in the context of non-bipartite lattices: as the name suggests, it is specifically the *geometry* of the lattice that precludes the existence of a state where all neighbouring pairs of spins between antiferromagnetic bonds are anti-aligned. We illustrate this concept in the next section with an important example: the Heisenberg model on a pyrochlore lattice.

2.2 Coulomb Phases in Geometrically-Frustrated Antiferromagnets

In this section, we first provide a short overview of geometrically frustrated magnets, concentrating particularly on the degeneracy of their ground states, and how these ground states may be described. Having introduced the concept of a Coulomb phase in Section 1.3, we also show how this sort of phase could be realised on a geometrically frustrated magnet. We will discuss two lattices that support a Coulomb phase: the pyrochlore lattice, which is equivalent to the

arrangement of magnetic ions in spinel compounds; and the less physical, but more mathematically convenient lattice of corner-sharing octahedra.

Geometrically-frustrated antiferromagnets (GFAFMs) are built out of a number of lattice units, called simplices, which share either edges or corners: the triangular lattice (not pictured) is a lattice of edge-sharing triangles, the kagomé (Figure 2.2(a)) a lattice of corner-sharing triangles. Generally, corner-sharing simplices provide a larger ground-state degeneracy. In discussing the ground states of GFAFMs that are built out of corner-sharing units, it is instructive to rewrite the Hamiltonian of Eq. (1.2) in the alternative form

$$E = J \sum_{\langle ij \rangle} \mathbf{S}_i \cdot \mathbf{S}_j = \frac{J}{2} \sum_{\alpha} \mathbf{L}_{\alpha}^2 - \frac{1}{2} NJS^2,$$

where α is an index which labels a simplex, and $\mathbf{L}_\alpha = \sum_{i \in \alpha} \mathbf{S}_i$ represents the total spin in that simplex (each spin belongs to two different simplices), and there are N sites in total. Looking at the Hamiltonian in this form, it is clear that the ground states are any configuration where the total spin vanishes in each simplex[51, 50], that is

$$\sum_{i \in \alpha}^{q} \mathbf{S}_i = 0 \qquad \text{for all } \alpha, \tag{2.1}$$

where each simpex α contains q sites. Armed with this condition, we may now calculate the dimension of the ground-state manifold and, perhaps most importantly, whether this dimension is an extensive quantity.

For n-component spins the total number of continuous degrees of freedom is $F = N(n-1)$, since each spin has a constraint on its length. Since each spin is shared between two simplices, the total number of simplices is $2N/q$, so the ground-state condition, Eq. (2.1), provides $K = 2nN/q$ constraints. Assuming linear independence of these constraints, the total dimension of the ground-state manifold is $D = F - K = N(n(1-2/q)-1)$. Thus the ground-state manifold is extensive provided that $n > (1-2/q)^{-1}$. For a Heisenberg antiferromagnet on a pyrochlore lattice, where $n = 3$ and $q = 4$, this condition is satisfied, giving a ground-state dimensionality of $D = N/2$. For a lattice of corner-sharing octahedra in which $q = 6$, we need $n > 3/2$ to give an extensively degenerate system.

We now discuss whether a GFAFM can exhibit a Coulomb phase, the first condition for which

is that the magnet must have an extensively degenerate ground-state manifold. In addition to this, two further conditions must be met for a system to support a Coulomb phase: the first is that thermal fluctuations must not induce order-by-disorder, in which an ordered phase can be selected on entropic grounds[65]. The other condition is that the lattice must be bi-simplex, meaning that the lattice of simplex centres is bipartite. An example of a spin system that fulfills all of these conditions is the Heisenberg model on a pyrochlore lattice (bipartite diamond simplex lattice). A further example is a lattice of corner-sharing octahedra, shown in Figure 2.5.

Whilst the preceeding material in this chapter has been a review of previously known results, the following work is original, and builds upon the results of References [30] and [28]. In the following subsection we will describe explicitly how a spin model on a lattice of corner-sharing octahedra may be mapped onto a system of solenoidal fields first introduced in Section 1.3.1; we will thus establish that such a system exhibits a Coulomb phase.

2.2.1 Demonstration of the Mapping from Spin Picture to Flux Picture

We have used a constraint-counting argument to show that a Heisenberg spin model on a pyrochlore lattice would have an extensively degenerate ground-state manifold. However, for the purposes of constructing an explicit mapping onto the solenoidal field model introduced in Section 1.3.1, we dispense with the pyrochlore lattice and choose to make this mapping on a lattice of corner-sharing octahedra. One reason for choosing this lattice is that it fulfils the three criteria that we stated in the previous section for a system to support a Coulomb phase. In addition, the lattice of corner-sharing octahedra contains three sites within its unit cell, compared with the pyrochlore lattice that has four sites within its unit cell. In the interests of keeping the mathematics as lucid as possible, we choose the lattice with the smaller unit cell.

Consider the lattice of corner-sharing octahedra, where interactions between n-component, classical spins $\mathbf{S}_i = (S_i^1, S_i^2, \ldots, S_i^n)$ are antiferromagnetic, and have strength J. These interactions are illustrated in Figure 2.5. The Hamiltonian for this system is written

$$\mathcal{H}_J = \sum_{ij} J_{ij}\, \mathbf{S}_i \cdot \mathbf{S}_j. \tag{2.2}$$

The simplex α is centred at $\mathbf{r}_\alpha$. The sites $\mathbf{r}_\alpha$ establish a Bravais lattice that is simple-cubic.

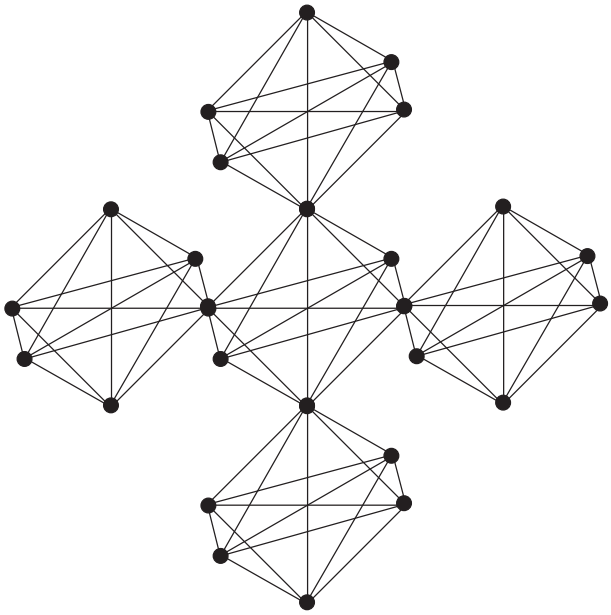

Figure 2.5: The lattice of corner-sharing octahedra. Sites of spins $\mathbf{S}_i$ are represented by filled circles, and antiferromagnetic interactions of strength J by lines. Note particularly that there is no spin at the centre of an octahedron. The position vector to the centre of octahedron α is denoted $\mathbf{r}_\alpha$.

At each lattice point $\mathbf{r}_\alpha$, the unit cell contains three sites $l = 1, 2, 3$, each displaced from $\mathbf{r}_\alpha$ by a vector $\boldsymbol{\delta}_l = \frac{1}{2}a\hat{\mathbf{e}}_l$, where $\hat{\mathbf{e}}_l$ is a unit vector in one of the three Cartesian directions, and a the lattice constant. In what follows we take $a = 1$. Spins $\mathbf{S}_{\alpha,l}$ (simplex α, site l) are located at $\mathbf{r}_\alpha + \widehat{\mathbf{e}}_l/2$. For a system containing N simplices ($3N$ spins), we define the following Fourier transformations:

$$\mathbf{S}_l(\mathbf{q}) = N^{-1/2} \sum_\alpha e^{-i(\mathbf{q}+\mathbf{k}_\pi)\cdot(\mathbf{r}_\alpha + \frac{1}{2}\hat{\boldsymbol{e}}_l)}\, \mathbf{S}_{\alpha,l}, \tag{2.3a}$$

$$\mathbf{S}_{\alpha,l} = N^{-1/2} \sum_{\mathbf{q}} e^{i(\mathbf{q}+\mathbf{k}_\pi)\cdot(\mathbf{r}_\alpha + \frac{1}{2}\hat{\boldsymbol{e}}_l)}\, \mathbf{S}_l(\mathbf{q}), \tag{2.3b}$$

where $\mathbf{k}_\pi = (\pi, \pi, \pi)$. Note that, with this convention for Fourier transformations, the $q = 0$ Fourier component corresponds to successive [111]-planes of alternating total magnetisation.

Following the treatment outlined in Reference [30], since the lattice of octahedral centres (the simplex-lattice) is simple-cubic, each link of this bipartite lattice may be assigned a unique directionality. On each link of the simplex lattice we assign a unit vector $\boldsymbol{\kappa}_{\alpha,l} \in \{\pm\widehat{\mathbf{e}}_l\}$ that points from the node chosen to be on sublattice A (say) to the node on sublattice B. Since spins

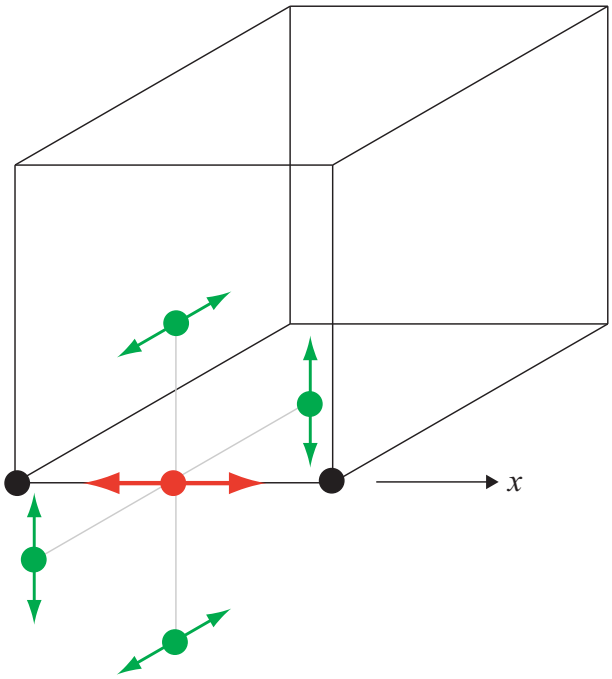

Figure 2.6: A diagram to highlight the location of $S^a, \mathbf{F}^a, \mathbf{A}^a$ and V^a. The cubic simplex lattice is shown as the black cube. The spin component $S^a_{\alpha,x}$ is represented by the red circle at the centre of the x-link. The field $\mathbf{F}^a(\mathbf{r}_\alpha + \frac{1}{2}\hat{\mathbf{e}}_x)$ by the red vector arrows along the $\pm\mathbf{e}_x$ direction at the site of $S^a_{\alpha,x}$. Vector potentials $\mathbf{A}^a$ are located at the centre of the faces of the simple-cubic lattice; these vectors point in the direction of the green arrows. Finally, scalar potentials V^a are at the nodes of the simple-cubic lattice; these are pictured as black circles.

are at the centre of each link, n flavours of field may now be defined on each link (α, l) through

$$\mathbf{F}^a(\mathbf{r}_\alpha + \widehat{\mathbf{e}}_l/2) = \boldsymbol{\kappa}_{\alpha,l}\, S^a(\mathbf{r}_\alpha + \widehat{\mathbf{e}}_l/2), \tag{2.4}$$

where the index a labels the spin component or field flavour. We note that the fields $\mathbf{F}^a_{\alpha,l}$ are directed along the links of the lattice so that $[\mathbf{F}^a_{\alpha,l}]_m \propto \delta_{lm}$. At each spin site the set of n fields $\mathbf{F}^a_{\alpha,l}$ may be decomposed as $\mathbf{F}^a_{\alpha,l} = \mathbf{B}^a_{\alpha,l} + \mathbf{I}^a_{\alpha,l}$, where $\mathbf{B}^a_{\alpha,l}$ is a lattice divergence-free part and $\mathbf{I}^a_{\alpha,l}$ the irrotational part. For the remainder of this section, it may be helpful to refer to Figure 2.6 for clarity. The divergence-free condition is solved by introducing a vector potential $\mathbf{A}^a_{\alpha,l}$ through

$$\begin{aligned} B_i(\mathbf{r}_\alpha + \widehat{\mathbf{e}}_i/2) &= [(\boldsymbol{\nabla} \times \mathbf{A})(\mathbf{r}_\alpha + \widehat{\mathbf{e}}_i/2)]_i \\ &= \sum_{jk} \varepsilon_{ijk} \Big[A_j(\mathbf{r}_\alpha + \widehat{\mathbf{e}}_i/2 + \widehat{\mathbf{e}}_k/2) - A_j(\mathbf{r}_\alpha + \widehat{\mathbf{e}}_i/2 - \widehat{\mathbf{e}}_k/2) \Big], \end{aligned} \tag{2.5}$$

so the vector potential is defined on the faces of the simple-cubic lattice. The field $\mathbf{I}^a_{\alpha,l}$ can be written as the gradient of a scalar potential V^a_α:

$$\begin{aligned}[\mathbf{I}(\mathbf{r}_\alpha + \widehat{\mathbf{e}}_i/2)]_i &= (\nabla_i V)(\mathbf{r}_\alpha + \widehat{\mathbf{e}}_i/2) \\ &= \Big[V(\mathbf{r}_\alpha + \widehat{\mathbf{e}}_i) - V(\mathbf{r}_\alpha)\Big] \end{aligned} \tag{2.6}$$

and the scalar potential is defined on the nodes of the simple-cubic lattice. Understanding $\boldsymbol{\nabla}$ to be a lattice operator, we may write

$$\mathbf{F}^a = \boldsymbol{\nabla} \times \mathbf{A}^a + \boldsymbol{\nabla} V^a. \tag{2.7}$$

From Equations (2.4), (2.5) and (2.6), for each spin component a the Fourier-transformed equations for this lattice model take the form

$$\begin{pmatrix} S_x(\mathbf{q}) \\ S_y(\mathbf{q}) \\ S_z(\mathbf{q}) \end{pmatrix} = 2i \begin{pmatrix} 0 & -s_z & s_y & s_x \\ s_z & 0 & -s_x & s_y \\ -s_y & s_x & 0 & s_z \end{pmatrix} \begin{pmatrix} A_x(\mathbf{q}) \\ A_y(\mathbf{q}) \\ A_z(\mathbf{q}) \\ V(\mathbf{q}) \end{pmatrix} \tag{2.8}$$

and we introduce the notation $s_m = \sin(q_m/2)$. Although this mapping appears to introduce an extra degree of freedom, we note that this is just a gauge degree of freedom from defining $\mathbf{B}^a = \nabla \times \mathbf{A}^a$, and by working in a fixed gauge there really are only three degrees of freedom.

2.2.2 Hamiltonian in the Flux Picture: A Verification of the Coulomb Phase

From the interactions illustrated in Figure 2.5, we see that the block-diagonalised form for the Hamiltonian $\mathcal{H}_J$ of Equation (2.2) is

$$\mathcal{H}_J = \sum_{\mathbf{q}} \sum_{mn}^{3} J_{mn}(\mathbf{q})\ \mathbf{S}_l(\mathbf{q}) \cdot \mathbf{S}_m(-\mathbf{q}), \tag{2.9}$$

where the interaction matrix is given by

$$J(\mathbf{q}) = 2J \begin{pmatrix} s_x^2 & s_x s_y & s_x s_z \\ s_x s_y & s_y^2 & s_x s_z \\ s_x s_z & s_x s_z & s_z^2 \end{pmatrix}, \tag{2.10}$$

and s_x, s_y and s_z have the same meaning as Eq. (2.8).

Under the parameterisation introduced in Equation (2.8), the $\mathcal{H}_J$ may now be written

$$\mathcal{H}_J = 8J \sum_a \sum_{\mathbf{q}} (s_x^2 + s_y^2 + s_z^2)^2 \left| V^a(\mathbf{q}) \right|^2. \tag{2.11}$$

Looking at the Hamiltonian of Eq. (2.11), the reasons for restating the problem in the language of solenoidal fields should be clear. This Hamiltonian exhibits no dependence on the divergence-free part of the fields $\mathbf{B}^a(\mathbf{q})$. Finding the ground-state manifold of $\mathcal{H}_J$ is now particularly simple: it corresponds to setting the scalar fields $V^a(\mathbf{q}) = 0$.

Within a coarse-grained description of such a phase, we see that any ground state corresponds to a continuum field $\mathbf{B}^a(\mathbf{r})$ that is everywhere solenoidal. In the limit of $J \to \infty$, such that only ground states are permitted, correlations between different components of the same field, $\langle F_i^a(\mathbf{r}) F_j^a(0) \rangle$ thus possess the algebraic, dipolar form as described in Section 1.3. The transformation back to spin variables preserves the dipolar form; we will show in Section 4.3.2 that spin-spin correlation functions $\langle S_i^a(\mathbf{r}) S_j^a(0) \rangle$ are also dipolar.

2.2.3 The Effect of Fluctuations off Ground-State Manifold

Strictly, the quasi-long-range correlations of the Coulomb phase only extend throughout the spin system in the limit of $J/T \to \infty$. For small but finite T/J, thermal fluctuations off the ground-state manifold cut off dipolar correlations at lengths greater than the cutoff length $\xi_c \sim (J/T)^{1/2}$[24], beyond which correlations fall off in the conventional exponential manner.

2.3 Summary

In this Chapter we have introduced the field of frustrated magnets. We have seen that geometrically frustrated antiferromagnets yield a rich range of behaviour, even if we consider only

classical spin systems. In a frustrated system with macroscopic ground-state degeneracy, we find that the interaction matrix has low-energy, wavevector independent flat bands. Furthermore, we have shown that a Coulomb phase can be supported on certain classes of GFAFM, and have provided an explicit demonstration of the mapping between a GFAFM and a system of divergence-free fields. We have seen that, in the limit of $J \to \infty$ correlations between spins inherit a dipolar nature.

Chapter 3

Some Approximation Schemes for Investigating Interacting Systems

Problems involving interactions between microscopic objects generates an extremely rich field of condensed-matter phenomena. Unfortunately – although perhaps not surprisingly given the very non-trivial behaviour that these systems exhibit – very few models have thermodynamics that can be solved exactly, and no single method is available for treating all the remaining models within condensed-matter theory. A number of very sophisticated approximation schemes have been developed in order to probe interacting systems in certain regimes and, when applied carefully, these approximation schemes can give an extremely precise description of the behaviour. In chapter 1 we touched upon one approximation scheme – the mean-field approximation – when studying the ferromagnet. This is often the first method that is applied to systems that are not exactly solvable. As an example of a classical system, in the mean-field treatment of the ferromagnet (Sec. 1.2.1), the approximation was that a single spin interacts with the *average* of all the other spins. Clearly this is an approximation, since in the model spins interact only with their immediate neighbours, however the Ginzburg criterion indicated that this becomes an accurate description of the physics in dimension $d > d_c^u$. In the short-range ferromagnet we found that $d_c^u = 4$; in fewer than four dimensions, alternative methods must be utilised.

We now discuss in more detail techniques for studying classical spin systems.

3.1 Continuum Descriptions as Field Theory

The most important object in statistical physics is the partition function, which here we write as an integral over all allowed field configurations (we assume that the continuum limit has been taken: the underlying lattice spacing has become small, and discrete n-component spins are replaced by n-component fields $\boldsymbol{\phi}(\mathbf{r}) = [\phi_1(\mathbf{r}), \phi_2(\mathbf{r}), \ldots, \phi_n(\mathbf{r})]$)

$$\mathcal{Z} = \int \mathcal{D}\boldsymbol{\phi}(\mathbf{r})\; e^{-S[\boldsymbol{\phi}(\mathbf{r})]}. \tag{3.1}$$

The functional $S[\boldsymbol{\phi}]$ causes particular problems because, for interacting systems, $S[\boldsymbol{\phi}]$ is not merely quadratic in $\boldsymbol{\phi}$: interactions are represented by quartic terms, and the partition function ceases to be a straightforward Gaussian integral. For $S[\boldsymbol{\phi}]$, which we call the effective Hamiltonian, we use the explicit form

$$S[\boldsymbol{\phi}] = \underbrace{\frac{1}{2}\int d\mathbf{r}\; \{r_0\; \boldsymbol{\phi}(\mathbf{r})\cdot\boldsymbol{\phi}(\mathbf{r}) + (\nabla\boldsymbol{\phi}(\mathbf{r}))^2\}}_{S_2[\boldsymbol{\phi}]} + \underbrace{\frac{1}{n}\;\frac{u_0}{4!}\int d\mathbf{r}(\boldsymbol{\phi}(\mathbf{r})\cdot\boldsymbol{\phi}(\mathbf{r}))^2}_{S_4[\boldsymbol{\phi}]}. \tag{3.2}$$

It is important to realise that this effective Hamiltonian does not represent all physical systems, or even all magnetic insulators. It serves as a prototype for a number of systems with short-range interactions, most notably at $n = 3$ it represents a short-range Heisenberg ferromagnet. Later in this chapter we investigate a short-range ferromagnet in the limit of $n \to \infty$; this is a useful exercise since it allows us, in this limit, to contrast conventional ferromagnetic transition with that of a less conventional one that will be introduced in Chapter 4.

A Landau approximation to the free-energy density of Eq. (3.2) is obtained from taking a uniform $\boldsymbol{\phi}(\mathbf{r}) = \boldsymbol{\Phi}$, giving

$$\frac{k_B T}{V} S(\Phi) \equiv U(\Phi) = k_B T \left(\frac{1}{2} r_0^{-1}\boldsymbol{\Phi}^2 + \frac{1}{n}\;\frac{u_0}{4!}(\boldsymbol{\Phi}^2)^2\right). \tag{3.3}$$

Similar to a mean-field theory, this Landau free energy succesfully encapsulates the critical behaviour at dimensions $d > d_c^u$.

For later analysis, it is convenient to write the effective Hamiltonian in Fourier space. The

quadratic and quartic parts are

$$S_2[\boldsymbol{\phi}] = \frac{1}{2} \sum_{\alpha\beta} \int \prod_i^2 \frac{d^d\mathbf{q}_i}{(2\pi)^d} \, \Gamma^{(2)}_{\alpha\beta}(\mathbf{q}_1, \mathbf{q}_2) \, \phi_\alpha(\mathbf{q}_1)\phi_\beta(\mathbf{q}_2) \tag{3.4}$$

$$S_4[\boldsymbol{\phi}] = \sum_{\alpha\beta\gamma\delta} \int \prod_i^4 \frac{d^d\mathbf{q}_i}{(2\pi)^d} \; \Gamma^{(4)}_{\alpha\beta\gamma\delta}(\mathbf{q}_1 \ldots \mathbf{q}_4) \, \phi_\alpha(\mathbf{q}_1)\phi_\beta(\mathbf{q}_2)\phi_\gamma(\mathbf{q}_3)\phi_\delta(\mathbf{q}_4), \tag{3.5}$$

where the $\mathbf{q}$-space integrals are cut off at $q_{max} = \Lambda \sim 1/a$ (lattice spacing a), effectively the wavevector at first Brillouin zone boundary. The two- and four-point functions are

$$\Gamma^{(2)}_{\alpha\beta}(\mathbf{q}_1, \mathbf{q}_2) = (2\pi)^d \delta(\mathbf{q}_1 + \mathbf{q}_2)\delta_{\alpha\beta}[G^{(0)}(\mathbf{q}_1)]^{-1} \tag{3.6}$$

$$\Gamma^{(4)}_{\alpha\beta\gamma\delta}(\mathbf{q}_1 \ldots \mathbf{q}_4) = \frac{1}{n} \, \frac{u_0}{4!}(2\pi)^d \delta(\sum_i \mathbf{q}_i) S_{\alpha\beta\gamma\delta} \tag{3.7}$$

where $G^{(0)}(\mathbf{q})$ is known as the bare propagator, which for the ferromagnetic Hamiltonian of Eq. (3.2) is $G^{(0)}(\mathbf{q}) = (q^2 + r_0)^{-1}$. Finally, the tensor $S_{\alpha\beta\gamma\delta}$ has the symmetric form

$$S_{\alpha\beta\gamma\delta} = \frac{1}{3}(\delta_{\alpha\beta}\delta_{\gamma\delta} + \delta_{\alpha\gamma}\delta_{\beta\delta} + \delta_{\alpha\delta}\delta_{\beta\gamma}).$$

It is important to stress that the exact form of $G^{(0)}(\mathbf{q})$ is valid only for the ferromagnetic Hamiltonian of Eq. (3.2). More generally, the bare propagator $G^{(0)}(\mathbf{q})$ is specific to the particular choice of effective Hamiltonian: different choices of Hamiltonians result in different functional dependence of the propagator on wavevector $\mathbf{q}$, but a universal feature of all propagators is that the parameter r_0 is controlled by temperature, and as its value passes through zero, a phase transition results.

3.2 Gaussian Field Theory

If $u_0 = 0$, the effective Hamiltonian reduces to only quadratic terms, $S[\boldsymbol{\phi}] = S_2[\boldsymbol{\phi}]$, and we have the partition function for a Gaussian Model. In this Gaussian model, stable in the symmetric phase ($r_0 > 0$), we can calculate the free energy exactly. For simplicity, we take $n = 1$ and consider a real, scalar-field theory. Starting from the integral

$$\int_{-\infty}^{\infty} dx \; \exp\left\{-\frac{1}{2a}x^2\right\} = (2\pi a)^{1/2},$$

the functional integral over $\phi(\mathbf{q})$ in the partition function becomes

$$\mathcal{Z} = \int \mathcal{D}\boldsymbol{\phi}(\mathbf{q})\; e^{-\frac{1}{2}\sum_{\mathbf{q}}[G^0(\mathbf{q})]^{-1}|\phi(\mathbf{q})|^2} = \prod_{\mathbf{q}}(2\pi G^0(\mathbf{q}))^{1/2}$$

and, using the identity $\ln\prod_{\mathbf{q}}\circ = \sum_{\mathbf{q}}\ln\circ$, the free-energy density is written

$$f = -\frac{k_BT}{2}\ln(2\pi) \;+\; \frac{k_BT}{2}\int\frac{d^d\mathbf{q}}{(2\pi)^d}\ln\,[G^0(\mathbf{q})]^{-1}.$$

This is an exact expression for the free energy which is manifestly dependent on the dimensionality of the system. From this free energy, all thermodynamic functions can be obtained for this Gaussian model.

3.3 Interacting Field Theories

For $u_0 > 0$ the partition function is no longer Gaussian, and contains quartic parts in the exponential. These terms cannot be integrated exactly, and we must resort to one of a number of approximation schemes to make further progress.

3.3.1 Weak-Coupling Expansion

We do not provide a full account of the weak-coupling expansion since it has been treated in detail in a vast number of books and articles[61, 57]. Instead, we sketch out a brief picture, without going into all of the technical details.

Consider a single-component field for simplicity. To treat $S_4[\phi]$ of Eq. (3.5) suppose the coupling parameter $u_0 \ll 1$. In this weak-coupling regime we assume that the quartic term can be expanded as a Taylor series so that $\exp\{-S_4[\phi]\} = \sum_{k=0}^{\infty}\frac{(S_4[\phi])^k}{k!}$. The partition function is now written in terms of Gaussian expectations of polynomial expressions. We have

$$\begin{aligned}\mathcal{Z} &= \sum_{k=0}^{\infty}\frac{1}{k!}\left(\frac{-u_0}{4!}\right)^k\int\mathcal{D}\phi(\mathbf{r})\;e^{-S_2[\phi(\mathbf{r})]}\prod_{i=0}^{k}\int d\mathbf{r}_i\;\phi^4(\mathbf{r}_i)\\ &= \sum_{k=0}^{\infty}\frac{1}{k!}\left(\frac{-u_0}{4!}\right)^k\left\langle\prod_{i=0}^{k}\int d\mathbf{r}_i\phi^4(\mathbf{r}_i)\right\rangle_0,\end{aligned}$$

where the $\langle\ldots\rangle_0$ denotes an expectation value with Gaussian weight $e^{-S_2[\phi]}$.

Provided that interactions are weak, so that $u_0 \ll 1$, the expansion is truncated at some $k = k_{max}$. There are now only a finite number of terms to consider. At a given order in k, we must calculate the Gaussian expectation of a product of $4k$ fields. Wick's theorem[68] allows us to decompose this Gaussian expectation into products of single-pair Gaussian expectation values, weighted by combinatorial factors:

$$\langle \phi_{x_1} \dots \phi_{x_l} \rangle_0 = \sum_{\substack{\text{all possible pairings} \\ P \text{ of } \{x_1 \dots x_l\}}} \langle \phi_{x_{P_1}} \phi_{x_{P_2}} \rangle_0 \dots \langle \phi_{x_{P_{l-1}}} \phi_{x_{P_l}} \rangle_0. \tag{3.8}$$

Single-pair expectation values are referred to as propagators, and the combinatorial factors associated with the pairings can be most readily evaluated using a graphical approach of Feynman diagrams, but we reserve the details of this for the next section.

3.3.2 Expansion in Number of Field Components

If the number of field components n is large, we may use a different approximation scheme from the weak-coupling expansion. This scheme does not truncate an expansion at some $k = k_{max}$, as was the case in a weak-coupling expansion, but instead includes contributions at all orders in k. As $n \to \infty$ only a reduced (but still infinite!) number of terms contribute. However, at $n \to \infty$, this infinite set of terms can be conveniently resummed to give finite quantities.

To understand the spirit of this approximation, consider the quartic part of the effective Hamiltonian, $S_4[\boldsymbol{\phi}]$. From the term $(\phi^2)^2 = \left(\sum_\alpha \phi_\alpha^2\right)^2$, the coefficient of a given ϕ_α^2 is $(2\phi^2 - \phi_\alpha^2)$. For n large, $2\phi^2$, which is the sum of n terms, is expected to be much larger than ϕ_α^2 so that, put more plainly, the coupling of each ϕ_α^2 to itself is much weaker than its coupling to the total sum ϕ^2 of all n components.

We expect small fractional fluctuations in ϕ^2; that is

$$\langle\, (\phi^2 - \langle\phi^2\rangle)^2 \,\rangle / \langle\phi^2\rangle^2 = \mathcal{O}(1/n)$$

or $\Delta\phi^2 \ll \langle\phi^2\rangle$ when n is large.

Using this approximation, the quartic part of the effective Hamiltonian, Eq. (3.5), reduces

to

$$S_4[\boldsymbol{\phi}] = \frac{u_0}{4!}\sum_{\mathbf{q}'\beta}\langle\phi_\beta(-\mathbf{q}')\phi_\beta(\mathbf{q}')\rangle\ \sum_{\mathbf{q}\alpha}\phi_\alpha(-\mathbf{q})\phi_\alpha(\mathbf{q}), \tag{3.9}$$

so that the partition function may now be written in the Gaussian form

$$\begin{aligned}\mathcal{Z} &= \int D\boldsymbol{\phi}(\mathbf{q})\ \exp\left\{-S_2[\boldsymbol{\phi}] - S_4[\boldsymbol{\phi}]\right\} \\ &= \int D\boldsymbol{\phi}(\mathbf{q})\ \exp\left\{-\frac{1}{2}\sum_{\mathbf{q}\alpha}[G_{\alpha\alpha}(\mathbf{q})]^{-1}\phi_\alpha(-\mathbf{q})\phi_\alpha(\mathbf{q})\right\},\end{aligned} \tag{3.10}$$

where we identify

$$[G_{\alpha\beta}(\mathbf{q})]^{-1} = [G^0_{\alpha\beta}(\mathbf{q})]^{-1} + \frac{u_0}{6}\sum_{\mathbf{q}'}\langle\phi_\alpha(-\mathbf{q}')\phi_\beta(\mathbf{q}')\rangle. \tag{3.11}$$

The object $G(\mathbf{q})$ can be identified as the full Green's function because it provides the correlations in the interacting theory. That this is true may be seen from the definition of the correlator

$$\begin{aligned}G_{\alpha\beta}(\mathbf{q}) = \langle\phi_\alpha(-\mathbf{q})\phi_\beta(\mathbf{q})\rangle &= \int D\boldsymbol{\phi}(\mathbf{q})\ \phi_\alpha(-\mathbf{q})\phi_\beta(\mathbf{q})\ \exp\left\{-\frac{1}{2}\sum_{\mathbf{q}',\gamma}[G(\mathbf{q}')]^{-1}\phi_\gamma(-\mathbf{q}')\phi_\gamma(\mathbf{q}')\right\} \\ &= \delta_{\alpha\beta}G(\mathbf{q}).\end{aligned} \tag{3.12}$$

Now Eqs. (3.11) and (3.12) may be used to write the Green's function through the self-consistent equation

$$G(\mathbf{q}) = \frac{1}{G^0(\mathbf{q})^{-1} - \Sigma}\ , \tag{3.13}$$

where $\Sigma = -(u_0/6)\sum_{\mathbf{q}'} G(\mathbf{q}')$ is called the "self-energy".

We have seen that within the framework of the large-n theory, integrating over fluctuations has modified the bare propagator $G^0(\mathbf{q})$ into $G(\mathbf{q})$, and describes correlation functions in the interacting theory. The coefficient of the $\mathbf{\Phi}^2$ term in the Landau approximation to the free energy, Eq. (3.3) is now modified from $\frac{k_BTr_0}{2n} = \frac{k_BT}{2n}[G^{(0)}(\mathbf{q}=0)]^{-1}$ to $\frac{k_BT}{2n}[G(\mathbf{q}=0)]^{-1}$. Likewise, interactions will modify the coefficient of the $(\mathbf{\Phi}^2)^2$ term, and this is particularly significant since a change in sign of this coefficient can dramatically affect the character of the transition. To investigate this coefficient more thoroughly, it is best to represent the equations in a diagrammatic form.

3.3.2.1 In a Diagrammatic Representation

Since the two-point function $\Gamma^{(2)}_{\alpha\beta}(\mathbf{q}_1, \mathbf{q}_2)$ of Eq. (3.6) is diagonal in both momentum and flavour space it is sufficient to represent it as a solid line, along which momentum and flavour are conserved (Fig. 3.1(a)). The four-point function $\Gamma^{(4)}_{\alpha\beta\gamma\delta}(\mathbf{q}_1 \dots \mathbf{q}_4)$ of Eq. (3.7) conserves total momentum, but provides coupling between fields of different flavours. For this reason, the four-point function, coupling the $\phi_\alpha(\mathbf{q}_i)$ with amplitude $\Gamma^{(4)}_{\alpha\beta\gamma\delta}(\mathbf{q}_1 \dots \mathbf{q}_4)$, is represented as an interaction vertex: the interaction is a dashed line connecting two solid lines of different flavours (Fig. 3.1(b)). Noting the fully-symmetric tensor of Eq. (3.7), this interaction vertex is split equally into three contributions.

(a) Bare Propagator

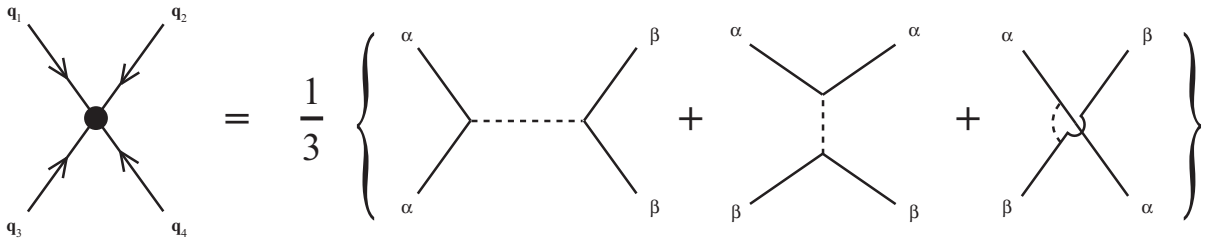

(b) Bare Interaction

Figure 3.1: Figure (a) represents the bare propagator. Figure (b) shows how the bare interaction couples different field flavours.

In order to see how this diagrammatic notation can simplify the calculation, we note some important points:

1. Each interaction term carries a factor of $1/n$.
2. If any diagram contains a *flavour loop*, the sum over field flavours provides a factor of n
3. In the limit of $n \to \infty$, diagrams that are higher order in $1/n$ do not contribute to the full propagator or full interaction.

These considerations allow us to write a Dyson equation that includes all the supplemental diagrams to the bare propagator

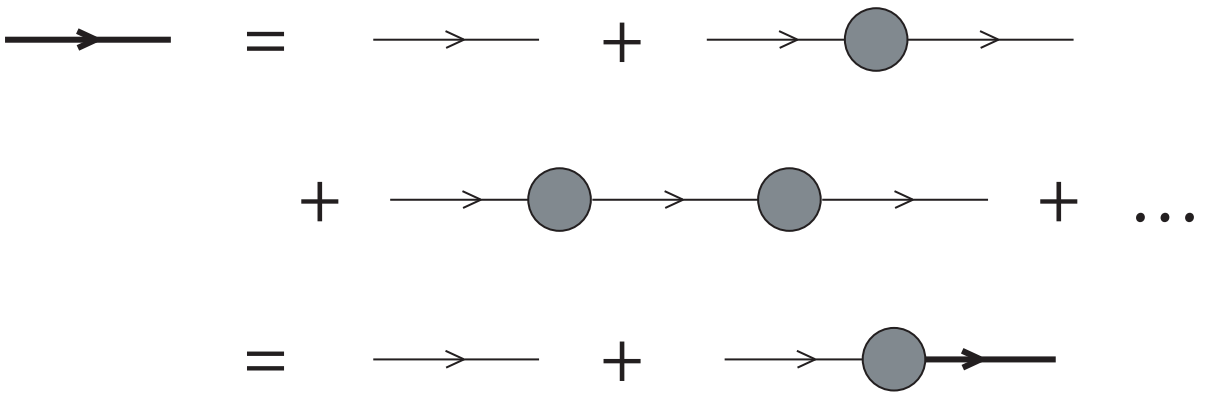

Figure 3.2: Dyson Equation. The grey circles denote the self-energy, Σ

where the self-energy Σ is equal to the sum of all one-particle-irreducible diagrams. This diagram, which can be written as the equation

$$G(\mathbf{q}) = G^0(\mathbf{q}) + G^0(\mathbf{q})\ \Sigma\ G(\mathbf{q}),$$

is equivalent to Eq. (3.13) and thus allows us to identify the self-energy as $\Sigma = -(u_0/6)\sum_{\mathbf{q}} G(\mathbf{q})$. This self-energy is represented diagrammatically

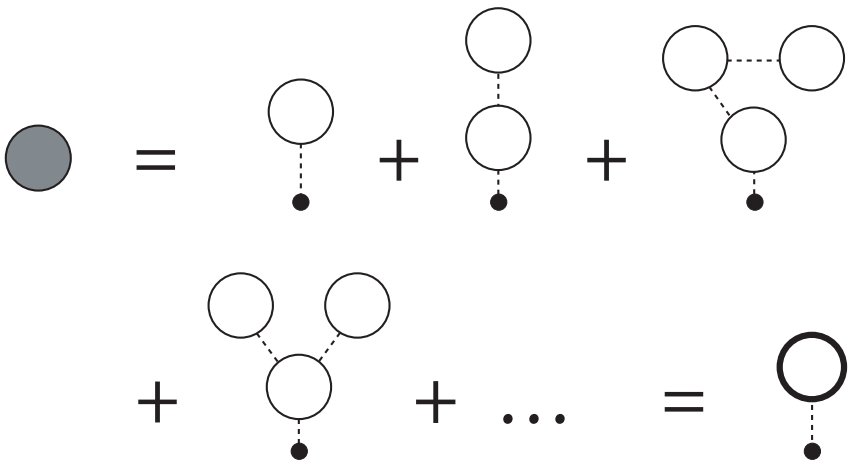

Figure 3.3: Self Energy Σ at $n = \infty$

We can use this diagrammatic representation to show how the full interaction vertex can be written in the form of a Bethe-Salpeter equation

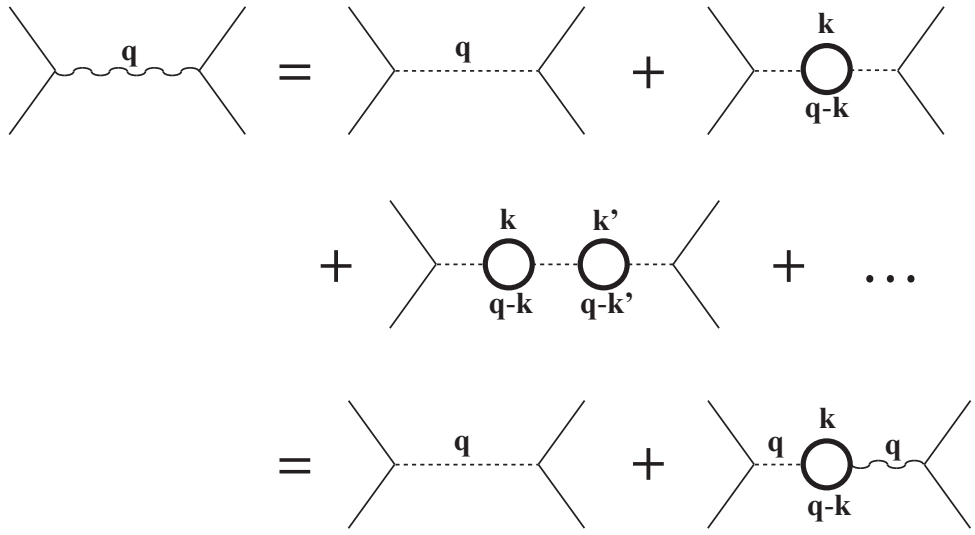

Figure 3.4: Bethe-Salpeter Equation

which is summed to provide the full interaction strength,

$$u(\mathbf{q}) = \frac{u_0}{1 + (u_0/6)I_2(\mathbf{q})}, \tag{3.14}$$

where

$$I_2(\mathbf{q}) = \int \frac{d^3\mathbf{k}}{(2\pi)^3} G(\mathbf{k})G(\mathbf{q}-\mathbf{k}).$$

The symmetrised version of the full interaction is written

$$g^{(4)}_{\alpha\beta\gamma\delta}(\mathbf{q}_1 \ldots \mathbf{q}_4) = \frac{1}{4!\,3n}[\delta_{\alpha\beta}\delta_{\gamma\delta}u(\mathbf{q}_1+\mathbf{q}_2) + \delta_{\alpha\gamma}\delta_{\beta\delta}u(\mathbf{q}_1+\mathbf{q}_3) + \delta_{\alpha\delta}\delta_{\beta\gamma}u(\mathbf{q}_1+\mathbf{q}_4)].$$

In order to see how replacing the bare interaction by the full interaction affects the Landau free energy of Eq. (3.3), we write $\boldsymbol{\phi}(\mathbf{r}) = \boldsymbol{\Phi} + \boldsymbol{\delta\phi}(\mathbf{r})$ and integrate over the fluctuations $\boldsymbol{\delta\phi}(\mathbf{r})$. Setting the external momenta $\mathbf{q}_i$ equal to zero picks out the spontaneous component of the field $\boldsymbol{\Phi}$. At zero momentum, $g^{(4)}_{\alpha\beta\gamma\delta}(\mathbf{q}_i = 0) = \frac{1}{n}S_{\alpha\beta\gamma\delta}\frac{u(\mathbf{q}=0)}{4!}$. Sufficiently close to the transition, the function $u_0 D_2(\mathbf{q}=0) \gg 1$, so that we approximate Equation (3.14) as $u(\mathbf{q}=0) \approx 6/I_2(\mathbf{q}=0)$. The Landau free energy of Eq. (3.3) is now replaced by

$$U(\boldsymbol{\Phi}) = \frac{1}{2}G^{-1}(\mathbf{q}=0)\ \boldsymbol{\Phi}^2 + \frac{1}{4n}I_2(\mathbf{q}=0)^{-1}\ (\boldsymbol{\Phi}^2)^2. \tag{3.15}$$

It is clear that the behaviour of $G(\mathbf{q})$ and $I_2(\mathbf{q})$ should be of great interest in studying phase

transitions in the limit of $n \to \infty$.

At this stage we pause to recap some key points. For the non-interacting, Gaussian theory of Section 3.2, we were able to construct (without approximation) a free energy that depended only on the form of the propagator $G^0(\mathbf{q})$, and the dimensionality of the system. Therefore, knowing the propagator can provide all of the thermodynamic functions for a given model in statistical mechanics. When interactions were included, we showed in Section 3.3.2 that, under the limiting condition of $n \to \infty$, the bare propagator $G^0(\mathbf{q})$ is renormalised to the full propagator $G(\mathbf{q})$. If the self-energy Σ turns out to be a finite quantity, this renormalisation corresponds to making the replacement $r_0 \to r$ in the propagator. Whether or not Σ is finite depends on the functional form of $G^0(\mathbf{q})$, and also on the dimensionality of the system, since the self-energy is got from integrating over $\mathbf{q}$.

In the next section we take the example of the short-range ferromagnet which we show has propagator $G^{(\mathrm{F})}(\mathbf{q}) = (q^2 + r)^{-1}$, where the superscript (F) refers to a ferromagnet. In this case, $r = r(t)$ where t is the reduced temperature. Clearly therefore, we should like to know the functional form of $r(t)$ in the large-n limit before we can reconstruct the critical behaviour. We then discuss how this is used to recover all of the thermodynamic functions around the phase transition.

3.4 Thermodynamics of a Ferromagnet in the Limit of $n \to \infty$

Throughout this chapter we have focussed on the effective Hamiltonian of Eq. (3.2). There the parameter u_0 in $S_4[\boldsymbol{\phi}]$ provides an energy cost to any configurations not satisfying $(\boldsymbol{\phi}(\mathbf{r}) \cdot \boldsymbol{\phi}(\mathbf{r}))^2 = 0$. This is referred to as a soft constraint, since configurations not satisfying the constraint simply cost a finite amount of energy; they are not disallowed.

For a system of n-component classical spins $\mathbf{S}_i$, where spins have length $\sqrt{n}$, a constraint is on allowed configurations is that they must satisfy $|\mathbf{S}_i|^2 - n = 0$. This is a called hard constraint, and configurations not satisfying it are disallowed[12, 64]. In this section, we enforce this length constraint with a delta function, which can be rewritten in integral form:

$$\delta(\mathbf{S}_i^2 - n) = \int D\lambda_i e^{-\beta J \sum_i \lambda_i (\mathbf{S}_i^2 - n)} \tag{3.16}$$

where the integration contour runs from $-i\infty$ to $+i\infty$, and the factor βJ is included for later convenience. In the limit of n large, we will see that the spin-length constraint can be imposed by taking a saddle-point approximation to λ_i.

Returning to the problem, we limit our attention to the high-temperature side of the ordering transtion and do not consider an applied field. We take advantage of translational invariance and write the Hamiltonian of the ferromagnet, (described by Eq. (1.2), but replacing $J \to -J < 0$), in Fourier space

$$H = -J \sum_{\mathbf{q}} \omega(\mathbf{q})\ \mathbf{S}_{\mathbf{q}} \cdot \mathbf{S}_{-\mathbf{q}},$$

where $\omega(\mathbf{q}) \propto q^2$ for a ferromagnet at small q. Using the integral representation of Eq. (3.16), the partition function

$$\mathcal{Z} = \int \mathcal{D}\mathbf{S}_i\ e^{-\beta H}\ \delta(\mathbf{S}_i^2 - n), \tag{3.17}$$

becomes

$$\mathcal{Z} = \int \mathcal{D}\lambda_{\mathbf{q}} e^{\beta J n V \lambda_{\mathbf{q}}} \int \mathcal{D}\mathbf{S}_{\mathbf{q}}\ e^{-\beta J \sum_{\mathbf{q}} (q^2 + \lambda_{\mathbf{q}}) \mathbf{S}_{\mathbf{q}} \cdot \mathbf{S}_{-\mathbf{q}}}. \tag{3.18}$$

The integrals over the $\mathbf{S}_{\mathbf{q}}$ may now be evaluated. There is one integral for each value of wavevector $\mathbf{q}$, and one for each spin component. We obtain

$$\mathcal{Z} = \int \mathcal{D}\lambda e^{\beta J n V \lambda} \left(\frac{\pi}{\beta J \prod_{\mathbf{q}} (q^2 + \lambda)} \right)^{n/2},$$

and (the singular part of) the integrand is exponentiated to give

$$\mathcal{Z}_{\rm sing} = \int \mathcal{D}\lambda_{\mathbf{q}} \exp -n \underbrace{\{-\beta J V \lambda + \frac{1}{2} \sum_{\mathbf{q}} \ln(q^2 + \lambda_{\mathbf{q}})\}}_{K(\lambda)}. \tag{3.19}$$

For n large we make a saddle-point approximation to the $\lambda_{\mathbf{q}}$-integrals: we first assume a uniform value of λ_i, so that only the $q = 0$ component contributes. For this ferromagnet, we now look for a saddle-point value $\lambda = \bar{\lambda}^{(\rm F)}$ that minimises $K(\lambda)$, providing the saddle-point condition

$$\beta J = \frac{1}{2} \int \frac{d^3\mathbf{q}}{(2\pi)^3} (q^2 + \bar{\lambda}^{(\rm F)})^{-1}. \tag{3.20}$$

At this point, we can make contact with the previous analysis for the soft constraint. This

equation is equivalent to the self-consistent equation (3.13) on making the replacements

$$\begin{aligned}\frac{1}{q^2+\bar{\lambda}^{(\mathrm{F})}} &\rightarrow G^{(\mathrm{F})}(\mathbf{q}) \\ \bar{\lambda}^{(\mathrm{F})} &\rightarrow r_0 - \Sigma^{(\mathrm{F})} \\ \beta J &\rightarrow -\frac{3}{u_0}\Sigma^{(\mathrm{F})}.\end{aligned}$$

Imposing the saddle-point value of $\bar{\lambda}^{(\mathrm{F})}$, the large-$n$ approximation to the free-energy density is

$$\begin{aligned}f_{\mathrm{sing}}^{(\mathrm{F})} = -\frac{1}{nV}k_BT\ln\mathcal{Z} &= \frac{k_BT}{V}K(\bar{\lambda}^{(\mathrm{F})}) + \mathcal{O}(n^{-1}\ln n) \\ &\overset{n\to\infty}{=} -J\bar{\lambda}^{(\mathrm{F})} + \frac{k_BT}{2}\int\frac{d^3\mathbf{q}}{(2\pi)^3}\ln(q^2+\bar{\lambda}^{(\mathrm{F})}).\end{aligned} \tag{3.21}$$

Next, we solve Eq. (3.20) for $\bar{\lambda}^{(\mathrm{F})}$ at temperatures $T \gtrsim T_c$. At the transition, where β takes its largest value of β_c, $\bar{\lambda}$ vanishes. Just above the transition $\bar{\lambda}^{(\mathrm{F})}$ is small, and we subtract Eq. (3.20) above criticality from its form at the critical point to give

$$J(\beta_c-\beta) = \frac{1}{2}\int\frac{d^3\mathbf{q}}{(2\pi)^3}\left\{\frac{1}{q^2} - \frac{1}{q^2+\bar{\lambda}^{(\mathrm{F})}}\right\}$$

which, in terms of $t=(T-T_c)/T_c$, reads

$$\frac{J}{k_BT_c}\,t = \frac{1}{2}\int\frac{d^3\mathbf{q}}{(2\pi)^3}\frac{\bar{\lambda}^{(\mathrm{F})}}{q^2(q^2+\bar{\lambda}^{(\mathrm{F})})}.$$

Rescaling the integral using $\mathbf{q} = (\bar{\lambda}^{(\mathrm{F})})^{1/2}\mathbf{Q}$ gives

$$\frac{J}{k_BT_c}t = (\bar{\lambda}^{(\mathrm{F})})^{1/2}\int\frac{d^3\mathbf{Q}}{(2\pi)^3}\frac{1}{Q^2(Q^2+1)}$$

where the integral is convergent at both limits, and so we obtain the result $\bar{\lambda}^{(\mathrm{F})} \propto t^2$ for small t. Thus we identify, in the limit of $n\to\infty$, the full Green's function for the short-range ferromagnet:

$$G^{(\mathrm{F})}(\mathbf{q}) = (q^2+ct^2), \tag{3.22}$$

where c is some positive constant.

3.4.1 Critical Exponents at the Transtion

At this stage most of the hard work is done, and it is straightforward to calculate the physical consequences through extracting the critical exponents[1, 69, 42]. At the transition, $f_{\rm sing}$ is stationary, as may be seen from evaluating $\partial f_{\rm sing}/\partial\bar{\lambda}$ in Eq. (3.21) and noting the saddle-point condition of Eq. (3.20). Here we will only evaluate the heat capacity and the susceptibility. Central to these is the use of the functional form of the saddle-point value $\bar{\lambda}^{(\rm F)}$ close to the transition, $\bar{\lambda}^{(\rm F)} \propto t^2$

3.4.1.1 Heat capacity

The singular contribution to the heat capacity, $C^{(\rm F)}_{\rm sing} \sim \partial^2 f^{(\rm F)}_{\rm sing}/\partial t^2$. We find

$$\begin{aligned} C^{(\rm F)}_{\rm sing} &\sim \frac{\partial^2 f^{(\rm F)}_{\rm sing}}{\partial\bar{\lambda}^2}\left(\frac{\partial\bar{\lambda}}{\partial t}\right)^2 \\ &\sim \underbrace{\int \frac{d^3\mathbf{q}}{(2\pi)^3}\frac{1}{(q^2+\bar{\lambda})^2}}_{D_2^{(\rm F)}(\bar{\lambda},\Lambda)} \times t^2 \\ &\sim t^2 D_2^{(\rm F)}(\bar{\lambda}^{(\rm F)},\Lambda) \sim t^2\bar{\lambda}^{-1/2} \sim t \end{aligned}$$

where in the second line we have used Eq. (3.21), and in the third line the asymptotics of $D_2^{(\rm F)}(\bar{\lambda}^{(\rm F)},\Lambda)$ from Appendix A.1. This result generates the first exponent, $\alpha = -1$.

3.4.1.2 Susceptibility

The susceptibility is obtained from

$$k_B T\chi \sim \sum_i \langle \mathbf{S}_i \cdot \mathbf{S}_0\rangle \sim G^{(\rm F)}(\mathbf{q}=0) \sim \frac{1}{\bar{\lambda}^{(\rm F)}} \sim t^{-2},$$

providing the second exponent $\gamma = 2$.

3.5 Summary

In this chapter we have discussed the need for approximation schemes to solve complicated problems in different limiting regimes. We concentrated on the large-n approximation, showing that integrating over fluctuations renormalises quantities such as the propagator at $n = \infty$.

We illustrated this approximation by studying the thermodynamics of a ferromagnet with n-component spins, and have seen that physical quantities such as the critical exponents are different from their values in, for example, a mean-field approximation.

Chapter 4

Ordering Transitions in Highly-Frustrated Antiferromagnets

We saw in Chapter 2 that, for frustrated spin systems built out of corner-sharing units, ground states may be described geometrically through the constraint – Eq. (2.1) – that the total spin of each simplex must vanish[51]. More specifically, we discussed the pyrochlore lattice and corner-sharing octahedral lattice, and showed that, as $J/T \to \infty$, these lattices support a Coulomb phase, with algebraic decay of correlations. In this chapter we discuss how to induce an ordering transition out of the Coulomb phase, using as an example the octahedral lattice. Ordering will be induced by lifting the ground-state degeneracy through weak additional interactions.

Algebraic decay of correlation functions in real systems has been established experimentally in neutron scattering measurements[22]. Quasi-long range ordering in the spin ice compound, $Ho_2Ti_2O_7$ is observed through sharp features in the neutron scattering profile called pinch points. These singularities are weaker than the sharp Bragg peaks of Néel ordering, but distinguish the phase from a conventional paramagnet with short-range correlations.

In addition to frustrated magnets displaying quasi-long range order, it was recently shown that a pressure-induced phase transition could be achieved in the material $Tb_2Ti_2O_7$[45, 46]. In these experiments, sharp features were observed in the neutron scattering profile at 2.1 K, indicative of Néel ordering, whereas at ambient pressure the profile was diffuse and correlations short range. A temperature-induced transition has also been observed in the spinel $ZnCr_2O_4$, where ordering is accompanied by spontaneous strain[38]. In principle, the results of the fol-

lowing four chapters should be able to be probed experimentally on single crystals of frustrated magnets under uniaxial stress. $Tb_2Ti_2O_7$ is a possible candidate; unfortunately this is a material that is at present poorly understood[19].

Returning to the theoretical work of this chapter, here present a full, detailed analysis of an ordering transition out of a Coulomb phase in the large-n limit. This involves a solution of the saddle-point equation, the equivalent to Eq. (3.20) of Chapter 3. We study the critical behaviour by performing the same analysis as in Section 3.4, but we also study the spontaneous magnetisation below T_c, and the response of the spins to an applied magnetic field. Finally we look at spin-spin correlation functions both above, at and below the transition temperature.

4.1 Spectrum of the Nearest-Neighbour Interaction Matrix J_{ij}

We begin by revisiting the model introduced in Section 2.2.1, in which all all non-zero interaction terms have strength J. In Section 2.2.2 we showed, by mapping the model onto a system of fields, that in the limit of $J/T \to \infty$ these fields become solenoidal and thus that the model exhibits a stable Coulomb phase.

We recall the Hamiltonian of Equation (2.2), where the interaction matrix J_{ij} identifies the interactions of Figure 2.5. After Fourier transforming this Hamiltonian, the interaction matrix of Eq. (2.10) is diagonalised by rotation in the space of unit cell sites. The spectrum of eigenvalues is shown in Fig. 4.1. Two branches of the eigenvalue spectrum are identically zero throughout the Brillouin zone: $J^{(1)}(\mathbf{q}) = J^{(2)}(\mathbf{q}) = 0$ are the non-dispersive (flat) low-lying branches that are a hallmark of macroscopic ground-state dengeracy. The third branch is dispersive with an energy scale set by J. It has the dispersion relation

$$J^{(3)}(\mathbf{q}) = 2J\ (s_x^2 + s_y^2 + s_z^2).$$

with the (normalised) eigenvector,

$$|e^{(3)}(\mathbf{q})\rangle = \frac{1}{\sqrt{s_x^2 + s_y^2 + s_z^2}}\Big(s_x,\ s_y,\ s_z\Big). \tag{4.1}$$

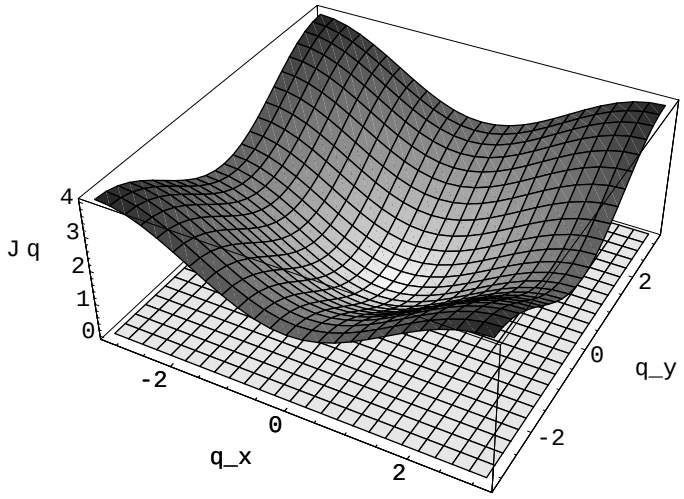

Figure 4.1: A Fourier space plot of the branches of the energy spectrum of $\mathcal{H}_J$ along the slice $q_z = 0$. The two non-dispersive branches are identically zero throughout the Brillouin zone, and the third, dispersive branch has dispersion $J^{(3)}(\mathbf{q})$. Lighter shading indicates regions of states most accessible through thermal fluctuations.

4.1.1 Flat band Eigenvalues of J_{ij} and the Projection Matrix

The flatband subspace is spanned by eigenvectors $|e^{(1)}(\mathbf{q})\rangle$ and $|e^{(2)}(\mathbf{q})\rangle$. We define the matrix $P(\mathbf{q})$

$$\begin{aligned} P(\mathbf{q}) &= \sum_{n=1}^{2} |e^{(n)}(\mathbf{q})\rangle\langle e^{(n)}(\mathbf{q})| \qquad (4.2) \\ &= \frac{1}{s_x^2+s_y^2+s_z^2} \begin{pmatrix} s_y^2+s_z^2 & -s_x s_y & -s_x s_z \\ -s_x s_y & s_x^2+s_z^2 & -s_y s_z \\ -s_x s_z & -s_y s_z & s_x^2+x_y^2 \end{pmatrix}, \end{aligned}$$

where $P(\mathbf{q})$ has the properties

$$P(\mathbf{q})|e^{(n)}(\mathbf{q})\rangle = |e^{(n)}(\mathbf{q})\rangle, \quad \text{for } n = 1, 2; \qquad P(\mathbf{q})|e^{(3)}(\mathbf{q})\rangle = 0.$$

That is, the matrix $P(\mathbf{q})$ projects a vector $|v\rangle$ onto the minimum-eigenvalue subspace of the interaction matrix J_{ij}.

For small q, $P(\mathbf{q})$ reduces to

$$P(\mathbf{q}) = \begin{pmatrix} 1 - \frac{q_x^2}{q^2} & -\frac{q_x q_y}{q^2} & -\frac{q_x q_z}{q^2} \\ -\frac{q_x q_y}{q^2} & 1 - \frac{q_y^2}{q^2} & -\frac{q_y q_z}{q^2} \\ -\frac{q_x q_z}{q^2} & -\frac{q_y q_z}{q^2} & 1 - \frac{q_z^2}{q^2} \end{pmatrix}. \tag{4.3}$$

Fourier transforming this projector into real space, we may write

$$[P(\mathbf{r})]_{ij} = \left(\frac{\partial^2}{\partial r_i \partial r_j} - \delta_{ij} \nabla^2 \right) \int \frac{d^3\mathbf{q}}{(2\pi)^3} \frac{e^{i\mathbf{q}\cdot\mathbf{r}}}{q^2}.$$

The integral evaluates to $(4\pi r)^{-1}$, so the elements of the projector are, in the long-distance limit

$$[P(\mathbf{r})]_{ij} = \frac{1}{4\pi} \frac{3r_i r_j - r^2 \delta_{ij}}{r^5}.$$

Note that this projector has the spatial dependence of a dipole-dipole interaction[71, 32]. In the regime $J/T \to \infty$, it will useful to use this projector to study the thermodynamics of the system using only states from the flat bands of J_{ij}. The projector $P(\mathbf{q})$ provides a means to achieve this.

4.2 Further Neighbour Interactions

To induce ordering of spins on the octahedral lattice of Figure 2.5, a suitable choice of perturbation is the modification of the strengths of certain interactions. Specifically, the interactions represented by dashed lines in Figure 4.2 are reduced in magnitude: in essence we include weak, additional ferromagnetic interactions at those links. We note that, in principle, a perturbation of this form can be achieved by applying uniaxial compression to the lattice in the [111]-direction to the lattice.

At zero temperature, spins align antiferromagnetically along stronger bonds, while the requirement of Eq (2.1) that the spin sum vanishes in each simplex forces ferromagnetic alignment across the weaker bonds. The perturbation corresponds to adding an extra term to the Hamil-

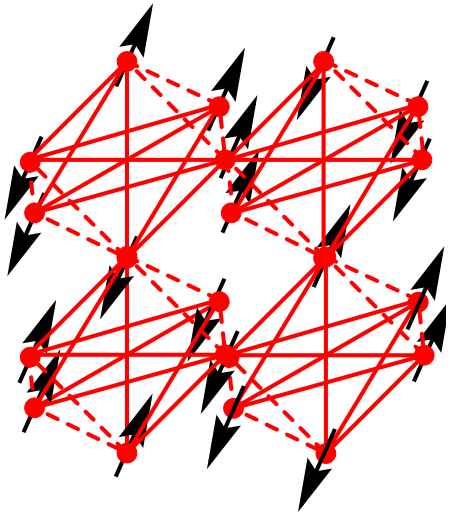

Figure 4.2: Here the solid lines have strength J and the dashed lines are weaker, having strength $J-\Delta$ (we take $\Delta \geq 0$). These weaker bonds form planes perpendicular to the [111]-direction. In the Néel phase, spins align antiferromagnetically on the stronger bonds, but frustration forces ferromagnetic alignment in each the planes of weaker bonds (for $\Delta \neq 0$). The collinear ordering is staggered at wavevector $\mathbf{k}_\pi$.

tonian:

$$\mathcal{H} = \mathcal{H}_J + \mathcal{H}_\Delta = \mathcal{H}_J + \sum_{\langle ij \rangle} \Delta_{ij}\, \mathbf{S}_i \cdot \mathbf{S}_j \tag{4.4}$$

where the nonzero elements of Δ_{ij} are $-\Delta < 0$, and $\mathcal{H}_J$ remains as defined in Eq. (2.2).

Written in Fourier space using Eq. (2.3), this perturbation term is

$$\mathcal{H}_\Delta = \sum_{\mathbf{q}} \sum_{lm}^{3} \Delta_{lm}(\mathbf{q})\, \mathbf{S}_l(\mathbf{q}) \cdot \mathbf{S}_m(-\mathbf{q}), \tag{4.5}$$

where

$$\Delta(\mathbf{q}) = -\Delta \begin{pmatrix} 0 & c_{xy} & c_{xz} \\ c_{xy} & 0 & c_{yz} \\ c_{xz} & c_{yz} & 0 \end{pmatrix}, \tag{4.6}$$

and we have introduced the notation $c_{mn} = \cos\big((q_m - q_n)/2\big)$.

The full Hamiltonian $\mathcal{H}$ contains an energy minimum $\mathcal{E}_0$ that corresponds to a unique (up to global spin rotations) Néel ordered state; this two-sublattice state is also within the ground-state manifold of $\mathcal{H}_J$, and is pictured in Figure 4.2. From Section 2.2.2, we remember that the limit of $J/T \to \infty$ is essential to ensure that a disordered phase is Coulombic. Hence, for

$J \gg \Delta > 0$, considering the effects of fluctuations in selecting either an ordered or disordered phase, we expect the system to undergo a transition from a Coulomb phase into an ordered Néel state at a temperature of $T_c \sim \mathcal{O}(\Delta)$. It is therefore the limit of $J/\Delta \to \infty$ which is of particular interest when studying this transition.

4.2.1 Projected Interaction Matrix $\widetilde{\Delta}_{ij}$

As the interaction strength $J \to \infty$, spin configurations are exclusively within the ground-state manifold of the undistorted lattice, and therefore only these configurations contribute to the thermodynamics. We thus study the thermodynamics of the system within this restricted sub-manifold of ground-state spin configurations. We thus define an operator $\mathcal{P}_J$ that leaves invarient any spin configuration in the ground-state manifold of $\mathcal{H}_J$.

Spin configurations from the ground-state manifold are, by definition, lowest energy configurations. Thermodynamic properties must therefore be determined only from the smallest eigenvalues of the interaction matrix J_{ij}, the subspace of flat bands. Therefore, in order to study the thermodynamics of the transition, we project the interaction matrix Δ_{ij} onto the flat-band subspace of J_{ij}. We define the projected interaction matrix $\widetilde{\Delta}_{ij}$ that, when Fourier transformed, is comprised of the elements

$$\widetilde{\Delta}^{lm}(\mathbf{q}) = \langle e^{(l)}(\mathbf{q})|\ P(\mathbf{q})\ \Delta(\mathbf{q})\ P(\mathbf{q})\ |e^{(m)}(\mathbf{q})\rangle. \tag{4.7}$$

This is a 3×3 matrix at each $\mathbf{q}$-wavevector: the 2×2 upper-left sub-matrix is within the flat band subspace. This sub-matrix may be diagonalised to generate two branches. These are the eigenvalues of the projected interaction matrix. Explicitly, the energy eigenvalues are

$$\begin{aligned} \mathcal{E}^{(1)}(\mathbf{q}) &= \Delta\Big(-2+\gamma(\mathbf{q})\Big) \\ \mathcal{E}^{(2)}(\mathbf{q}) &= \Delta, \end{aligned} \tag{4.8}$$

where $\gamma(\mathbf{q})$ is a positive function of $\mathbf{q}$, written

$$\begin{aligned} \gamma(\mathbf{q}) &= \frac{1}{s_x^2+s_y^2+s_z^2}\Big\{(s_x+s_y+s_z)^2 \\ &-2\Big(\ s_x s_y\ (1-c_{xy}) + s_x s_z(1-c_{xz}) + s_y s_z(1-c_{yz})\Big)\Big\}. \end{aligned} \tag{4.9}$$

The spectrum of $\widetilde{\Delta}_{ij}$ attains its minimum value of $\mathcal{E}_0 = -2\Delta$ in the $\mathcal{E}^{(1)}(\mathbf{q})$ branch at the point where $\gamma(\mathbf{q}) \to 0$. Since the function $\gamma(\mathbf{q})$ is non-analytic at $q = 0$, its value there is determined by the direction of approach. The minimum in $\gamma(\mathbf{q})$ is contained within the plane $\mathbf{q} \cdot \hat{\mathbf{n}} = 0$, where $\hat{\mathbf{n}}$ is a unit vector in the [111]-direction. Writing $\mathbf{q} \cdot \hat{\mathbf{n}} = q_\parallel$, in the vicinity of $q = 0$, we expand $\gamma(\mathbf{q})$ as

$$\gamma(\mathbf{q}) = 3\frac{q_\parallel^2}{q^2} + q^2 + \mathcal{O}(q_\parallel q_\perp, q_\parallel^2, \frac{q_\parallel^4}{q_\perp^4}, q_\perp^4, \ldots) \tag{4.10}$$

where $q^2 = q_\parallel^2 + q_\perp^2$.

At this point we pause to note that $\gamma(\mathbf{q})$ is identical to the dispersion found in ferromagnets and ferroelectrics with a long-range dipole-dipole interaction[35, 37, 3].

In essence, we have shown that this magnet with short range interactions – at values of J/T large enough that the physics is determined solely by its flat bands – has thermodynamics identical to a system interacting though long-range, uniaxial dipolar interactions. In addition, given that we have induced an ordering transtion through the weak, additional short-range interaction, we may proceed to see how the critical behaviour is influenced by these effective long-range interactions.

In a similar observation, a recent paper by Isakov, Moessner and Sondhi[32] introduces a concept that they term "projective equivalence", whereby there exist pairs of interaction matrices that share the same low-lying flat bands and eigenvectors, and whose physics is thus equivalent under projection onto these flat bands. They consider a spin-ice system, where strong easy axis anisotropy leads to short-range Ising-type exchange terms $\mathcal{J}$ and, because of the large magnetic moments, additional long-range dipolar interactions $\mathcal{D}$. They then construct a model interaction $\mathcal{P}$ that, crucially, possesses the same low-energy manifold and eigenvectors as $\mathcal{J}$: they choose this to take the form of a projection operator. In addition to having identical ground states to $\mathcal{J}$, and thus recovering the low-temperature entropy of $\mathcal{J}$ (identical to water ice), the model interaction $\mathcal{P}$ has the same leading-order long-distance form as the dipolar interaction $\mathcal{D}$, but with corrections at $\mathcal{O}(r^{-5})$.

Returning to our spin model, there remains, however, an issue for its analytical treatment: since ground-state spin configurations $|0\rangle = \sum_{\mathbf{q}} \sum_{\mu=1,2} a_\mu(\mathbf{q}) |e^{(\mu)}(\mathbf{q})\rangle$ are written as a linear

combination of eigenvectors from the flatbands, where the coefficients $a_\mu(\mathbf{q})$ of these eigenvectors must be chosen to respect the constraint on spin length, under projection this coupling between coeffiecents generates a very complicated set of equations. This issue can only be resolved in the limit of a large number of spin components since, as $n \to \infty$, the constraint can be relaxed and applied to each spin component on the average, and therefore enforced using a single Lagrange multiplier. In order to investigate the thermodynamic properties of the spin-system, we now turn to the solvable limit of $n \to \infty$.

4.3 Large-n Limit of the Transition

The large-n calculation now proceeds in the same way as in Section 3.4, generating equations equivalent to the saddle-point equation and the free-energy expression of Equation (3.20) and (3.21), which described a conventional ferromagnet at $n \to \infty$.

In analogy with Equation (3.20), the saddle-point equation for the GFAFM is written

$$3\beta\Delta = \frac{1}{2}\sum_{n}^{3}\int \frac{d^3\mathbf{q}}{(2\pi)^3}\left(\frac{1}{\Delta}\mathcal{E}^{(n)}(\mathbf{q}) + \bar{\lambda}^{(GFAFM)}\right)^{-1}, \tag{4.11}$$

where the factor of 3 on the left-hand side of this equation is due to the 3 sites in the unit cell. In the remainder of this section we describe the solution to this equation, looking at the dependence of the parameter $\bar{\lambda}^{(GFAFM)}$ on temperature, including both high- and low-temperature phases.

The projected interaction matrix $\tilde{\Delta}$ of Eq. (4.7) contains three branches $\mathcal{E}^{(n)}$ in its energy spectrum. Branch $\mathcal{E}^{(3)} = \mathcal{O}(J)$, and its contribution to the sum of Eq. (4.11) vanishes as $J \to \infty$. Using the explict form of the other two branches from Eq. (4.8), the energy minimum $\mathcal{E}_0$ occurs in the branch $\mathcal{E}^{(1)}$. We shift $\bar{\lambda}^{(GFAFM)}$ and write in terms of a new variable s, defined by $\bar{\lambda}^{(GFAFM)} + \mathcal{E}_0/\Delta = s$, where $s = s(t)$ is non-negative, and depends only on temperature. Inserting the $\mathbf{q}$-dependence of the eigenvalues, we obtain

$$3\beta\Delta = \frac{1}{2}(3+s)^{-1} + \frac{1}{2}\int \frac{d^3\mathbf{q}}{(2\pi)^3}(\gamma(\mathbf{q})+s)^{-1}. \tag{4.12}$$

Far above the transition, when $s \gg 1$, Equation (4.12) is solved by taking

$$s \overset{\beta\Delta\ll 1}{=} \frac{1}{6\beta\Delta}. \tag{4.13}$$

Close to the transition ($s \to 0$), the first term on the right-hand side of Eq. (4.12) may be neglected compared to the second. We have

$$3\beta\Delta = \frac{1}{2}\int \frac{d^3\mathbf{q}}{(2\pi)^3} \underbrace{\frac{1}{\gamma(\mathbf{q})+s}}_{G^{(GFAFM)}(\mathbf{q})}, \tag{4.14}$$

where we identify the integrand of Eq. (4.14) as the full Green's function for the frustrated magnet.

For s small, we expand Eq. (4.12) in powers of s: making the replacement $\beta \approx \beta_c(1-t)$ on the left-hand side we find

$$6\beta_c\Delta\big(1-t+\mathcal{O}(t^2)\big) = \underbrace{\left\{\int \frac{d^3\mathbf{q}}{(2\pi)^3}\frac{1}{\gamma(\mathbf{q})}\right\}}_{D_1(s=0,\Lambda)} - \underbrace{\left\{\int \frac{d^3\mathbf{q}}{(2\pi)^3}\left(\frac{1}{\gamma(\mathbf{q})}-\frac{1}{\gamma(\mathbf{q})+s}\right)\right\}}_{s\ D_2(s,\Lambda)}. \tag{4.15}$$

The functions $D_1(s,\Lambda)$ and $D_2(s,\Lambda)$ are discussed in Appendix A.2. In the remainder of this section we will quote the results of that appendix. At the transition $s = 0$ and so the critical temperature is evaluated by comparing leading terms in Eq. (4.15):

$$T_c = \frac{6\Delta}{k_B D_1(s=0,\Lambda)}.$$

Comparing the next-highest order terms we find

$$6\beta_c\Delta t = \int \frac{d^3\mathbf{q}}{(2\pi)^3}\frac{s}{\gamma(\mathbf{q})(\gamma(\mathbf{q})+s)} = sD_2(s,\Lambda).$$

Taking the small-s form of $D_2(s,\Lambda)$ from Appendix A.2.1, we obtain the result

$$t \sim \frac{1}{6\beta_c\Delta} s \ln 1/s. \tag{4.16}$$

Inverting Eq. (4.16) for small s and t gives the important relationship

$$s \sim t\left(\ln\frac{1}{t}\right)^{-1}. \tag{4.17}$$

At this stage we go further and also investigate the solution to Equation (4.12) in the low-

temperature phase. This symmetry-broken phase is characterised by a non-zero expectation of spin along some direction. Specifying this longitudinal direction $\hat{\mathbf{e}}_1$ as the 1-axis in spin space, we separate spins into a single longitudinal component and $n-1$ transverse components. We subtract off any spontaneous magnetisation m_i in the longitudinal direction by writing

$$\mathbf{S}_i = \mathbf{S}'_i + \, m_i \, n^{1/2} \, \hat{\mathbf{e}}_1, \tag{4.18}$$

so that $\mathbf{S}'_i = (\sigma_i, \vec{\pi}_i)$ represents the fluctuating part of the magnetisation, and $\langle \mathbf{S}'_i \rangle = 0$. The factor $n^{1/2}$ is included to make m_i of order unity.

The exponent in the partition function now picks up terms linear in σ_i, and the partition function becomes:

$$\mathcal{Z} = \left(\frac{\beta}{2\pi}\right)^{3N} \prod_i \int d\mathbf{S}'_i d\lambda_i \; e^{-n\beta \mathcal{W}'[\mathbf{S}'_i, \lambda_i]},$$

where

$$\begin{aligned} \mathcal{W}'[\mathbf{S}'_i, \lambda_i] = \; & - \; \sum_i \lambda_i + \sum_{ij} \left(\tilde{\Delta}_{ij} + \lambda_i \delta_{ij}\right) \Big(\frac{1}{n} \vec{\pi}_i \cdot \vec{\pi}_j + m_i m_j \\ & + \; n^{-1/2} (m_i \sigma_j + m_j \sigma_i) + n^{-1} \sigma_i \sigma_j \Big) \end{aligned} \tag{4.19}$$

For the ensemble average $\langle \sigma_i \rangle$ to vanish, the coefficient of terms linear in σ_i from $\mathcal{W}'$ must also vanish. This generates the condition

$$0 = \sum_i (\tilde{\Delta}_{ij} + \lambda_i \delta_{ij}) m_i. \tag{4.20}$$

Looking for a uniform saddle-point $\lambda_i = \bar{\lambda}$, in Fourier space Eq. (4.20) is transformed into the condition

$$0 = m \sum_{lm} (\tilde{\Delta}^{lm}(\mathbf{q} = 0) + \bar{\lambda} \delta^{lm}), \tag{4.21}$$

indicating either that $m = 0$ (as is the case in the high-T phase) or that $m \neq 0$ (below the transition), in which case $\bar{\lambda}$ must satisfy the extra condition

$$\bar{\lambda} = -\frac{1}{3} \sum_{lm} \tilde{\Delta}^{lm}(\mathbf{q} = 0).$$

The evaluation of this sum is at first unclear due to the non-analyticity in the spectrum of $\tilde{\Delta}^{lm}$ at $q = 0$. For this reason, we should take the limit of $T/J \to 0$ after having set $\mathbf{q} = 0$. The unprojected quantity $\sum_{lm} \Delta^{lm}(\mathbf{q} = 0)$ may be read directly off Eq. (4.6), giving

$$\bar{\lambda} = -\frac{1}{3}(-6\Delta) = 2\Delta = -\mathcal{E}_0 \quad \text{for} \quad m \neq 0. \tag{4.22}$$

Taken together, Eqs. (4.21) and (4.22) completely determine the magnetization m and the saddle-point value $\bar{\lambda}$ in both phases of the system.

Putting together the results of Eqs. (4.13), (4.17) and (4.22), we have

$$s = \begin{cases} 0 & \text{if } T < T_c, \\ kt(\ln 1/t)^{-1} & \text{if } T \gtrsim T_c, \\ k_B T/3\Delta & \text{if } T \gg T_c. \end{cases} \tag{4.23}$$

4.3.1 Critical Exponents

In the same vein as Section 3.4.1, having found a solution of the saddle-point equation for a complete range of temperature, extracting the critical exponents is a simple job. Using the form of s close to the transition (Eq. (4.23)) we now investigate physical observables around the transition.

The free energy is obtained in the same way as in Section 3.4.1, except that the function $K(\lambda)$ from Eq. (3.19) is modified to

$$K(\lambda) = -3N\beta\Delta + \frac{1}{2}\sum_n \sum_{\mathbf{q}} \ln(\mathcal{E}^{(n)}(\mathbf{q}) + \lambda),$$

so that the free energy becomes, in terms of s,

$$f_{\text{sing}} = -3\beta\Delta s + \frac{1}{2}\int \frac{d^3\mathbf{q}}{(2\pi)^3} \ln(\gamma(\mathbf{q}) + s). \tag{4.24}$$

4.3.1.1 Heat capacity

The singular contribution to the heat capacity, $C_{sing} \sim \partial^2 f_{\rm sing}/\partial t^2$. On account of the stationarity of the free energy at the transition, $\partial f_{\rm sing}/\partial s = 0$, we have

$$\begin{aligned} C_{\rm sing} &= \left(\frac{\partial s}{\partial t}\right)^2 \frac{\partial^2 f_{sing}}{\partial s^2} \\ &\sim \left((\ln 1/t)^{-1}\right)^2 \int \frac{d^3\mathbf{q}}{(2\pi)^3} (\gamma(\mathbf{q}) + s)^{-2}. \end{aligned}$$

The integral is of the form $D_2(s, \Lambda)$, and we use the asymptotic behaviour $D_2(s, \Lambda) \sim \ln 1/s$ to obtain

$$C_{\rm sing} \sim (\ln 1/t)^{-1}. \tag{4.25}$$

4.3.1.2 Susceptibility

The susceptibility at the ordering wavevector $\mathbf{k} = (\pi, \pi, \pi)$ (that is $q = 0$ from the definition of Fourier transformation in Eq. (2.3)) is obtained from

$$k_B T \chi = \sum_i (-1)^i \langle \mathbf{S}_i \cdot \mathbf{S}_0 \rangle \sim G(\mathbf{q} = 0) \propto (\tilde{\Delta}(q = 0) + \bar{\lambda})^{-1}.$$

Since, after projection, the eigenvalues of the interaction matrix are non-analytic at $q = 0$, we delay taking the limit of $J \to \infty$. From the definition of Eq. (4.6), the minimum eigenvalue of $\Delta(q = 0)$ is $\mathcal{E}_0 = -2\Delta$. The susceptibility thus diverges as

$$\chi \sim (\mathcal{E}_0 + \bar{\lambda})^{-1} \sim s^{-1} \sim t^{-1}(\ln 1/t). \tag{4.26}$$

4.3.1.3 Magnetisation

At the critical temperature, we may investigate the magnetisation as a function of an applied field h that couples to the spins. To be commensurate with the symmetry of the ordered phase this field must point in opposite directions on the two sublattices: we thus apply a field at the wavevector $\mathbf{k} = (\pi, \pi, \pi)$. The field has the form $\mathbf{h}^{lm}(\mathbf{q}) = hN\delta(\mathbf{q})\hat{\mathbf{e}}_1$. The Hamiltonian is

modified by the application of the field:

$$\mathcal{H} \to \mathcal{H}' = \mathcal{H} - \sum_i \mathbf{h}_i \cdot \mathbf{S}_i. \tag{4.27}$$

This change in the Hamiltonian adds another term to the coefficient of the linear term in σ_i of Eq. (4.19), and Eq. (4.21) becomes

$$3h = m \sum_{lm} (\Delta^{lm}(q=0) + \bar{\lambda}\delta^{lm}). \tag{4.28}$$

As a result of the applied field, the saddle-point value of $\bar{\lambda}$ is modified from its zero-field value. We incorporate this change by writing $\bar{\lambda}(h) = \bar{\lambda}(0) + r(h)\Delta$. Exactly at the critical temperature ($t = s = 0$), Eq. (4.28) reduces to

$$h = m\,\Delta\, r(h). \tag{4.29}$$

At $s = 0$ the saddle-point condition Eq. (4.11) becomes

$$-3N\beta_c\Delta(1-m^2) + \frac{1}{2}\sum_{\mathbf{q}}^{N} \Big(\gamma(\mathbf{q}) + r\Big)^{-1} = 0,$$

and using the same manipulations that led to Eq. (4.16), we find $m^2 \sim r\,\ln(1/r)$. Inverting, we find $r \sim m^2\,\ln(1/m^2)$, and combining with Eq. (4.29) leads finally to $h \sim m^3\,\ln(1/m)$, or

$$m \sim h^{1/3}\,(\ln(1/h))^{1/3}.$$

We note that we have obtained a set of exponents ($\alpha = 0$, $\beta = 1/2$, $\gamma = 1$ and $\delta = 3$) that are consistent with a mean-field treatment of a short-range ferromagnet. However, in addition there are logarithmic corrections to these power-law scalings, and these are characteristic of a system at its upper critical dimension. In effect, the correlations of the Coulomb phase control the critical behaviour, and place the transition in the same class as a transition in a magnet with uniaxial dipolar interactions, where $d_c^u = 3$.

Finally, we compare these results to ones obtained by Larkin and Khmel'nitskii from an important work on phase transitions in ferroelectrics with dipole-dipole interactions[37]. From Equation (A2.7) of that work, we extract the results at $n = \infty$: $C \sim (\ln 1/t)^{-1}$, $\quad \chi \sim t^{-1} \ln 1/t$

and $m \sim t^{1/2}$. These results are identical to the set of exponents we have derived in this Section.

4.3.2 Correlation Functions

In Section 2.2 we showed that the spins on an octahedral lattice have dipolar correlations as $J/T \to \infty$. In this Chapter we introduced distortion into this lattice, and now discuss how this affects the resultant spin correlations.

We begin by writing the partition function as an unconstrained integral over spin configurations,

$$\mathcal{Z} \sim \int D\mathbf{S} \exp\Big\{ -\sum_{\mathbf{q}} \sum_{lm} \big[G^{-1}(\mathbf{q})\big]_{lm} \mathbf{S}_l(\mathbf{q}) \cdot \mathbf{S}_m(\mathbf{q}) \Big\}, \tag{4.30}$$

where the subscript l, m denotes the sublattice. In the large-n limit, we impose the saddle-point value $\bar{\lambda}$ to set the spin length, so that G^{-1} is given by

$$G^{-1}(\mathbf{q}) = \beta\big[J(\mathbf{q}) + \Delta(\mathbf{q}) + \bar{\lambda}\delta(\mathbf{q})\big].$$

Inverting this yields the Green's matrix $G(\mathbf{q})$, the elements of which correspond to sublattice-sublattice correlators. In the limit of $J/\Delta \to \infty$ we obtain the results

$$\big\langle \mathbf{S}_x(\mathbf{q}) \cdot \mathbf{S}_x(-\mathbf{q}) \big\rangle = \frac{k_B T}{\Delta(3+s)} \, \frac{2(s_y s_z + s_y^2 + s_z^2) + s\,(s_y^2 + s_z^2)}{(s_x + s_y + s_z)^2 + s\,(s_x^2 + s_y^2 + s_z^2)} \tag{4.31}$$

$$\big\langle \mathbf{S}_x(\mathbf{q}) \cdot \mathbf{S}_y(-\mathbf{q}) \big\rangle = \frac{k_B T}{\Delta(3+s)} \, \frac{2s_x s_y + s_z(s_x + s_y - s_z) + s\, s_x s_y}{(s_x + s_y + s_z)^2 + s\,(s_x^2 + s_y^2 + s_z^2)} \tag{4.32}$$

and the other correlators follow from the symmetries of these.

Introducing strain into the system renders the directions parallel and perpendicular to the strain inequivalent; we label these directions $r_\parallel$ and $\mathbf{r}_\perp$. Recall that $r_\parallel$ is the direction [111], and so the sublattices are still equivalent.

It is an difficult task to calculate correlation functions for a general value of the strain, but nevertheless it is possible to study the correlations in various regimes, which we do in the remainder of this Chapter. Firstly, for small strain, we expect correlations to be similar to the dipolar correlations of the unstrained system, but now with inequivalent $r_\parallel$ and $\mathbf{r}_\perp$. We will show how this inequivalence varies as a function of the strain. Secondly, we study correlations at temperatures just above the transition temperature. Since at the transition we expect a

divergence of the correlation length, we use this regime to investigate quantitative features of that divergence. We also study the form of correlations exactly at the critical point and show that this is qualitatively different from behaviour away from the critical point.

4.3.2.1 At High Temperatures

We parameterise the strain using the quantity $\epsilon = (2+s)^{-1}$. The unstrained system now corresponds to $\epsilon = 0$, and the transition is located at $\epsilon = 1/2$. The same-sublattice correlation function is

$$\langle S_x(\mathbf{r})S_x(0)\rangle = \frac{k_BT}{\Delta}\frac{\epsilon}{1+\epsilon}\int \frac{d^3\mathbf{q}}{(2\pi)^3}e^{i\mathbf{q}\cdot\mathbf{r}}\frac{s_y^2+s_z^2+2\epsilon s_y s_z}{(s_x^2+s_y^2+s_z^2)+\epsilon[(s_x+s_y+s_z)^2-2(s_x^2+s_y^2+s_z^2)]} \tag{4.33}$$

which we write as

$$\langle S_x(\mathbf{r})S_x(0)\rangle = \frac{k_BT}{\Delta}\frac{\epsilon}{1+\epsilon}\mathcal{I}_{xx}(\mathbf{r}) \tag{4.34}$$

and, in the long-distance limit, the function $\mathcal{I}_{xx}(\mathbf{r})$ may be written $\mathcal{I}_{xx}(\mathbf{r}) = D_{xx}\mathcal{J}(\mathbf{r})$, where the differential operators are defined

$$D_{xx} = -\left(\frac{\partial^2}{\partial y^2}+\frac{\partial^2}{\partial y^2}+2\epsilon\frac{\partial^2}{\partial y\partial z}\right), \tag{4.35}$$

$$D_{xy} = -\left(\frac{\partial^2}{\partial x\partial y}+\epsilon\frac{\partial}{\partial z}\left(\frac{\partial}{\partial x}+\frac{\partial}{\partial y}-\frac{\partial}{\partial z}\right)\right), \tag{4.36}$$

(others may be obtained through symmetry), and the function

$$\mathcal{J}(\mathbf{r}) = \int \frac{d^3\mathbf{q}}{(2\pi)^3}\, e^{i\mathbf{q}\cdot\mathbf{r}}\, \frac{1}{3\epsilon\, q_\parallel^2+(1-2\epsilon)\, q^2}. \tag{4.37}$$

In Appendix B.1 we show that

$$\mathcal{J}(\mathbf{r}) = \frac{1}{4\pi(1-2\epsilon)^{1/2}}\left[r_\parallel^2(1-2\epsilon)+(\boldsymbol{r}_\perp)^2(1+\epsilon)\right]^{-1/2}, \tag{4.38}$$

a result that is valid throughout the high-temperature phase in the long-distance limit. In the absence of strain, we note that this reduces to $(4\pi r)^{-1}$, and that the sublattice-sublattice correlation functions obtain the dipolar form predicted in Section 2.2. As strain is introduced into the system, this result indicates that the directions $r_\parallel$ and $r_\perp$ scale differently from each

other, and the overall factor $(1-2\epsilon)^{-1/2}$ shows that correlations become stronger as the system approaches the transition.

4.3.2.2 Close to the Critical Temperature

The divergence of the function $\mathcal{J}(\mathbf{r})$ as $\epsilon \to 1/2_-$ is indicative of a qualitative change of correlations at the critical point. Close to the transition we know the asymptotic form of $s = (\epsilon^{-1} - 2)$ is $s \sim t \left(\ln \frac{1}{t}\right)^{-1}$ and so we write the correlation functions in terms of this parameter:

$$\left\langle \mathbf{S}_i(\mathbf{r}) \cdot \mathbf{S}_j(0) \right\rangle = s^{-1/2} \left(A_{ij} \frac{\partial}{\partial r_\parallel} + B_{ij} \frac{\partial}{\partial r_\perp} \right)^2 \left[s\, r_\parallel^2 + 3 r_\perp^2 \right]^{-1/2}.$$

where we have checked by explicit calculation that the coefficients A_{ij}, B_{ij} are $\mathcal{O}(1)$.

The asymptotic behaviour of the correlation functions are

$$\left\langle \mathbf{S}_i(\mathbf{r}) \cdot \mathbf{S}_j(0) \right\rangle \sim \begin{cases} s^{-1/2} r_\perp^{-3} & \text{for } r_\parallel \ll s^{-1/2} r_\perp, \\ s^{-1} r_\parallel^{-3} & \text{for } r_\parallel \gg s^{-1/2} r_\perp. \end{cases}$$

4.3.2.3 At the Critical Temperature

The divergence of the correlations as the critical point is approached suggests that, exactly at the critical point, the previous analysis is insufficient to determine the correlation functions. Looking at the definition of $\mathcal{J}(\mathbf{r})$ in Eq. (4.37), we see that at $\epsilon = 1/2$ the coefficient of the q^2 term in the denominator vanishes, and the integral diverges. In fact, returning to the original definition of the real-space correlation functions, Eq. (4.33), we see that no such divergence occurs, even at $\epsilon = 1/2$. We have simply neglected higher powers of q from the original lattice formulation. At this stage we reintroduce them by including a term cq^4 in the denominator to ensure convergence of the integral at large q.

For simplicity, we sum over the same-sublattice correlation functions so that any angular dependence is averaged over. Starting from Eq. (4.34) with $\epsilon = 1/2$, we have

$$\sum_i \left\langle \mathbf{S}_i(\mathbf{r}) \cdot \mathbf{S}_i(0) \right\rangle = \frac{k_B T_c}{3\Delta} \sum_{i=\{x,y,z\}} \mathcal{I}_{ii}(\mathbf{r}), \tag{4.39}$$

and inserting the expression for $\mathcal{I}_{ii}(\mathbf{r})$ of Eq. (4.34), we find

$$\sum_i \left\langle \mathbf{S}_i(\mathbf{r}) \cdot \mathbf{S}_i(0) \right\rangle = \frac{k_B T_c}{3\Delta} \int \frac{\mathrm{d}^3\mathbf{q}}{(2\pi)^3} e^{i\mathbf{q}\cdot\mathbf{r}} \frac{3q_\parallel^2 + q^2}{3q_\parallel^2 + cq^4} \tag{4.40}$$

where the range of integration in $\mathbf{q}$-space is up to some lattice cutoff $q < \Lambda$ where $\Lambda \sim 1/a \sim \mathcal{O}(1)$. The largest contribution to the integral is from the region $q_\parallel \ll q_\perp \ll 1$, so we may neglect the $q_\parallel$ term in the numerator. We ignore numerical factors that do not qualitatively affect the asymptotic behaviour at large r, and so we investigate the integral

$$I_c(\mathbf{r}) = \int \frac{\mathrm{d}^3\mathbf{q}}{(2\pi)^3} \frac{e^{i\mathbf{q}\cdot\mathbf{r}}}{(q_\parallel/q)^2 + q^2} \tag{4.41}$$

in directions parallel and perpendicular to the strain axis.

The detail of the calculation is described in Appendix B.2, but here we simply present the results for large r:

$$I_c(\mathbf{r}) \sim \begin{cases} \dfrac{1}{8\pi r}, & \text{for } \mathbf{r} \text{ along } \hat{\mathbf{r}}_\parallel, \\ \dfrac{e^{-r/2}}{4\pi r}, & \text{for } \mathbf{r} \text{ along } \hat{\mathbf{r}}_\perp. \end{cases} \tag{4.42}$$

We note the power-law decay of correlations along the parallel direction at the critical point, and also the contrast between this and the short-range exponential falloff of correlations in directions perpendicular to the strain.

4.3.2.4 At Low Temperatures in the Ordered State

At $T = 0$, the spins align in a Néel state, with the symmetry-broken component defining the $a = 1$ axis in spin-space. This Néel state corresponds to spins $\vec{S}_i$ having Fourier components

$$S_l^a(\mathbf{q}) = N^{1/2}\, \delta_{\mathbf{q},0}\, \delta^{a,1}.$$

For $k_B T \ll \Delta$, spins exhibit small fluctuations around this ground state. Labelling the $a \neq 1$ transverse spin components as $\vec{\pi}$, the spin $\vec{S}_i = \Big(\pm (1 - \vec{\pi}_i^2)^{1/2}, \vec{\pi}_i \Big) \approx \Big(\pm (1 - \frac{1}{2}\vec{\pi}_i^2 + \ldots), \vec{\pi} \Big)$, where the sign of the $a = 1$ component depends on the sublattice.

We expand the Hamiltonian of Eq. (4.4) to quadratic order in $\vec{\pi}$:

$$\mathcal{H} \overset{J\to\infty}{=} -2N\Delta + \Delta \sum_{\mathbf{q}} \gamma(\mathbf{q})\ \vec{\pi}(\mathbf{q}) \cdot \vec{\pi}(-\mathbf{q}).$$

Connected correlation functions $\langle \vec{S}(\mathbf{q}) \cdot \vec{S}(-\mathbf{q}) \rangle_c = \langle \vec{S}(\mathbf{q}) \cdot \vec{S}(-\mathbf{q}) \rangle - \langle \vec{S}(\mathbf{q}) \rangle \cdot \langle \vec{S}(-\mathbf{q}) \rangle = \langle \vec{\pi}(\mathbf{q}) \cdot \vec{\pi}(-\mathbf{q}) \rangle$ can be obtained directly from the partition function $\mathcal{Z} = \int \mathcal{D}\vec{\pi} \exp\{-\beta \mathcal{H}[\vec{\pi}]\}$ to give

$$\langle \vec{\pi}(\mathbf{q}) \cdot \vec{\pi}(-\mathbf{q}) \rangle = \frac{1}{\beta \Delta \gamma(\mathbf{q})}.$$

This may in turn be Fourier transformed to yield the low-T correlations,

$$\langle \vec{S}(\mathbf{r}) \cdot \vec{S}(0) \rangle_c = \frac{k_B T}{\Delta} \int \frac{d^3\mathbf{q}}{(2\pi)^3} \frac{e^{i\mathbf{q}\cdot\mathbf{r}}}{\gamma(\mathbf{q})} = \frac{k_B T}{\Delta} I_c(\mathbf{r}),$$

where $I_c(\mathbf{r})$, defined in Eq. (4.41), is evaluated in Eq. (4.42). Thus, the low-T correlations scale as T for $k_B T \ll \Delta$.

4.4 Summary

In this Chapter we have shown how to induce an ordering transition into the octahedral lattice. We did this by including weak further-neighbour interactions between certain pairs of spins. Taking the limit of $J \to \infty$ so that the high-temperature phase of the system corresponds to a Coulomb phase, we studied the thermodynamics of the ordering transition where the number of spin components $n = \infty$. We found that the critical exponents are not the same as for a conventional paramagnetic–ferromagnetic transition in the large-n limit, but instead correspond to a transition with *uniaxial dipolar interactions*[37]. This result is surprising since the model we studied contained only *short-range interactions*, but it provides a stark illustration of the controlling influence that the correlations of the Coulomb phase have on the critical behaviour.

Chapter 5

Flux Picture of the Transition

In this Chapter we present an alternative treatment of the transition introduced in the previous chapter, in which we arrive at a continuum description of the system by considering the degrees of freedom of the high temperature phase. We will see that a continuum description cannot be constructed through the conventional Landau-Ginzburg-Wilson framework, but instead requires a mapping of the spin configurations onto configurations of solenoidal fields, so that the necessary description is in terms of the degrees of freedom of these solenoidal fields.

Previously, in continuum descriptions of a Coulomb phase, the entropic weight on states was to be postulated[30, 31], rather than explicity derived. In Chapter 1, to provide a coarse-grained theory of a Coulomb phase in a close-packed dimer model, the entropic weight on states was taken to be

$$\mathcal{P}[\mathbf{B}(\mathbf{r})] = \exp\left\{-\frac{\kappa}{2}\int d\mathbf{r}[\mathbf{B}(\mathbf{r})]^2\right\},$$

where κ is a phenomenological "stiffness" parameter. In this Chapter, we provide a new insight on this entropic weight by deriving it for the first time, using the large-n limit to control correlations. We take n-component spins on an octahedral lattice as our starting point.

We proceed in the following manner: first we write the full Hamiltonian, Eq. (4.4) in terms of the set of variables introduced in Section 2.2.2. To recap, instead of n-component spins on the sites of the octahedral lattice, we represent a configuration by a mapping onto n flavours of field on the links of the octahedral lattice. These fields are then decomposed into a divergence-free part, and an irrotational part. The ground-state manifold of Hamiltonian $\mathcal{H}_J$ can then be specified by restricting the set of allowed fields to have zero lattice divergence.

In the next section, we will see how, $\mathcal{H}_\Delta$, is written in the space of divergence-free fields: in effect we project $\mathcal{H}_\Delta$ onto the set of ground states of $\mathcal{H}_J$. After diagonalising $\mathcal{H}_\Delta$ in the space of these fields, a critical field will emerge: this controls the thermodynamics of the transition and the long-distance properties of this field will provide a clearer understanding of the behaviour at criticality.

5.1 Hamiltonian in Flux Picture

We recall the mapping of Section 2.2.1, where the model of n-component spins on a lattice of corner-sharing octahedra was translated into a system of n separate fields where, in the limit of $J \to \infty$, the fields became solenoidal: this corresponds to setting the scalar potential $V^a(\mathbf{q}) = 0$.

We now look at how $\mathcal{H}_\Delta$ transforms when written solely in terms of the vector potential $\mathbf{A}^a(\mathbf{q})$. After making the change of variables using Eq. (2.8), $\mathcal{H}_\Delta$ is put into the diagonal form

$$\mathcal{H}_\Delta = 4\Delta \sum_{i}^{3} \sum_{\mathbf{q}} \mu_i(\mathbf{q}) \left|\vec{v}_i(\mathbf{q})\right|^2, \tag{5.1}$$

by making a unitary transformation on the 3 components of $\mathbf{A}^a(\mathbf{q})$ to generate the fields $\vec{v}_i(\mathbf{q})$ $(i = 1, 2, 3)$. Explicitly, the eigenvalues in Equation (5.1) are

$$\begin{aligned} \mu_1(\mathbf{q}) &= (s_x^2 + s_y^2 + s_z^2)\,(-2 + \gamma(\mathbf{q})) \\ \mu_2(\mathbf{q}) &= s_x^2 + s_y^2 + s_z^2 \qquad (5.2) \\ \mu_3(\mathbf{q}) &= 0. \qquad (5.3) \end{aligned}$$

The unitary transformation on components of the vector potential, written

$$v_i^a(\mathbf{q}) = U_{ij}(\mathbf{q})\, A_j^a(\mathbf{q}), \tag{5.4}$$

is brought about by the matrix $U(\mathbf{q})$, the columns of which are

$$\begin{aligned} \mathbf{U}_1^T(\mathbf{q}) &= c_1\,(s_{yz}, s_{zx}, s_{xy}) \\ \mathbf{U}_3^T(\mathbf{q}) &= c_2\,(s_x, s_y, s_z) \end{aligned}$$

and $\mathbf{U}_2(\mathbf{q}) = \mathbf{U}_3(\mathbf{q}) \times \mathbf{U}_1(\mathbf{q})$. The factors $c_i(\mathbf{q})$ ensure the normalisation of the columns of $U(\mathbf{q})$.

In a fixed gauge, only two of these fields fluctuate independently: implementing the Coulomb gauge – the lattice equivalent of $\boldsymbol{\nabla} \cdot \mathbf{A} = 0$ – results in $v_3(\mathbf{q}) = 0$. In this Coulomb gauge the lattice equation $\mathbf{B} = \nabla \times \mathbf{A}$, written in Fourier space as

$$\mathbf{B}(\mathbf{q}) = 2i \begin{pmatrix} 0 & -s_z & s_y \\ s_z & 0 & -s_x \\ -s_y & s_x & 0 \end{pmatrix} \mathbf{A}(\mathbf{q}), \tag{5.5}$$

is inverted by

$$\mathbf{A}(\mathbf{q}) = \frac{i}{2(s_x^2 + s_y^2 + s_z^2)} \begin{pmatrix} 0 & -s_z & s_y \\ s_z & 0 & -s_x \\ -s_y & s_x & 0 \end{pmatrix} \mathbf{B}(\mathbf{q}). \tag{5.6}$$

5.2 Effective Theory of Transition

In the small-q limit, the fields of Eq. (5.4) recover particularly simple forms

$$\begin{aligned} v_1(\mathbf{q}) &= c_0\, \hat{\mathbf{n}} \times \hat{\mathbf{q}} \cdot \mathbf{A}(\mathbf{q}) = c_0\, \hat{\mathbf{q}} \times \mathbf{A}(\mathbf{q}) \cdot \hat{\mathbf{n}} \\ v_2(\mathbf{q}) &= c_0\, \hat{\mathbf{q}} \times (\hat{\mathbf{n}} \times \hat{\mathbf{q}}) \cdot \mathbf{A}(\mathbf{q}) \overset{\text{Coulomb}}{=} c_0\, \hat{\mathbf{n}} \cdot \mathbf{A}(\mathbf{q}) \\ v_3(\mathbf{q}) &= \hat{\mathbf{q}} \cdot \mathbf{A}(\mathbf{q}) \overset{\text{Coulomb}}{=} 0, \end{aligned}$$

where the second equalities in the second and third lines are true only in the Coulomb gauge ($\hat{\mathbf{q}} \cdot \mathbf{A}(\mathbf{q}) = 0$). In these equations $\hat{\mathbf{n}}$ is a unit vector in the [111]-direction, and the factor $c_0 = (1 - (\hat{\mathbf{n}} \cdot \hat{\mathbf{q}})^2)^{-1/2}$ is necessary from the normalisations in Eq (5.4).

Within the Coulomb gauge, the continuum versions of Eqs (5.5) and (5.6) can be written

$$\mathbf{B}^a(\mathbf{q}) = i\, \mathbf{q} \times \mathbf{A}^a(\mathbf{q}) \tag{5.7}$$

$$\mathbf{A}^a(\mathbf{q}) = i\, q^{-2}\, \mathbf{q} \times \mathbf{B}^a(\mathbf{q}) \tag{5.8}$$

This inversion allows us to write the fields $V_i^a(\mathbf{q})$ in terms of $\mathbf{B}^a(\mathbf{q})$. On rescaling the fields

$\vec{\varphi}_n(\mathbf{q}) = q\vec{v}_n(\mathbf{q})$ we have

$$\varphi_1^a(\mathbf{q}) = \hat{\mathbf{n}} \cdot \mathbf{B}^a(\mathbf{q}) \equiv B_\parallel^a(\mathbf{q}) \tag{5.9}$$

$$\varphi_2^a(\mathbf{q}) = \hat{\mathbf{n}} \cdot \mathbf{q} \times \mathbf{B}^a(\mathbf{q}) \tag{5.10}$$

Hence, in the continuum limit we may write the Hamiltonian of Eq. (5.1) as

$$\mathcal{H} = \mathcal{H}_J + \mathcal{H}_\Delta = 4\Delta \sum_i^3 \sum_{\mathbf{q}} \frac{\mu_i(\mathbf{q})}{q^2} \left|\vec{\varphi}_i(\mathbf{q})\right|^2 \tag{5.11}$$

$$= \mathcal{E}_0 + \Delta \sum_a \int \frac{d^3\mathbf{q}}{(2\pi)^3} \left(\gamma(\mathbf{q}) \left|B_\parallel^a(\mathbf{q})\right|^2 + 3\left|\hat{\mathbf{n}} \cdot \mathbf{q} \times \mathbf{B}^a(\mathbf{q})\right|^2\right), \tag{5.12}$$

We note that this integrand is valid only for $(\hat{\mathbf{n}} \cdot \hat{\mathbf{q}})^2 \ll 1$. We identify the critical field as $\varphi_1^a(\mathbf{q}) = \hat{\mathbf{n}} \cdot \mathbf{B}^a(\mathbf{q}) = B_\parallel^a(\mathbf{q})$.

5.2.1 Spin-Length Constraint in Flux Picture

At this stage we note that the spin-length constraint is enforced by using the saddle-point value $\lambda_i = \bar{\lambda}$ in Equation (3.17). Within this integral over spins $\mathbf{S}_i$, the spin-length constraint, in the limit of n large, is written

$$\exp\left\{-\bar{\lambda} \sum_{\mathbf{q}} \mathbf{S}(-\mathbf{q}) \cdot \mathbf{S}(\mathbf{q})\right\}.$$

In this new representation, the scalar product $\mathbf{S}(-\mathbf{q}) \cdot \mathbf{S}(\mathbf{q})$ is

$$\mathbf{S}(-\mathbf{q}) \cdot \mathbf{S}(\mathbf{q}) = 4 \sum_a \Big[(s_x^2 + s_y^2 + s_z^2)\Big(|A_x^a(\mathbf{q})|^2 + |A_y^a(\mathbf{q})|^2 + |A_z^a(\mathbf{q})|^2 + |V^a(\mathbf{q})|^2\Big) - \left|s_x A_x^a(\mathbf{q}) + s_y A_y^a(\mathbf{q}) + s_z A_z^a(\mathbf{q})\right|^2\Big].$$

Furthermore, we notice that in the small-q limit this simplifies to

$$\mathbf{S}(-\mathbf{q}) \cdot \mathbf{S}(\mathbf{q}) = \sum_a \left[q^2(|\mathbf{A}^a(\mathbf{q})|^2 + |V^a(\mathbf{q})|^2) - |\mathbf{q} \cdot \mathbf{A}^a(\mathbf{q})|^2\right] = \sum_a [|\mathbf{q} \times \mathbf{A}^a(\mathbf{q})|^2 + q^2|V^a(\mathbf{q})|^2] \tag{5.13}$$

The first term in the final expression can be recognised simply as $\sum_a |\mathbf{B}^a(\mathbf{q})|^2$. Taking $V^a(\mathbf{q}) = 0$, spin-length constraint is transformed back to real space to give the coarse-grained entropic

weight on states

$$\mathcal{P}[\mathbf{B}(\mathbf{r})] = \exp\left\{-\bar{\lambda}\sum_a \int d\mathbf{r}\ |\mathbf{B}^a(\mathbf{r})|^2\right\} = e^{-\mathcal{S}_0[\mathbf{B}^a(\mathbf{r})]}, \tag{5.14}$$

as has been previously postulated.

5.2.2 Effective Hamiltonian

Thus, in order to describe a phase transition between the Coulomb and Néel phases, we incorporate the effect of non-zero Δ into the continuum theory of Eq. (5.14)

$$\mathcal{Z} = \int\limits_{\nabla\cdot\mathbf{B}^a(\mathbf{r})=0} \mathcal{D}\mathbf{B}^a(\mathbf{r})\ \mathcal{P}[\mathbf{B}^a(\mathbf{r})]\ e^{-\beta\mathcal{H}_{crit}}$$

Writing this schematically in terms of a temperature-dependent control parameter t, with $t = 1$ for $T \gg \Delta$ and $t < 0$ for $T \ll \Delta$, the analysis of this chapter may be most readily summed up by the overall effective Hamiltonian $\mathcal{H} = \mathcal{H}_2 + \mathcal{H}_4$, where $\mathcal{H}_4$ is required for stability in the ordered phase. Fourier transforming back to real space, the effective Hamiltonian reads

$$\mathcal{H}_2 = \frac{\kappa}{2}\sum_a \int \mathrm{d}^3\mathbf{r}\ \left\{\ t\left|\mathbf{B}^a_{\parallel}(\mathbf{r})\right|^2 + \left|\mathbf{B}^a_{\perp}(\mathbf{r})\right|^2 + \left|\boldsymbol{\nabla}\times\mathbf{B}^a(\mathbf{r})\right|^2\right\}$$
$$\mathcal{H}_4 = \frac{u_0}{n}\times\frac{1}{4!}\int \mathrm{d}^3\mathbf{r}\ \left\{\sum_a \left|\mathbf{B}^a(\mathbf{r})\right|^2\right\}^2. \tag{5.15}$$

In $\mathcal{H}_4$ the interaction strength u_0/n is chosen to make $\mathcal{H}_2$ and $\mathcal{H}_4$ are of the same order for $n \to \infty$. At $t = 1$, Eq. (5.15) is simply $\mathcal{H}_J$ supplemented by gradient and quartic terms that are irrelevant in the scaling sense in the Coulomb phase. On reducing t a transition occurs (at $t = 0$ within mean field theory) to an ordered phase in which $\langle B^a_{\parallel}(\mathbf{r})\rangle \neq 0$.

5.3 Summary and Discussion

In this Chapter we have taken the spin model introduced in Chapter 4 and derived a continuum theory for it in the limit of $J \to \infty$. To achieve this we explicitly mapped the lattice spin model onto a lattice flux model, where flux is carried around the links of the bipartite simplex lattice. In the limit of $n \to \infty$, the spin length constraint is implemented by introducing a Lagrange multiplier; this multiplier turns out to be analagous to the stiffness parameter in the

flux model. Taking the continuum limit of the flux model results in the effective Hamiltonian of Equation (5.15), and allows us to identify the critical field as $\hat{\mathbf{n}} \cdot \mathbf{B}^a(\mathbf{r}) = B_{\|}(\mathbf{r})$. The quantity $\langle \mathbf{B}^a(\mathbf{r}) \rangle$ is zero above the transtion (Coulomb phase) and below the transition (Néel phase) the field condenses along the real-space direction $\mathbf{n} = [111]$ with a corresponding breaking of the $O(n)$-symmetry of flavour space.

We recall from Section 1.3.1 ordering transitions out of Coulomb phases in classical dimer models, for which numerical simulation data is available. References [4] and [49] both point to continuous phase transitions in these dimer systems. Although classical dimer transitions and the transition in the spin model described in this chapter are both examples of ordering transitions from the Coulomb phase, we now briefly outline some fundamental differences between these two systems. For the dimer model, a gauge field description of the columnar phase corresponds to small plaquettes of circulating flux: after coarse graining the flux in these small regions averages to zero. By contrast, the low temperature phase of the spin model may be described as a macroscopic condensation of the gauge field $\mathbf{B}^a(\mathbf{r})$: under coarse graining the condensation of this field persists. We have succeeded in providing an effective continuum description of this ordering transition based on the coarse-grained gauge field. In this case we have shown how the dipolar correlations alter the critical behaviour from a conventional magnetic transition. By contrast, an equivalent approach to the dimer problem does not seem possible because the coarse-grained gauge field disappears in the ordered phase. Dimer transitions still appear to exhibit non-LGW criticality[15].

Chapter 6

Towards a More Complete Understanding of the Ordering Transition

In Chapter 4 we introduced a system of frustrated classical spins in which the high-temperature phase was Coulombic, and the low-temperature phase had Néel ordering. We proceeded to study the thermodynamics of the transition, and showed it was identical to that of a system of spins coupled via long-range, uniaxial dipolar interactions. In Chapter 5 we showed that this spin system could be more naturally represented using continuum description that involved dynamically fluctuating solenoidal fields. We found that a phase transition corresponded to a breaking of the $\mathcal{O}(n)$-symmetry of flavour space, and that the symmetry broken component condensed along the axis $\hat{\mathbf{n}}$, defining $B^{\alpha}_{\parallel}(\mathbf{r}) = \hat{\mathbf{n}} \cdot \mathbf{B}^{a}(\mathbf{r})$. We thus arrived at the coarse-grained description encapsulated by the Hamiltonian $\mathcal{H} = \mathcal{H}_2 + \mathcal{H}_4$ of Equation (5.15), and valid for any n.

In a recent work it was shown, by numerical simulations of classical Heisenberg spins on a pyrochlore lattice, that the ordering transition is discontinuous[59]. Evidence of this is shown in Figure 6.1. However, from the analytical work of Chapters 4 and 5, we have seen that at $n \to \infty$ the transition is continuous.

In this Chapter we attempt to show how these two results are compatible. To do this, we provide two separate analytical treatments: firstly we perform an expansion of the free energy

in powers of $1/n$, where n is large; secondly, we integrate out fluctuations of the non-critical mode in a local approximation.

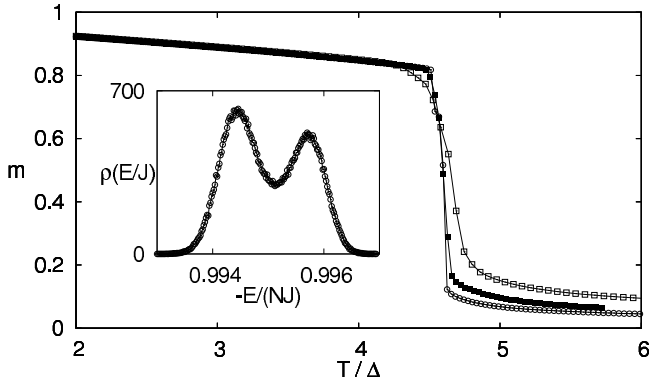

Figure 6.1: Evidence for a first-order transition from simulations with $\Delta = 10^{-3}J$. Main panel: m vs. T/J for $L = 6$ (□), 8 (■), and 10 (○). Inset: probability distribution $\rho(E/J)$ for the energy E at the estimated transition temperature, $T/J = 4.6 \times 10^{-3}$, for $L = 6$.

6.1 $1/n$ Expansion

At the phase transition, where (in mean-field theory) the coefficient t in $\mathcal{H}_2$ of Eq. (5.15) changes sign from positive to negative, one flavour component of the solenoidal field $\mathbf{B}(\mathbf{r})$ condenses along the real-space direction $\hat{\mathbf{n}}$. We choose flavour of the condensed field to be $a = 1$ and separate out B_0 by writing

$$\mathbf{B}^a(\mathbf{r}) = B_0\, \hat{\mathbf{n}}\, \delta^{a1} \;+\; \delta\mathbf{B}^a(\mathbf{r}). \tag{6.1}$$

From Eqs. (5.4) and (5.5), we note that $\sum_i |v_i(\mathbf{q})^a|^2 = |\mathbf{A}^a(\mathbf{q})|^2$ and, since $\varphi_i(\mathbf{q})^a = q\, v_i(\mathbf{q})^a$, in the Coulomb gauge we have

$$\mathbf{B}^a(-\mathbf{q}) \cdot \mathbf{B}^a(\mathbf{q}) = \sum_i |\varphi_i^a(\mathbf{q})|^2.$$

Taking the interaction strength $u_0 = 0$, we have the partition function for the free theory:

$$\mathcal{Z}_0 = \int \mathcal{D}\mathbf{B}^a(\mathbf{q}) \exp\{-\mathcal{H}_2[\mathbf{B}^a(\mathbf{q})]\}.$$

Of most significance for later, we have

$$\begin{aligned}\sum_a \langle \mathbf{B}^a(\mathbf{q})\cdot\mathbf{B}^a(-\mathbf{q})\rangle_0 &= B_0^2\delta(\mathbf{q}=0)+\sum_a\langle\delta\mathbf{B}^a(\mathbf{q})\cdot\delta\mathbf{B}^a(-\mathbf{q})\rangle_0\\ &= B_0^2\delta(\mathbf{q}=0)+\sum_a\langle\varphi_1^a(\mathbf{q})\varphi_1^a(-\mathbf{q})\rangle_0+\sum_a\langle\varphi_2^a(\mathbf{q})\varphi_2^a(-\mathbf{q})\rangle_0,\end{aligned}$$

since $\varphi_3 = 0$. For $\varphi_1^a(\mathbf{q})$ and $\varphi_2^a(\mathbf{q})$ we have, for small $\mathbf{q}\cdot\hat{\mathbf{n}} \ll 1$,

$$\langle\varphi_1^a(\mathbf{q})\varphi_1^a(-\mathbf{q})\rangle_0 = \left[(q_\parallel^2/q^2)+q^2+t\right]^{-1}, \qquad \langle\varphi_2^a(\mathbf{q})\varphi_2^a(-\mathbf{q})\rangle_0 = \left[\,3+q^2\,\right]^{-1} \tag{6.2}$$

where the angled brackets $\langle\bullet\rangle_0$ denote an expectation over the Gaussian weight $\exp\{-\mathcal{H}_2\}$. We observe that the field φ_2 has short-range correlations in real space. In contrast, the field φ_1 is long-ranged due to the singularity at $q = 0$ that results from the projected interaction; thus it is this critical field that determines the long-distance behaviour of the system. This fact allows the simplification

$$\langle\delta\mathbf{B}^a(\mathbf{q})\cdot\delta\mathbf{B}^a(-\mathbf{q})\rangle_0 \approx \langle\varphi_1^a(\mathbf{q})\varphi_1^a(-\mathbf{q})\rangle_0 = \left[(q_\parallel^2/q^2)+q^2+t\right]^{-1}.$$

The expectation value of these fluctuations, which are averaged over the *quadratic* part of the Hamiltonian only, becomes the *bare* propagator $\langle\varphi_1^a(\mathbf{q})\varphi_1^a(-\mathbf{q})\rangle_0$ in the language of field theory. Introducing a diagramatic representation, this is displayed as a thin, solid line where the flavour label a is conserved.

6.1.1 Interactions

Below the transition, where a spontaneous B_0 develops, the quadratic Hamiltonian $\mathcal{H}_2$ is insufficient to provide a stable theory. In the spin model, the length constraint on each spin couples together the different components of a spin (represented in the field theory as flavours of field), and therefore we include a quartic interaction term $\mathcal{H}_4$ of Eq. (5.15) that couples together the n different flavours of field.

Within mean-field theory, the free energy f for this system is given by $\mathcal{Z} = \exp\{-\beta n V f\}$

$$n\beta f = \frac{t}{2}B_0^2 + \frac{u_0}{24n}B_0^4$$

where $B_0 = \mathcal{O}(n^{1/2})$, and so both terms of the free energy are of comparable size.

By contrast, we may make a Landau approximation to the free energy for $n = \infty$, using Eq. (3.15). In the new solenoidal field representation of the spin model, B_0 plays that same role as Φ. Since B_0 is provided by the $\mathbf{q} = 0$ Fourier coefficient of $B^{\alpha=1}(\mathbf{q})$, the Landau approximation to the free energy can be obtained by setting all of the external momenta to zero. Close to the transition, s is small, and we may use the aysmptotic form of $I_2(\mathbf{q} = 0, s) \sim s \ln 1/s$ for small s:

$$U(\mathbf{\Phi}) = \frac{1}{2} G^{-1}(\mathbf{q} = 0) B_0^2 + \frac{1}{24n} u(\mathbf{q} = 0) B_0^4 \tag{6.3}$$

where we recall $G^{-1}(\mathbf{q}) = \gamma(\mathbf{q}) + s$, so that the inverse susceptibility, $G^{-1}(\mathbf{q} = 0) = s$, where $s(t)$ has the temperature dependence described in Eq. (4.23). At small s, from Eqs. (3.14) and (A.6) the function $u(\mathbf{q} = 0)$ vanishes as $u(\mathbf{q} = 0) \sim (\ln(1/s))^{-1}$. Thus this quartic coefficent in the free energy vanishes more slowly than the quadratic coefficient around the transition, and at $n = \infty$ the transition is continuous, generating the critical exponents of Section 3.4.1.

6.1.2 Free Energy to $\mathcal{O}(1/n)$

From the parameterisation of Eq. (6.1), in the low temperature phase, expectation values of $\langle \{ |\sum_a \mathbf{B}^a|^2 \}^2 \rangle_0$ contain terms of the form $B_0^2 \langle \delta\mathbf{B}^a(\mathbf{q}) \cdot \delta\mathbf{B}^a(-\mathbf{q}) \rangle_0$. We represent the condensed part B_0 as a double line, and note that this carries zero momentum.

In order to calculate the order in $1/n$ of a diagram in a perturbative expansion, we introduce the parameter $D = N_v - N_l$, where N_v is the number of vertices and N_l the number of propagator loops. Below we remind ourselves of the $n = \infty$ results and proceed to calculate the $\mathcal{O}(1/n)$ corrections to them.

6.1.2.1 Coefficient of B_0^2 to $\mathcal{O}(1/n)$

At $n = \infty$, the contribution to the two-point function comes from a $D = 0$ object. Allowing additional diagrams at $D = 1$ corresponds to a further mass renormalisation, which we think of as an $\mathcal{O}(1/n)$ correction to the self-energy Σ.

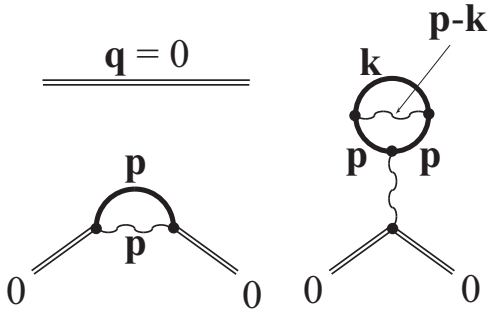

Figure 6.2: B_0^2 terms in free energy.

From this point onwards in the $\mathcal{O}(1/n)$ treatment, whenever we draw a thick, solid line for the propagator we regard it as representing the propagator to $\mathcal{O}(1/n)$. That is, the sum of these three diagrams. Equivalently, the function $G(\mathbf{q}) = (\gamma(\mathbf{q}) + \tilde{s}(t))^{-1}$, where $\tilde{s} = s - \Sigma_{1/n}$. Since this just shifts the transition temperature by a small amount, we do not concern ourselves with evaluating Σ to $\mathcal{O}(1/n)$, and understand the parameter $\tilde{s} \to s$ to represent s to $\mathcal{O}(1/n)$.

6.1.2.2 Coefficient of B_0^4 to $\mathcal{O}(1/n)$

At the transition, the coefficient s of the B_0^2 term in the free-energy expansion vanishes. In this section we calculate the coefficient of the B_0^4 term as $s \to 0$.

The leading order four-point function is a $D = 1$ object. At $D = 2$ we can identify 5 distinct free energy diagrams. We display these "faithful" diagrams (those that explicitly show field flavour) below in Figure 6.3.

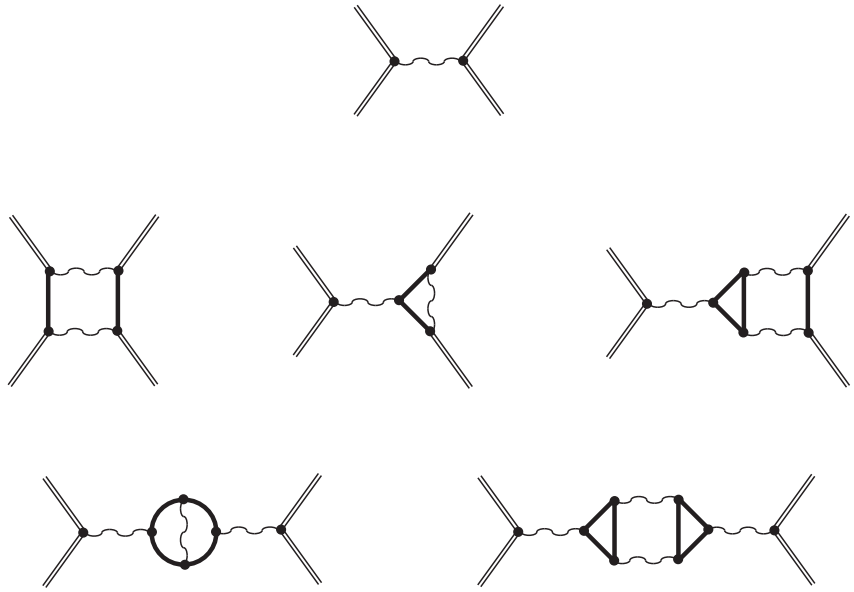

Figure 6.3: B_0^4 terms in free energy. Double lines correspond to a uniform field B_0, and thus carry no momentum. The first diagram, (a), is a $D = 1$ contribution, and the following five $(b, c, d, e \text{ and } f)$ are $D = 2$ contributions.

To see why there should only be five contributory diagrams at $D = 2$ we propose the following argument. First join up the external legs to produce the free energy diagrams: any further topologically distinct diagram must be constructed from any of these five, with the addition of as many propagator loops as additional vertices. Simply replacing —interaction— with —interaction—loop—interaction— is not allowed since this has been included in the renormalised interaction. Adding a —interaction—loop onto any propagator is likewise not allowed since this has been included in the renormalised propagator. We are left with the options of joining two propagators together with an —interaction—, a process that increases D, or joining a propagator to the boundary with an —interaction—, also a process that increases D. Thus we must conclude that these are the only five diagrams available.

Faithful diagrams are generated from the structural diagrams (where four-point interactions are represented at a point) with the following coefficients.

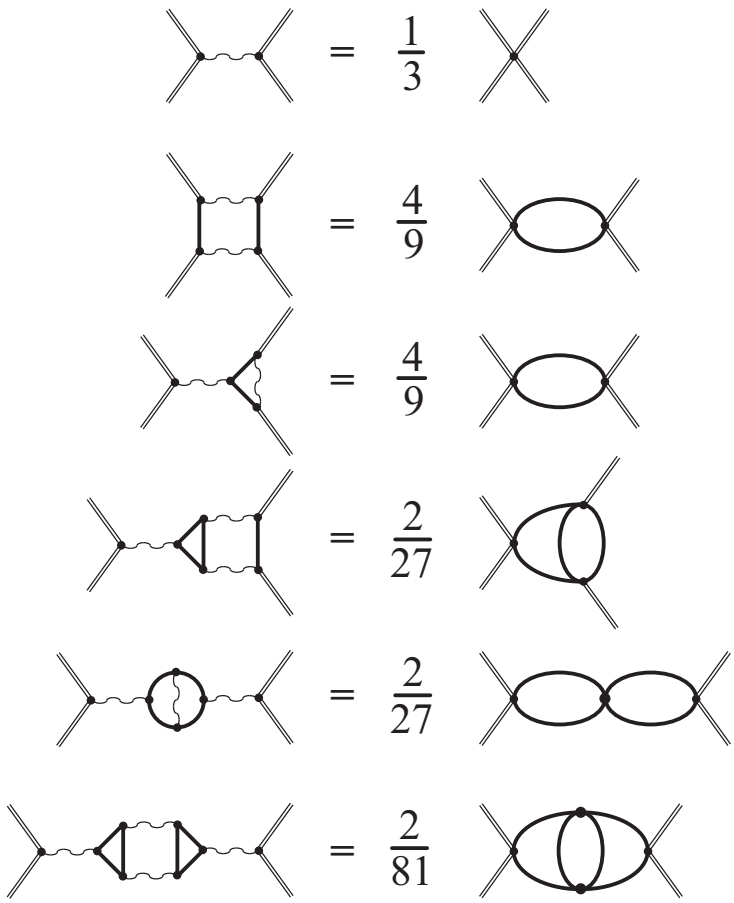

Figure 6.4: Combinatorial factors for faithful diagrams. The structural diagrams have the symmetry factors, respectively: $(a)\ -u$; $(b)\ u^2/2$; $(c)\ u^2/2$; $(d)\ -u^3/8$; $(e)\ -u^3/4$; $(f)\ u^4/4$.

Diagram (a) This $D = 1$ contribution contains no momentum or flavour integrals. Its value is

$$X_a = -\frac{1}{3}u(0).$$

Since, from Eqs. (3.14) and (A.6) we have the result $u(\mathbf{q} = 0) \sim (\ln(1/s))^{-1}$ for small s, we find $X_a \to 0$ as $s \to 0$.

Diagram (b) The first $D = 2$ diagram contains one momentum loop but no flavour loops. Setting all external momenta to be zero corresponds to the integral

$$X_b = +\frac{1}{2}\,\frac{4}{9}\int \frac{d^3\mathbf{q}}{(2\pi)^3}\,[G(\mathbf{q})]^2\,[u(\mathbf{q})]^2 \equiv \frac{2}{9}F_2(s,\Lambda).$$

In Appendix A.2.4 we show that $F_2(s,\Lambda)$ is a finite, positive quantity at $s=0$, and so $X_b = +2F_2(s=0,\Lambda)/9$.

Diagram (c) The second $D=2$ contribution is obtained from the same structural diagram as the first, and again contains one momentum loop and no flavour loops. The integral in this case is

$$X_c = +\frac{1}{2}\,\frac{4}{9}u(0)\int\frac{d^3\mathbf{q}}{(2\pi)^3}\,[G(\mathbf{q})]^2\,u(\mathbf{q}) = \frac{2}{9}u(0)\;F_1(s,\Lambda),$$

where we remember $u(0)$ tends to zero as $(\ln(1/s))^{-1}$. In Appendix A.2.4 we note that, for small s, $F_1(s,\Lambda)\sim\ln(\ln(1/s))$. However, the factor of $(\ln(1/s))^{-1}$ from $u(0)$ means that $X_c\to 0$ as $s\to 0$.

Diagram (d) The third diagram contains two momentum loops and one flavour loop. It is given by

$$X_d = -\frac{1}{8}\,\frac{2}{27}[u(0)]^2\int\frac{d^3\mathbf{p}}{(2\pi)^3}\int\frac{d^3\mathbf{q}}{(2\pi)^3}\,[G(\mathbf{q})]^2\,[G(\mathbf{p})]^2u(\mathbf{q}-\mathbf{p}).$$

Since the quantity $\int\frac{d^3\mathbf{p}}{(2\pi)^3}\,[G(\mathbf{p})]^2 = D_2(s,\Lambda)\to\left(\ln\frac{1}{s}\right)$ has a divergent contribution at $p\to 0$, we have the result

$$\int\frac{d^3\mathbf{p}}{(2\pi)^3}[G(\mathbf{p})]^2u(\mathbf{q}-\mathbf{p}) = \left(\ln\frac{1}{s}\right)u(\mathbf{q}).$$

Using this result, we integrate first on $\mathbf{p}$. The factor $\ln 1/s$ cancels one power of $u(0)$ to give

$$X_d = -\frac{1}{8}\,\frac{2}{27}[u(0)]\int\frac{d^3\mathbf{q}}{(2\pi)^3}\,[G(\mathbf{q})]^2u(\mathbf{q}) = -\frac{1}{108}u(0)F_1(s,\Lambda).$$

Comparing this with X_c we conclude that $X_d\to 0$ as $s\to 0$.

Diagram (e) This diagram contains two momentum loops and one flavour loop again. We write

$$X_e = -\frac{1}{4}\,\frac{2}{27}\int\frac{d^3\mathbf{p}}{(2\pi)^3}\,G(\mathbf{p})\,[u(\mathbf{p})]^2\;\underbrace{u(0)\int\frac{d^3\mathbf{q}}{(2\pi)^3}\,G(\mathbf{p}-\mathbf{q})\,[G(\mathbf{q})]^2}_{K(\mathbf{p})}.$$

In Appendix A.2.3 we show why $K(\mathbf{p})$ reduces to $G(\mathbf{p})$ as $s\to 0$. The remaining $\mathbf{p}$ integral is identical to the function $F_2(s,\Lambda)$, and for $s=0$ we find $X_e = -F_2(s=0,\Lambda)/54$.

Diagram (f) The final diagram contains 3 momentum integrals. We write this diagram as

$$X_f = +\frac{1}{4}\,\frac{2}{81}\int \frac{d^3\mathbf{k}}{(2\pi)^3}\,[u(\mathbf{k})]^2\,\underbrace{u(0)\int \frac{d^3\mathbf{q}}{(2\pi)^3}[G(\mathbf{q})]^2\,G(\mathbf{k}-\mathbf{q})}_{G(\mathbf{k})}\,\underbrace{u(0)\int \frac{d^3\mathbf{p}}{(2\pi)^3}[G(\mathbf{p})]^2 G(\mathbf{k}-\mathbf{p})}_{G(\mathbf{k})}\,,$$

so that the remaining $\mathbf{k}$-integral is $F_2(s,\Lambda)$ and we find $X_f = F_2(s=0,\Lambda)/162$.

Since each four-point diagram has three permutations of the external legs 12|34, 13|24 and 14|23, there is an additional factor of three in the B_0^4 term in the free energy. For any finite value of n, this coefficient remains finite through the transition. Its value is $-3\sum_i X_i$ and is equal to

$$-3\left\{\frac{1}{n}\,(u(0)) + \frac{1}{n^2}\left(\frac{2F_2(s=0,\Lambda)}{9} + 0 + 0 - \frac{F_2(s=0,\Lambda)}{54} + \frac{F_2(s=0,\Lambda)}{162}\right)\right\}.$$

6.1.3 Critical Behaviour at $\mathcal{O}(1/n)$

Including the $D=2$ corrections to the free energy of Eq. (6.3), we have

$$U(\mathbf{\Phi}) = \frac{1}{2}\,s\,B_0^2 + \frac{1}{4!n}\left(u(0) - \frac{17F_2(s=0,\Lambda)}{81\,n}\right)B_0^4 \tag{6.4}$$

so that, in the regime where $n \ll F_2(s=0,\Lambda)\ln(1/s)$,

$$U(\mathbf{\Phi}) = \frac{1}{2}\,s\,B_0^2 - \frac{1}{n^2}\frac{17F_2(s=0,\Lambda)}{81\times 4!}B_0^4. \tag{6.5}$$

The negative coefficient of the B_0^4 term necessitates including B_0^6 terms for stability. Within the framework of the Landau free energy expansion, a negative ϕ^4 coefficient indicates a first-order transition. Therefore we find that the $1/n$ expansion has yielded a first order transition for any finite value of n.

6.2 Local approximation to the free energy

In this section we describe another approach to determining the form of the free energy for finite n. From the form of the propagators in Eq. (6.2), we note that the correlation function $\langle\vec{\varphi}_2(\mathbf{r})\cdot\vec{\varphi}_2(0)\rangle$ is a finite-range object. We therefore make the approximation that the values of

$\vec{\varphi}_2(\mathbf{r})$ are uncorrelated in space, and integrate out this mode.

We begin from the Hamiltonian

$$H[\vec{\varphi}_1(\mathbf{r}), \vec{\varphi}_2(\mathbf{r})] = H_2[\vec{\varphi}_1(\mathbf{r})] + a\vec{\varphi}_2(\mathbf{r})^2 + u_{11}\vec{\varphi}_1(\mathbf{r})^4 + 2u_{12}\vec{\varphi}_1(\mathbf{r})^2\vec{\varphi}_2(\mathbf{r})^2 + u_{22}\vec{\varphi}_2(\mathbf{r})^4$$

where H_2 contains only terms quadratic in $\vec{\varphi}_1(\mathbf{r})$. Here, $\vec{\varphi}_1(\mathbf{r})^4$ should be understood to mean $(\vec{\varphi}_1(\mathbf{r})^2)^2$. We wish to find $H_{eff}[\vec{\varphi}_1(\mathbf{r})]$ such that

$$e^{-H_{eff}[\vec{\varphi}_1(\mathbf{r})]} = \int \mathcal{D}\vec{\varphi}_2(\mathbf{r}) e^{-H[\vec{\varphi}_1(\mathbf{r}), \vec{\varphi}_2(\mathbf{r})]}.$$

Within the local approximation we identify

$$H_{eff}[\vec{\varphi}_1(\mathbf{r})] = H_2[\vec{\varphi}_1(\mathbf{r})] + \mathcal{H}, \tag{6.6}$$

where

$$\mathcal{H} = -\int d^3\mathbf{r} \ln I\left[\vec{\varphi}_1(\mathbf{r})\right]$$

and

$$I\left[\vec{\varphi}_1(\mathbf{r})\right] = \int d\vec{\varphi}_2 \exp\left\{-a\vec{\varphi}_2^2 - u_{11}\vec{\varphi}_1^4 - 2u_{12}\vec{\varphi}_1^2\vec{\varphi}_2^2 - u_{22}\vec{\varphi}_2^4\right\}.$$

For $\vec{\varphi}_1$ small we expand $I[\vec{\varphi}_1(\mathbf{r})]$ in a power series $I\left[\vec{\varphi}_1(\mathbf{r})\right] = I_0 + I_2\vec{\varphi}_1(\mathbf{r})^2 + I_4\vec{\varphi}_1(\mathbf{r})^4 + \ldots$, with

$$\begin{aligned} I_0 &= \int d\vec{\varphi}_2 \exp\left\{-a\vec{\varphi}_2^2 - u_{22}\vec{\varphi}_2^4\right\} \\ I_2 &= -2u_{12}\int d\vec{\varphi}_2\ \vec{\varphi}_2^2\ \exp\left\{-a\vec{\varphi}_2^2 - u_{22}\vec{\varphi}_2^4\right\} \\ I_4 &= -u_{11}I_0 + 2u_{12}^2\int d\vec{\varphi}_2\ \vec{\varphi}_2^4\ \exp\left\{-a\vec{\varphi}_2^2 - u_{22}\vec{\varphi}_2^4\right\}. \end{aligned}$$

Taking the logarithm of this series, we obtain

$$\ln\left[I\left(\vec{\varphi}_1(\mathbf{r})\right)\right] = \ln I_0 - 2u_{12}\langle\vec{\varphi}_2^2\rangle_0\ \vec{\varphi}_1(\mathbf{r})^2 - \left[u_{11} - 2u_{12}^2(\langle\vec{\varphi}_2^4\rangle_0 - \langle\vec{\varphi}_2^2\rangle_0^2)\right]\ \vec{\varphi}_1(\mathbf{r})^4 + \ldots$$

where the notation $\langle \ldots \rangle_0$ represents

$$\langle \ldots \rangle_0 = \frac{\int d\vec{\varphi}_2 \ldots e^{-a\vec{\varphi}_2^2 - u_{22}\vec{\varphi}_2^4}}{\int d\vec{\varphi}_2 e^{-a\vec{\varphi}_2^2 - u_{22}\vec{\varphi}_2^4}}$$

Thus, $H_{eff}[\vec{\varphi}_1(\mathbf{r})]$ of Eq. (6.6) contains a term $u_{eff} \int d^3\mathbf{r}\ \vec{\varphi}_1(\mathbf{r})^4$, where

$$u_{eff} = u_{11} - 2u_{12}^2 \Big\langle \big(\vec{\varphi}_2^2 - \langle \vec{\varphi}_2^2 \rangle_0\big)^2 \Big\rangle_0. \tag{6.7}$$

Rescaling $\vec{\Phi}_2 = a^{-1/2}\vec{\varphi}_2$ we have

$$u_{eff} = u_{11} - 2\frac{u_{12}^2}{a^2} f_n\left(\frac{u_{22}}{a^2}\right) \tag{6.8}$$

where the function $f_n(x) = \langle \vec{\Phi}_2^4 \rangle - \langle \vec{\Phi}_2^2 \rangle^2$, and

$$\langle \ldots \rangle = \frac{\int d\vec{\Phi}_2 \ldots e^{-\vec{\Phi}_2^2 - x\vec{\Phi}_2^4}}{\int d\vec{\Phi}_2 e^{-\vec{\Phi}_2^2 - x\vec{\Phi}_2^4}}.$$

For small and large argument, the function $f_n(x)$ has the asymptotic forms

$$f_n(x) \sim \begin{cases} \frac{n}{2} & x = 0 \\ \frac{c_n}{x} & x \gg 1 \end{cases}$$

where $c_n = n/4 - \big(\Gamma(1/2 + n/4)/\Gamma(n/4)\big)^2$ is a monotonically increasing function of n bounded between $c_1 = 0.136\ldots$ and $c_\infty = 1$.

Returning to the u_{eff} of Eqs. (6.7) and (6.8), and taking $u_{11} = u_{22} = u$, and $u_{12} = ku$, and writing $x = u/a^2$, we have

$$u_{eff} = \begin{cases} u & x \to 0 \\ u\left[1 - 2k^2 c_n\right] & x \to \infty. \end{cases}$$

Thus we find that the nature of the transition, determined by the sign of u_{eff}, can be changed by the parameter k. We note that the transition is continuous for $k^2 < 1/2c_n$, and discontinuous for $k^2 > 1/2c_n$. Thus, for large x (parameter a small) we can change the nature of the transition by tuning the couplings u_{ij} between the critical and non-critical modes.

6.3 Conclusions

We began this chapter by with the aim of bridging the gap between two observations: (i) for $n \to \infty$ the analytical work of Chapters 4 and 5 predicted a continuous transition; (ii) for $n = 3$, simulations of the ordering transition showed a discontinuous transtion[59]. In this chapter we have provided two complementary approaches to building an analytical understanding of the transition. In the first, we wrote the free energy as an expansion in powers of $1/n$ and found that, for any finite n the transition appears to be discontinous. In the second, we integrated out fluctuations of the non-critical mode and showed that both continuous and discontinuous transitions are achievable within this framework.

It is important to recognise that both these approaches represent a preliminary attempt to understand the transition. In the first approach, it would be possible to add extra parameters into the propagators of Eq. (6.2) to choose these parameters phenomenologically. More precisely, the term q^2 in the propagator $\langle \varphi_1^a(\mathbf{q})\varphi_1^a(-\mathbf{q})\rangle_0$ could be modified to cq^2 to allow for an additional, model-dependent parameter. In the second approach we allowed more flexibility by having a larger set of adjustable parameters, $\{a, u_{11}, u_{12}, u_{22}\}$, and so a richer variety of critical behaviour is perhaps not too surprising.

Finally, we remark that both the approaches represent a first attempt at understanding the transition. A more sophisticated and complete treatment would involve a full renormalisation group calculation. We leave this for future work.

Chapter 7

Effects of Disorder on Frustrated Lattices

7.1 Motivation

A characteristic feature of GFAFMs with a macroscopically degenerate ground-state manifold is that their interaction matrices diagonalise to generate low-lying, dispersionless energy bands. This immediately leads to the interesting question of what might be the impact of applying a disorder-induced perturbation to any system whose interaction matrix contains such flat bands. Motivated by this observation, in this Chapter we investigate a specific example of such a situation: we provide a numerical study of a tight-binding model on a two-dimensional pyrochlore lattice with nearest-neigbour hopping in the presence of on-site disorder. Tight binding models with disorder have been very extensively studied as models for conductors with impurities, and we start with a short review of ideas from that field.

7.2 Background on Localisation

7.2.1 Physical Origin of Quenched Disorder

In any real crystalline lattice, some amount of disorder is inevitable. Disorder may enter through many processes, the most notable of which for systems studied in this thesis is atomic impurities within the crystal. Since the positions of the component atoms of a given crystalline lattice are fixed unless the crystal melts, disorder from random atomic impurities is a form of *quenched*

disorder. Using a tight-binding approximation to model a system with quenched disorder, we treat on-site energies and hopping strengths as random variables taken from some statistical distribution, the exact form of which affects physical properties.

7.2.2 Localisation in Eigenfunctions of Linear Operators

In a seminal work of 1958 [6], P.W. Anderson recognised that single-particle wavefunctions of Hamiltonians of disordered quantum systems could be exponentially localised to finite regions of space. Subsequently, mathematicians and mathematical physicists began work on looking at the eigenfunctions of more general linear operators whose matrix elements have a component of randomness. This randomness can be either in the diagonal, or off-diagonal matrix elements. Eigenfunctions were found to be localised under the conditions of high disorder strength or at energies close to the edges of the energy spectrum[52, 34].

Such operators can describe a large number of physical systems. Localisation as a phenomenon is observed in, for example: localised electrons in an insulating solid, the effect of disorder on spin-wave dispersion, single-electron states in quantum Hall systems.

7.2.3 Localisation in Tight-Binding Models

Within the framework of the tight-binding model of a crystalline solid, the Hamiltonian is constructed as a sum of the energies of individual atomic states (on-site energies), plus hopping matrix elements that result from weak overlap between the atomic states on neigbouring sites. Whether or not the single-particle eigenstates of the Hamiltonian are extended or localised depends on the variance in the energy of on-site terms, the range of the hopping elements, and the lattice dimensionality. For example, in one- or two-dimensional lattices, any disorder in on-site energies results in localisation of one-particle states[2].

In the 1960s it was shown by Mott [53] that localised and extended states (those not confined to a finite region of space) could not coexist at a given energy. Without disorder, the density of states profile contains sharp band edges. Since disorder smears out these sharp band-edges, in the tails of the density of states, there should be regions where the this density is so low that states are localised. The energy at which there is a transition between extended and localised states defines the "mobility edge" within these tails [41]. Thus, there are two mobility edges:

E_c at the lower end of the energy spectrum, and E_c' at the upper end. As the disorder is increased, these mobility edges move towards the centre of the band until, at some critical value of disorder, the two mobility edges coincide and the crystal becomes insulating. Alternatively, if in the metallic phase the Fermi energy is not in the centre of the band, a transition can be achieved when either of the mobility edges crosses the Fermi energy. Both of these situations are disorder-induced metal–insulator transition. For a recent review of metal–insulator transitions, see Reference [21].

The quantum mechanical nature of the localisation process makes it difficult to predict in a straightforward way which systems exhibit localisation. A classically localised particle stuck in a potential well can delocalise through quantum-mechanical tunnelling; as seen in Bloch states of a metal. Conversely, a classically delocalised particle may become localised through coherent quantum-mechanical backscattering. A survey of many of the theoretical tools for investigating the issue of localisation, as well as much experimental data, is provided in Reference [34].

7.2.4 Characterisation of Localised States

In a system where the single-particle states are localised it is possible to introduce a localisation length λ as the decay length of the envelope of a single-particle wavefunction. A single-particle wavefunction can become localised in an accidental potential well; outside this well, in the exponentially decaying tails of the state, we define

$$\psi(\mathbf{r}) = f(\mathbf{r})e^{-r/\lambda} \qquad \text{as } r \to \infty, \tag{7.1}$$

where $f(\mathbf{r})$ is a randomly varying function whose variance does not depend on $\mathbf{r}$. Close to a mobility edge, the localisation length diverges with the characteristic form[17, 40, 67]

$$\lambda \sim (E_c - E)^{-\nu} \qquad \text{for localised states.} \tag{7.2}$$

On the metallic side of the mobility edge, it is possible to characterise extended states through the d.c. conductivity, $\sigma_{d.c.} \sim (E - E_c)^s$. Using a scaling relation, Wegner[67] showed the conductivity is related to the divergence of the localisation length in that $s = \nu$. Here, however, it is sufficient to note that extended states have $\lambda \to \infty$.

7.2.5 Models with Long-Range Hopping

It was recognised as early as the 1958 paper of Anderson[6] that whether or not quantum states localise depends on the range of hopping matrix elements. Consider a Hamiltonian of the form

$$\mathcal{H} = \sum_{ij} |\mathbf{r}_i\rangle V_{ij} \langle \mathbf{r}_j| \tag{7.3}$$

where $V_{ij} = |\mathbf{r}_i - \mathbf{r}_j|^{-\alpha} G_{ij}(1-\delta_{ij})$, and each matrix element G_{ij} is selected independently from a box distribution of width $2W$. This Hamiltonian describes a tight-binding model with no randomness in on-site terms, and random hopping strength that decays in distance with the power-law form $r^{-\alpha}$. When these hopping terms decay sufficiently slowly with distance, the long-range hopping processes between atomic sites ensures that single-particle states will be extended; conversely, for hopping terms that fall off sufficiently quickly with distance, states may be localised. At a critical value of $\alpha = \alpha_c$, the state will be critical. Anderson's paper recognised that the critcal value between localised ($\alpha > \alpha_c$) and extended ($\alpha < \alpha_c$) states occurs at $\alpha_c = d$.

Some time later, in the investigation of models with long-range hopping, the critical case of $\alpha = d = 1$ was studied in two limits: the weak coupling limit was given a systematic analytical treatment through mapping onto a non-linear σ-model by Mirlin *et al.*[48] (analogous to a conventional Anderson transition at $d = 2 + \varepsilon$ with $\varepsilon \ll 1$); the strong coupling case, analogous to a conventional Anderson transition at $d \gg 1$, was treated in detail using another RG method developed earlier by Levitov for related problems[39, 47]. Later, by studying fluctuations of wavefunctions (specifically the inverse participation ratios, $\langle |\psi(\mathbf{r})|^{2q} \rangle$) for a family of critical points in one-dimenstion, Evers and Mirlin[20] investigated the critical states in detail in both the weak- and strong-coupling regimes. The model of power-law random banded matrices (PRBM) takes the matrix elements of V_{ij} to have the variance $\langle |V_{ij}|^2 \rangle = a^2(|\mathbf{r}_i - \mathbf{r}_j|)$, where $a^2(r) = \left[1 + (r/b)^{2\alpha}\right]^{-1}$, and so introduces the additional parameter b. Taking $\alpha = 1$ generates a line of critical points as a function of b, and allows for a systematic investigation of both the strong- ($b \ll 1$) and weak-coupling ($b \gg 1$) regimes.

7.3 Localisation in Models with Flat Bands

7.3.1 Random Perturbations on Eigenstates from a Flat Band

The Hamiltonians in this chapter may decomposed into two pieces:

$$\mathcal{H} = \mathcal{H}_0 + \mathcal{H}_{dis}, \tag{7.4}$$

where the translationally-invariant part $\mathcal{H}_0$ is characterised by nearest-neighbour interactions of energy J and has low-lying flat-bands in its energy spectrum; the Hamiltonian containing quenched disorder in on-site energies, $\mathcal{H}_{dis}$, is characterised by energy scale W. We now discuss these two terms separately.

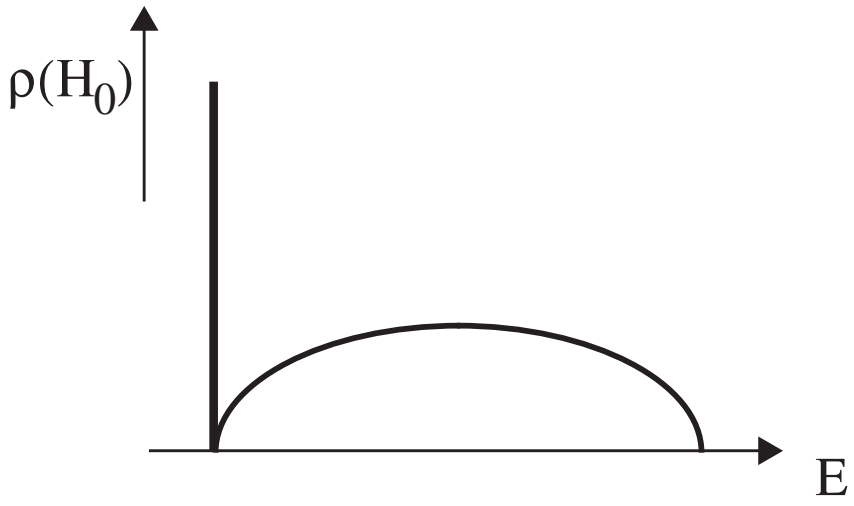

Figure 7.1: Schematic representation of the density of states, $\rho(\mathcal{H}_0)$, plotted as a function of energy E. The broad band has a width $\mathcal{O}(J)$.

The interaction matrix J_{ij} of $\mathcal{H}_0$, may be diagonalised and leads to the existence of wavevector-independent low-lying "flat bands"; these flat bands produce a delta function in the density of states (DoS) at the flat-band energy, $\mathcal{E}_0$, which we choose to define as the zero of energy. For $\mathcal{H}_0$ a generic profile for the DoS, $\rho(\mathcal{H}_0)$, is illustrated in Figure 7.1. In the same way as we did in Section 2.2, we define another operator that projects only onto states of energy $\mathcal{E}_0$: this operator, $\mathcal{P} = \sum_{\mathbf{q}} |\psi^{flat}(\mathbf{q})\rangle\langle\psi^{flat}(\mathbf{q})|$, is again non-analytic in q-space. The non-analyticity is at the wavevector where the dispersive band touches the flat band(s). The impact of this non-analyticity is that, in real space, the projector is of a power-law form, having a decay envelope r^{-d}, where d is the dimensionality of the lattice.

The Hamiltonian of the quenched, random disorder, $\mathcal{H}_{dis}$, contains only on-site energies. For disorder of width $2W$ we may write

$$\mathcal{H}_{dis} = W \sum_i \epsilon_i |\psi_i\rangle\langle\psi_i|,$$

where ϵ_i is a random variable chosen from a box distribution on the interval $[-1, 1]$, and $|\psi_i\rangle$ is the amplitude of a state on the ith site.

In the regime $W \ll J$, the DoS $\rho(\mathcal{H})$ is similar to $\rho(\mathcal{H}_0)$: the main difference being that the delta function in $\rho(\mathcal{H}_0)$ is broadened into a narrow peak of width $O(W)$. This is illustrated in Figure 7.2. Note that for $W \neq 0$ the narrow peak in $\rho(\mathcal{H}_0)$ merges into the continuum of other states. Only in the limit of $W \to 0$ is this low-lying narrow peak distinct from the broad band. In order to probe behaviour for $W \to 0$ it is justfied to project $\mathcal{H}_{dis}$ onto the manifold of ground states of $\mathcal{H}_0$, and see how the lifting of the degeneracy reorganises these states.

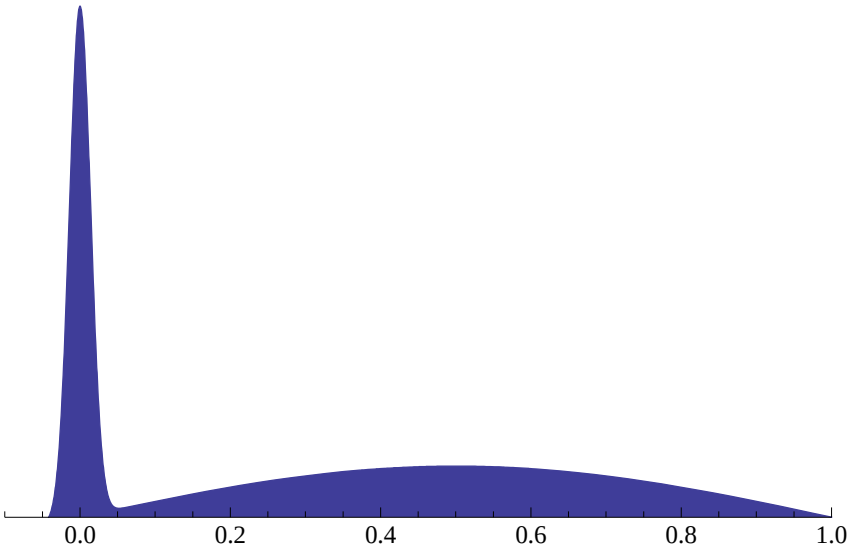

Figure 7.2: Schematic representation of the density of states, $\rho(\mathcal{H})$, plotted as a function of energy E (arbitrary units). The narrow peak has characteristic width W, and the broad band width J. In this example, $W \ll J$.

Projecting $\mathcal{H}$ onto the set of states $\{|\psi^{flat}\rangle\}$ generates the effective Hamiltonian

$$\mathcal{H}_{eff} = \mathcal{P}\mathcal{H}\mathcal{P} = \mathcal{P}\mathcal{H}_{dis}\mathcal{P},$$

where $\mathcal{H}_{eff}$ has the form

$$\mathcal{H}_{eff} = W \sum_{ij} |\psi_i\rangle V_{ij} \langle\psi_j|, \tag{7.5}$$

and $W\,V_{ij}$ is the strength of interactions between lattice sites i and j

By projecting the on site disorder terms onto the flat bands of $\mathcal{H}_0$, the energy scale J that was present in Eq. (7.4) has dropped out of the Hamiltonian $\mathcal{H}_{eff}$. After projection we have $\langle V_{ij}\rangle = 0$. Furthermore, as a result of the long-range nature of the projection operator, and most crucially, the off-diagonal elements of V_{ij} have, for $|\mathbf{r}_i - \mathbf{r}_j| \gg 1$, the asymptotic form $\langle |V_{ij}|^2\rangle^{1/2} \sim |\mathbf{r}_i - \mathbf{r}_j|^{-d}$.

Comparing $\mathcal{H}_{eff}$ with $\mathcal{H}$ of Equation (7.3), and through the discussion of Section 7.2.5, $\mathcal{H}_{eff}$ contains hopping elements that fall off in distance as $r^{-\alpha_c}$, and so single-particle eigenstates $|\psi_{eff}\rangle$ are expected to be critical.

In Section 7.5 we will introduce a tight-binding model with a Hamiltonian of the form of Eq. (7.5) for $d = 2$, and use numerical methods to investigate the nature of its single-particle eigenstates states as $W \to 0$..

7.3.2 Application to spin-waves in GFAFMs

Although the motivation for this work, as outlined in Section 7.1, arises from the physics of frustrated magnets, we will make no direct reference to magnetic systems in the following sections. Nevertheless, localisation in the presence of flat bands does have application to GFAFMs. To see this, consider the Hamiltonian $\mathcal{H} = \sum_{ij} J_{ij}\,\mathbf{S}_i \cdot \mathbf{S}_j$. Studying low-energy excitations of this Hamiltonian is possible provided the classical ground state has translational invariance. Provided that this is the case spin-wave excitations can be investigated by expanding the Hamiltonian to quadratic order in $\delta\mathbf{S}_i$, where $\delta\mathbf{S}_i$ is a small deviation of the ith spin from the classical ground-state orientation. Where the ground state has no translational invariance, studying excitations is generally very difficult. Therefore, as a particularly simple case, consider a GFAFM with disorder in elements of J_{ij}, but with the spins fully polarised by a strong magnetic field in the z-direction. Low-energy excitations may now be investigated by performing a Holstein-Primakoff transformation[29] to expand the Hamiltonian about the spin-polarised ground state.

Writing the Hamiltonian of the Heisenberg model in the presence of a field

$$\mathcal{H} = \sum_{ij} J_{ij} \mathbf{S}_i \cdot \mathbf{S}_j - h \sum_i S_i^z,$$

we can recast the operators for the spin components in terms of bosonic creation and annihilation operators $a_i^\dagger$ and a_i, with

$$S_i^z = S - a_i^\dagger a_i, \quad S_i^+ = (2S)^{1/2} a_i, \quad S_i^- = (2S)^{1/2} a_i^\dagger,$$

to obtain

$$\mathcal{H} = S \sum_{ij} J_{ij} (a_i^\dagger a_j + a_j^\dagger a_i) - \mu \sum_i a_i^\dagger a_i + \mathcal{O}(S^0), \tag{7.6}$$

where $\mu = zJS - h$, and z is the coordination number of the lattice.

In this way, it is possible to see the connection between the Hamiltonian of Eq. (7.6) and that of Eq. (7.5).

7.3.3 Recent developments on flat-band localisation

There has been a small amount of earlier work of flat-band localisation. Here we provide a brief review of that work. It is well known that, for $d = 3$, a disorder-induced delocalisation–localisation transition happens at some critical value of $W = W_c \neq 0$, with extended states at $W < W_c$ and localised states for $W > W_c$.

Recent work by Goda *et al.*[26] on disorder-induced transitions in the presence of *flat bands* claimed to identify an additional feature: a localisation–delocalisation transition at W_c', where $W_c' < W_c$. However, for finite W, the flat band is no longer present. In later work[55], they clarify that the localisation persists even when the strength of disorder is numerically as small as possible, and thus that random perturbation on the flat band appears to lead to localisation. In another work, a flat-band model with interactions is analysed using dynamical mean-field theory is in Reference [63], and they note that the presence of interactions in that model enhances delocalisation.

7.4 Transfer Matrix Methods

In order to investigate the localisation length in a disordered crystal, we study finite-sized lattice systems on a strip-like geometry of length L, and cross-section N^{d-1}, where $N \ll L$. We will calculate localisation lengths by analysing products of random matrices[58, 43].

Considering first a tight-binding model in a one-dimensional system, we have the single-particle wavefunction $|\psi\rangle$ with amplitude ψ_n at each lattice site. For a given site n, we take the incoming probability amplitudes from the left and right to be z_n and w_{n+1} respectively. Defining a random scattering matrix S_n at the nth site we have

$$\begin{pmatrix} z_{n+1} \\ w_n \end{pmatrix} = S_n \begin{pmatrix} z_n \\ w_{n+1} \end{pmatrix},$$

where w_n and z_{n+1} are the outgoing probability amplitudes to the left and right respectively. This situation is illustrated in Figure 7.3. Also, by current conservation we have

$$|z_{n+1}|^2 - |w_{n+1}|^2 = |z_n|^2 - |w_n|^2$$

, a condition that requires the matrix S_n to be unitary. Alternatively we may choose to study

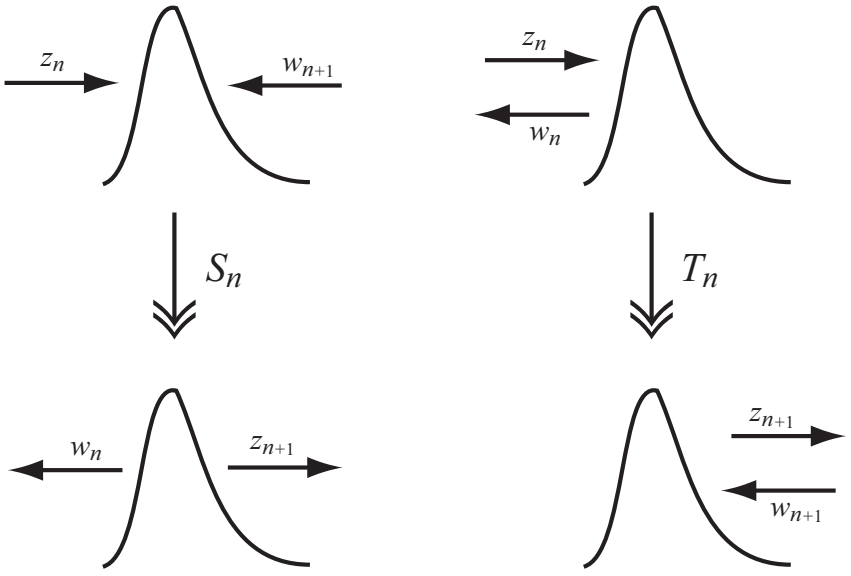

Figure 7.3: Representation of scattering matrix S_n (*left*) and transfer matrix T_n (*right*) acting at the random potential of site n.

the problem in the less physical but, for numerical calculations, more convenient transfer matrix

framework. We define a transfer matrix T_n according to

$$\begin{pmatrix} z_{n+1} \\ w_{n+1} \end{pmatrix} = T_n \begin{pmatrix} z_n \\ w_n \end{pmatrix},$$

and again illustrated in Figure 7.3. Now current conservation requires $T_n^\dagger J T_n = J$, where $J = \mathrm{diag}(1, -1)$. By defining the product of random matrices $Q_L = \prod_{n=0}^{L-1} T_n$, we set the current exiting from the left end of the sample $w_0 = 0$ and thus obtain

$$\begin{pmatrix} z_L \\ w_L \end{pmatrix} = Q_L \begin{pmatrix} 1 \\ 0 \end{pmatrix}.$$

Oseledec's theorem [56] states that there exists a limiting matrix

$$\Gamma = \lim_{L \to \infty} (Q_L Q_L^\dagger)^{1/2L} \tag{7.7}$$

with eigenvalues $\exp(\pm\gamma)$, where $\pm\gamma$ denotes the characteristic Lyapunov exponents of Q_L. Localised eigenstates of a Hamiltonian $\mathcal{H}$ at a given E are exponentially increasing from the left and right end of the system. Matching these states in the bulk of the sample [52], we may identify the inverse localisation length λ^{-1}, defined in Eq. (7.1), of this state with the Lyapunov exponent γ.

7.4.1 Transfer Matrix for a Tight-Binding Model

To find Lyapunov exponents using the transfer matrix method, we begin by writing the Schrödinger equation for the tight-binding model in one dimension: for an eigenstate $|\Psi\rangle$ of energy E having site amplitudes $\langle \mathbf{r}_i | \Psi \rangle = \psi_i$, on-site energies ϵ_i and nearest-neighbour hopping of strength t we have

$$E\psi_i = \epsilon_i \psi_i + t(\psi_{i-1} + \psi_{i-1}). \tag{7.8}$$

We rearrange this to give

$$\psi_{i+1} = t^{-1}(E - \epsilon_i)\psi_i - \psi_{i-1}.$$

This equation can be written in the form

$$\underbrace{\begin{pmatrix}\psi_{i+1}\\ \psi_i\end{pmatrix}}_{v_{i+1}} = \underbrace{\begin{pmatrix}t^{-1}(E-\epsilon_i) & -1\\ 1 & 0\end{pmatrix}}_{T_i}\underbrace{\begin{pmatrix}\psi_i\\ \psi_{i-1}\end{pmatrix}}_{v_i},$$

so that, by comparing the amplitudes of ψ_{L+1} and ψ_L to a known ψ_1 and ψ_0 to obtain growth rates, the single Lyapunov exponent γ can be obtained from the two eigenvalues $\exp(\pm\gamma)$ of the limiting matrix $\Gamma = \lim_{L\to\infty}(Q_L Q_L^\dagger)^{1/2L}$.

The extension to two-dimensions is straightforward: the strip is split into L "slices", each of width N. The N site amplitudes on the ith slice are represented by the N-component vector $\boldsymbol{\psi}_i$. The matrix T_i has size $2N \times 2N$, and so Γ will have $2N$ eigenvalues, leading to N plus–minus pairs of distinct Lyapunov exponents $\pm\gamma_j$. Since Γ is Hermitian, its eigenvectors $u^{(j)}$ form an orthogonal set. The γ_j characterise the growth rates in each of these orthogonal directions. The smallest positive Lyapunov exponent γ_0 corresponds to the longest localisation length in the system.

7.4.2 Numerical Implementation

Introduce vectors $\{\mathbf{v}_i\}$ constructed from the site amplitudes $\mathbf{v}_i = (\boldsymbol{\psi}_{i+1} \quad \boldsymbol{\psi}_i)^T$. Here, the index i represents the slice, and the component $[\boldsymbol{\psi}_i]_j$ the site j on that slice. Thus $i = 0, 1, \ldots L-1$, and $j = 1, 2, \ldots 2N$.

Since we wish to calculate the $2N$ Lyapunov exponents, we introduce $2N$ starting vectors that form an orthonormal set: we call these $\hat{\mathbf{u}}_0^{(k)}$, where the superscript k denotes a vector within the set. We take as the orthonormal set $\left[\hat{u}_0^{(k)}\right]_j = \delta_{jk}$.

In this subsection we also introduce a set of vectors $\{u\}$, where the orthogonal set $\{u_i\}$ will be obtained from orthogonalising within the set $\{v_i\}$. Further, we define unit vectors $\{\hat{u}\}$, where $\{\hat{u}_i\}$ are obtained from normalising the set $\{u_i\}$.

We follow the numerical procedure of Reference [8, 9].

Take as a starting set the orthonormal set of vectors $\hat{u}_0^{(k)}$ that have the entries $\left[\hat{u}_0^{(k)}\right]_j = \delta_{jk}$.

1. From the set $\hat{\mathbf{u}}_0^{(k)}$, obtain the set $\mathbf{v}_1^{(k)}$ using $\mathbf{v}_i^{(k)} = \mathbf{T}_{i-1}\hat{\mathbf{u}}_{i-1}^{(k)}$.

2. To obtain the set $\mathbf{u}_1^{(k)}$, perform a Gram-Schmidt orthogonalisation procedure on the set

$\mathbf{v}_1^{(k)}$ by doing, in sequence for $k = 1, 2, \ldots 2N$,

$$\mathbf{u}_i^{(k)} = \mathbf{v}_i^{(k)} - \sum_{k'<k} \frac{\mathbf{v}_i^{(k)} \cdot \mathbf{u}_i^{(k')}}{|\mathbf{u}_i^{(k')}|^2} \mathbf{u}_i^{(k')}.$$

3. Calculate logarithmic growth rates $g_1^{(k)}$ using $g_i^{(k)} = \ln |\mathbf{u}_i^{(k)}|$, and then normalise to obtain the orthonormal set of vectors $\hat{\mathbf{u}}_1^{(k)}$ using $\hat{\mathbf{u}}_i^{(k)} = e^{-g_i^{(k)}} \mathbf{u}_i^{(k)}$.

Repeat Steps 1 – 3, replacing $i = 1$ with, in sequence, $i = 2, 3, \ldots, L$, and then calculate the average of these logarithm of the growth rates as

$$\overline{g^{(k)}} = \frac{1}{L} \sum_{i=1}^{L} g_i^{(k)},$$

where the error on $\overline{g^{(k)}}$ may be reduced by taking a longer sample length L. Writing the set $\overline{g^{(k)}}$ in order of descending size, the first N values correspond to Lyapunov exponents $\gamma_{N-1}, \gamma_{N-2}, \ldots, \gamma_0$, and the $N+1$ to $2N$ values to exponents $-\gamma_0, -\gamma_1, \ldots, -\gamma_{N-1}$.

To calculate all $2N$ exponents, this algorithm requires a number of operations that scales as $N^3 L$ (this is dominated by the orthogonalisation procedure). In order to reduce processor time, it is possible to orthogonalise the vectors every L_{orth} iterations, provided that L_{orth} is small enough that directions with large growth rates do not cause data for small growth rates to be lost due to a limitation in processor precision. The value of L_{orth} will be determined on an ad hoc basis.

For $L_{orth} \neq 1$, we make the modifications $g_i^{(j)} \to g_i^{(j)}/L_{orth}$, and $\gamma_j \to \frac{L_{orth}}{L} \sum_{i=0}^{L/L_{orth}} g_i^{(j)}$.

7.4.3 Finite size scaling

The scaling description of localisation, introduced by E. Abrahams and others[67, 2] in 1979[2], is based on the assumption that, close to a metal–insulator transition, only one variable is needed to describe the critical behaviour. In essence, the scaling theory states that the conductance of a disordered electronic system depends in a universal manner only on the length scale of the system compared to the localisation length (or correlation length in a metal).

For a state $\psi(\mathbf{r})$ of the form in Eq. (7.1), it is straightforward to determine the localisation

length as

$$-\frac{2}{\lambda} = \lim_{L\to\infty} \frac{1}{L} \ln(\psi_L^2 + \psi_{L+1}^2),$$

where, using the formalism of Section 7.4, we have $\lambda = \lambda(W, N)$. In order to extrapolate to infinite lattices, we would like to take $N \to \infty$.

It turns out that[13]

$$\frac{\lambda(W,N)}{N} = f\left(\frac{\lambda_\infty(W)}{N}\right),$$

where the function f depends only on a system's dimension, and not the disorder strength W.

For localised states in a system having with very large width N, such that $\lambda(W, N) \ll N$, we must have

$$\lim_{N\to\infty} \lambda(W,N) = \lambda_\infty(W),$$

indicating that the scaling function $f(x) \sim x$ as $x \to 0$. For localised states, the Lyapunov exponent $\gamma = 1/\lambda_\infty$ will be independent of N at large N.

In a system of extended states, where $\lambda(W, N) \gg N$ even for N large, the number of Lyapunov exponents scales as N^{d-1}: the largest of these is fixed, and set of exponents form a uniformly spaced set, so the smallest exponent scales as N^{1-d}[16, 44]. Hence, extended states are identified through

$$\lambda(W,N) \sim N^{d-1}$$

for N large.

The crossover between localised and extended states is the case of critical states. Such states have $\lambda_\infty \to \infty$, and so their characteristic size can only be set by the system width. For these states we therefore have

$$\lambda(W,N) \sim N,$$

indicating that $\gamma(W,N) = \frac{1}{\lambda(W,N)} \sim N^{-1}$.

At $d = 2$, the scaling of critical states with system size is identical to that of extended states, since both scale as $\sim N$. It is therefore useful to consider another quantity to distinguish critical from extended states; we briefly discuss such a method now.

7.4.3.1 Inverse Participation Ratio

The inverse participation ratio (IPR) is a quantity that stems directly from eigenfunctions of a Hamiltonian, rather than Lyapunov exponents. The IPR is the second moment of the probability density[66], $\langle|\psi(\mathbf{r})|^4\rangle$. In a d-dimensional system of linear dimension L, extended states are homogeneous in space: $|\psi(\mathbf{r})|^2 \sim L^{-d}$, indicating that $\langle|\psi(\mathbf{r})|^4\rangle \sim L^{-2d}$. States that are localised within a finite region λ have $|\psi(\mathbf{r})|^2 \sim \lambda^{-d}$ with probability $(\lambda/L)^d$, and have $|\psi(\mathbf{r})|^2 = 0$ otherwise. Therefore $\langle|\psi(\mathbf{r})|^4\rangle \sim \lambda^{-2d} \cdot (\lambda/L)^d$. We thus have

$$\langle|\psi(\mathbf{r})|^4\rangle \sim \begin{cases} L^{-2d} & \text{for extended states} \\ L^{-d} & \text{for localised states.} \end{cases} \tag{7.9}$$

Critical states have the form $\langle|\psi(\mathbf{r})|^4\rangle \sim L^{-x}$, for $d < x < 2d$.

7.5 Two-Dimensional Pyrochlore Lattice

We take as our example of a flat band tight-binding model the two-dimensional pyrochlore lattice illustrated in Fig 7.4. We choose this because the interaction matrix of this lattice has a low-lying flat band in its energy spectrum when $t_1 = t_2$, and also two-dimensional lattices are less computationally intensive to study in the transfer matrix formalism than are three-dimensional lattices.

7.5.1 Exact Results in the absence of Disorder

The Hamiltonian of the clean system is written

$$\mathcal{H}_0 = \sum_{ij} |\psi_i\rangle t_{ij} \langle\psi_j|,$$

where the energy minimum is chosen to be at $\mathcal{E}_0 = 0$. The elements of the matrix t_{ij} are t_1 for nearest-neighbours and t_2 for some next-nearest-neighbour hopping terms, as shown by the dashed lines of Figure 7.4. There is a flat band in the interaction matrix for $t_1 = t_2$, but for the purposes of computation is will be necessary to lift this degeneracy with $t_1 \neq t_2$, hence we discuss a general $t_1 - t_2$ model.

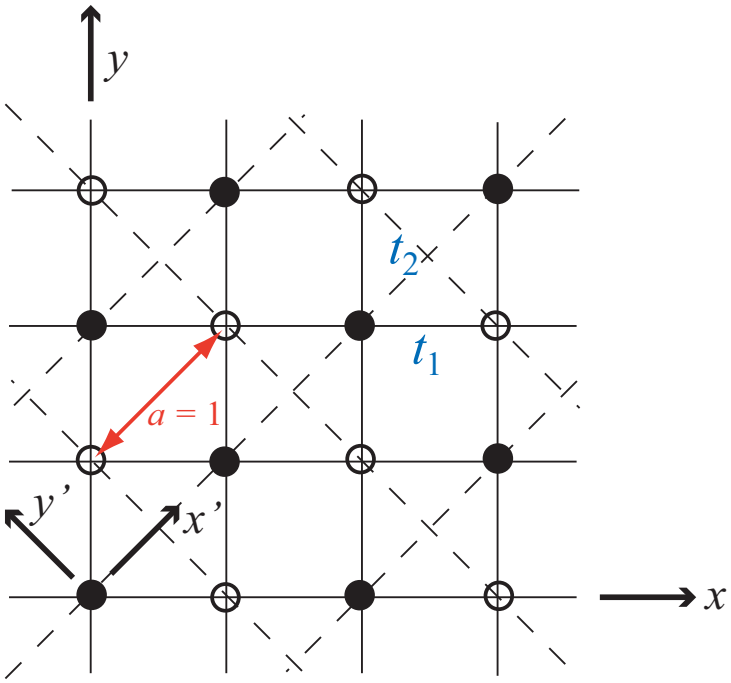

Figure 7.4: The two-dimensional pyrochlore lattice with hopping strengths t_1 and t_2 labelled. Solid circles represent a-type sites, and hollow circles b-type sites.

Taking the distance between two adjacent a-sites to be $a = 1$ and the direction x' along the lines of a-sites and the direction y' along the lines of b sites, the matrix t_{ij} is block-diagonalised under the Fourier transformation

$$\psi^a(\mathbf{q}) = \sum_{i\in a} e^{-i\mathbf{q}\cdot\mathbf{r}_i}\psi_i; \qquad \psi^b(\mathbf{q}) = \sum_{i\in b} e^{-i\mathbf{q}\cdot\mathbf{r}_i}\psi_i \tag{7.10}$$

to give, in the (a, b) basis

$$t(\mathbf{q}) = 2t \begin{pmatrix} c_{x'}^2 & (1+\sigma)c_{x'}c_{y'} \\ (1+\sigma)c_{x'}c_{y'} & c_{y'}^2 \end{pmatrix},$$

where $t_1 = t(1+\sigma)$, $t_2 = t$; $c_{x'} = \cos(q_{x'}/2)$ and $c_{y'} = \cos(q_{y'}/2)$. The matrix $t(\mathbf{q})$ has the eigenvalues $E^{\pm}(\mathbf{q})$, where

$$\frac{1}{t}E^{\pm}(\mathbf{q}) = c_{x'}^2 + c_{y'}^2 \pm \left[(c_{x'}^2 + c_{y'}^2)^2 + 4\sigma(2+\sigma)c_{x'}^2 c_{y'}^2\right]^{1/2}. \tag{7.11}$$

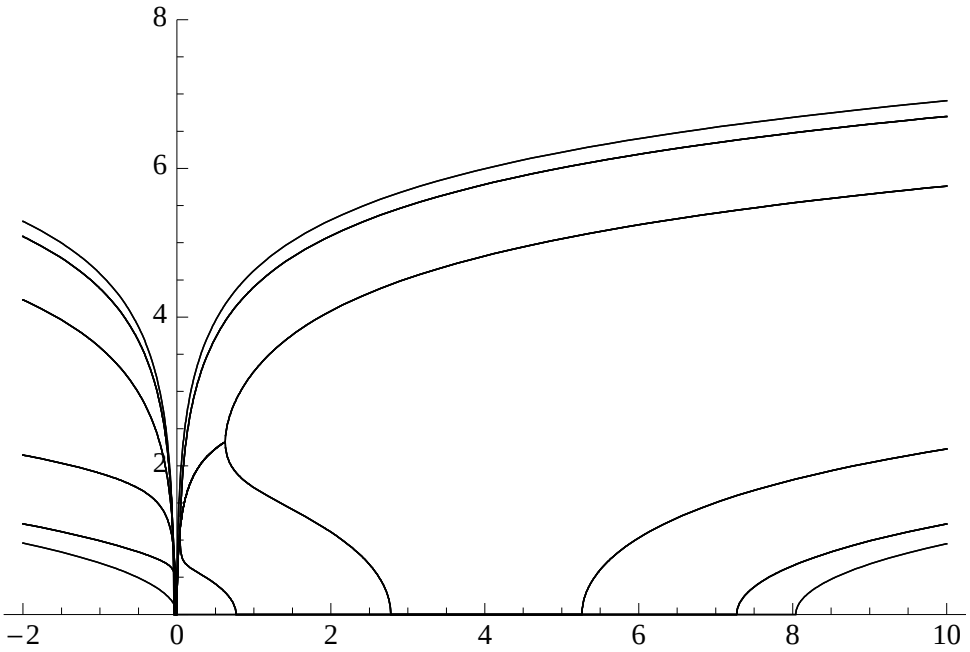

Figure 7.5: Exact results for a system of width 10 for $t = 2$ and $\sigma = 0.01$. x-axis is energy E and y-axis is inverse decay length $\lambda^{-1} = \mathrm{Im}\{q_x\}$.

Now taking $\sigma = 0$ and introducing the states

$$\psi^+(\mathbf{q}) = \frac{1}{\sqrt{c_{x'}^2 + c_{y'}^2}} \left(c_{x'}\psi^a(\mathbf{q}) + c_{y'}\psi^b(\mathbf{q}) \right)$$

and

$$\psi^-(\mathbf{q}) = \frac{1}{\sqrt{c_{x'}^2 + c_{y'}^2}} \left(c_{y'}\psi^a(\mathbf{q}) - c_{x'}\psi^b(\mathbf{q}) \right),$$

the Hamiltonian of the clean system is

$$\mathcal{H}_0 = \sum_{\mathbf{q}} \left\{ E^-|\psi^-(\mathbf{q})\rangle\langle\psi^-(\mathbf{q})| + E^+(\mathbf{q})|\psi^+(\mathbf{q})\rangle\langle\psi^+(\mathbf{q})| \right\}$$

where

$$E^- = 0; \qquad E^+(\mathbf{q}) = 2t[c_{x'}^2 + c_{y'}^2]. \tag{7.12}$$

For periodic solutions (real $q_{x'}$ and $q_{y'}$ in Eq. (7.10)), Eq (7.12) shows that $E_{min} < E < E_{max}$, where $E_{min} = 0$ and $E_{max} = 4t$. Outside these limits on E, complex values of $q_{x'}$ and $q_{y'}$ correspond to evanescent modes.

In order to determine whether modes are periodic or evanescent for a given energy, we can

invert Eq. (7.11) at a given σ. However, we would like to know the transport in the x-direction of Figure 7.4. We thus make the change of variables $x = (y' - x')/2$ and $y = (x' + y')/2$. We require periodic boundary conditions in the y-direction, and open boundary conditions in the x-direction. Taking as an example a system of width $N = 10$, ($q_y = n\pi/5$ for integer $n = -4, \ldots, 5$), the inverse decay length along x, $\lambda^{-1} = \mathrm{Im}\{q_x\}$ for each of the ten modes is plotted in Figure 7.5 as a function of energy E.

We now describe some of the key features of Figure 7.5. At $E = 0$, the location of the flat band, decay lengths $\lambda \to \infty$, and all modes are extended and periodic in the x-direction. With $t = 2$, $E_{min} = 0$ and $E_{max} = 8$. We find that all modes are localised for $E < E_{min}$ and for $E > E_{max}$. Within the band $E_{min} < E < E_{max}$, the number of extended states is: 1 for $E_{min} < E < 0.75$; 3 for $0.75 < E < 2.75$; 5 for $2.75 < E < 5.75$; 3 for $5.75 < E < 7.25$; 1 for $7.25 < E < E_{max}$. For $E < E_{min}$ and $E > E_{max}$ there appear to be 6 lines; in fact, the degeneracies of these six lines are $1, 2, 2, 2, 2$ and 1. This degeneracy is explained by the pairings of q_y wavevectors into $q_y = \{0, \pm\pi/5, \pm 2\pi/5, \pm 3\pi/5, \pm 4\pi/5, \pi\}$.

In Figure 7.6 we display data for the same parameters as Figure 7.5 except that $\sigma = 10^{-6}$. The features of the lowest $N/2$ exponents are identical (note that all modes are zero for $E = 0$); the principal difference is that the highest $N/2$ exponents are larger. In fact, for these largest $N/2$ exponents we find that $\lambda_i^{-1} \propto \log 1/\sigma$ as $\sigma \to 0$.

At all energies, we confirm that the lower $N/2$ correspond to modes $\psi^-(\mathbf{q})$, and the upper $N/2$ to $\psi^+(\mathbf{q})$. Recalling the discussion of Section 7.3.1, in order to enforce the function of $\mathcal{P}$ and project onto the flat band subspace, it is necessary to take the limit of $\sigma \to 0$ and study only the lowest $N/2$ exponents.

7.5.2 Weak Disorder

The Hamiltonian of the disorder, $\mathcal{H}_{dis}$ contains only onsite energies

$$\mathcal{H}_{dis} = W \sum_i \epsilon_i |\psi_i\rangle\langle\psi_i|$$

where ϵ_i is a random variable chosen from a uniform distribution on the energy interval $[-1, 1]$.

A system without disorder corresponds to $W = 0$. In the absence of disorder, the lattice is frustrated when $t_1 = t_2$: we thus require $\sigma = 0$ to enforce frustration, and take $E = 0$ to

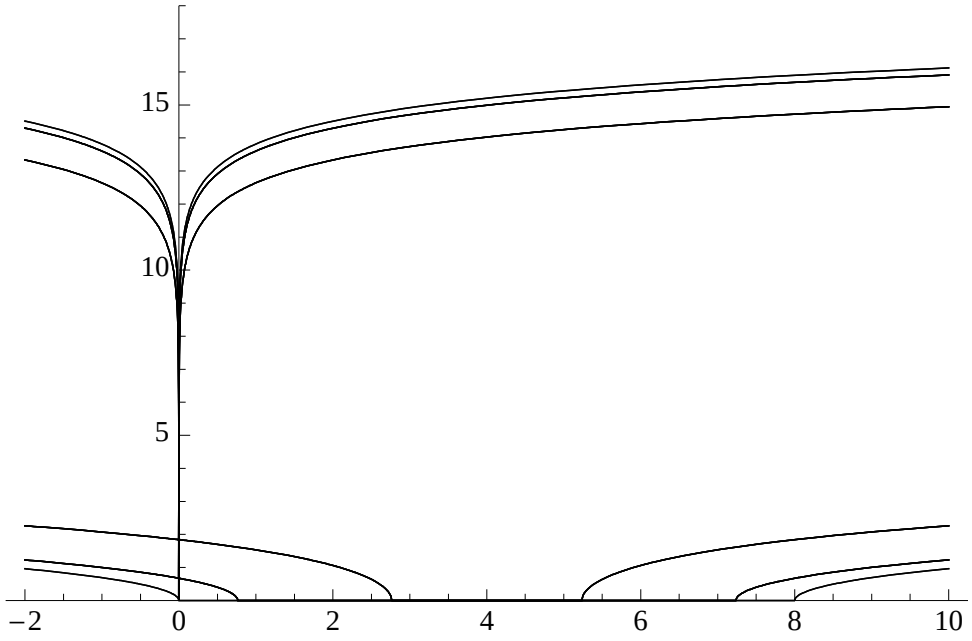

Figure 7.6: Exact results for a system of width 10 for $t = 2$ and $\sigma = 10^{-6}$. x-axis is energy E and y-axis is inverse decay length $\lambda^{-1} = \mathrm{Im}\{q_x\}$.

investigate the flat band. However, in order to keep the transfer matrices well-defined, it will be necessary to take $\sigma \neq 0$ in setting up the numerical implementation. Since we wish to study the *weak-disorder limit* of a *frustrated lattice*, we are ultimately interested in the quantity

$$\lim_{W\to 0}\left\{\lim_{\sigma\to 0}\gamma_i(E=0,W,\sigma)\right\}. \tag{7.13}$$

Consider the alternative of taking $W \to 0$ with σ finite. At $E = 0$, taking the limit of $W \to 0$ with finite σ, all Lyapunov exponents will tend to zero. The reason for this is that, as $W \to 0$, the Lyapunov exponents will recover the form of Figure 7.5 for $\sigma = 0.01$.

7.5.2.1 Explicit Form of Transfer Matrices

We now use the transfer matrix formalism to study the localisation propeties of the two-dimensional pyrochlore lattice in the presence of onsite disorder. In order to make the transfer matrices well-defined, we must take t_1 and t_2 in $\mathcal{H}_0$ to be inequivalent, and later take the limit $t_1/t_2 \to 1$ to study the frustrated case.

Using a tight-binding model in the (x, y) basis, we may write the Schrödinger equation:

$$E\Psi_{m,i} = \epsilon_{m,i}\Psi_{m,i} + t_1(\Psi_{m+1,i} + \Psi_{m-1,i} + \Psi_{m,i+1} + \Psi_{m,i-1}) + t_2(\Psi_{m+1,i+1} + \Psi_{m-1,i-1})$$

if (m,i) is a site of type a, and

$$E\Psi_{m,i} = \epsilon_{m,i}\Psi_{m,i} + t_1(\Psi_{m+1,i} + \Psi_{m-1,i} + \Psi_{m,i+1} + \Psi_{m,i-1}) + t_2(\Psi_{m+1,i-1} + \Psi_{m-1,i+1})$$

if (m,i) is a site of type b. We employ a numbering convention that, for an a-site, $m+i$ is even, and for a b-site, $m+i$ is odd.

We can eliminate from these two equations to generate a "transfer matrix" form. For $m+i$ even we have

$$\begin{aligned}\Psi_{m,i} = &\Big[\delta\Psi_{m-1,i-2} + \beta_{m-1,i-1}\Psi_{m-1,i-1} + \alpha_{m-1,i}\Psi_{m-1,i} - \gamma\Psi_{m-1,i+1}\Big] \\ &+\Big[\zeta\Psi_{m-2,i-2} + \delta\Psi_{m-2,i-1} - \gamma\Psi_{m-2,i} - \delta\Psi_{m-2,i+1}\Big] \end{aligned} \tag{7.14}$$

and for $m+i$ odd

$$\begin{aligned}\Psi_{m,i} = &\Big[-\gamma\Psi_{m-1,i-1} + \alpha_{m-1,i}\Psi_{m-1,i} + \beta_{m-1,i+1}\Psi_{m-1,i+1} + \delta\Psi_{m-1,i+2}\Big] \\ &+\Big[-\delta\Psi_{m-2,i-1} - \gamma\Psi_{m-2,i} + \delta\Psi_{m-2,i+1} + \zeta\Psi_{m-2,i+2}\Big] \end{aligned} \tag{7.15}$$

where we have defined the site-dependent quantities

$$\alpha_{m,i} = \frac{(1+\sigma)(E-\epsilon_{m,i}+1)}{\sigma(2+\sigma)}; \quad \beta_{m,i} = -\frac{(1+\sigma)^2 + E - \epsilon_{m,i}}{\sigma(2+\sigma)}$$

and site-independent quantities

$$\gamma = \frac{(1+\sigma)^2}{\sigma(2+\sigma)}; \quad \delta = \frac{1+\sigma}{\sigma(2+\sigma)}; \quad \zeta = \frac{1}{\sigma(2+\sigma)},$$

and E and $\epsilon_{m,i}$ are in units of t, and we have made the replacements $t_1 = t(1+\sigma), t_2 = t$.

It may be simpler to picture these two equations as a transfer matrix "motif" of Figure 7.7

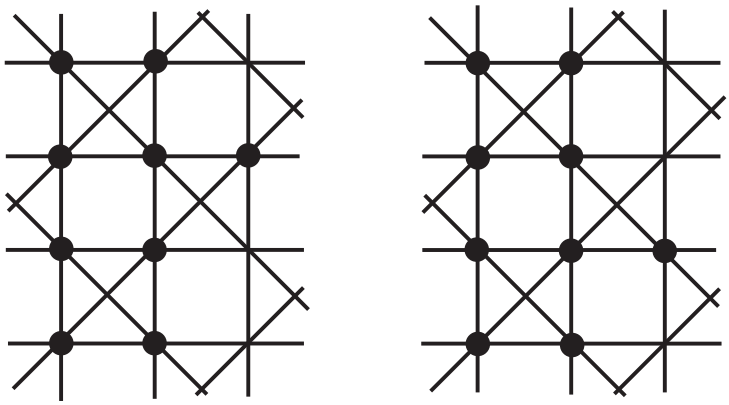

Figure 7.7: A pictorial representation of the transfer matrix equation. (*Left*) For the a site of the right column, the coefficients on the different sites are obtained from Eq. (7.14): left column from top, $-\delta, -\gamma, \delta, \zeta$; middle column from top $-\gamma, \alpha, \beta, \delta$. (*Right*) For the b site of the right column, the coefficients on the different sites are obtained from Eq. (7.15): left column from top, $\zeta, \delta, -\gamma, -\delta$; middle column from top $\delta, \beta, \alpha, -\gamma$.

For m even we have

$$\mathbf{T}_m^{even} = \begin{pmatrix} \mathbf{H}_m^{even} & \mathbf{V}^{even} \\ \mathbf{1} & \mathbf{0} \end{pmatrix} \tag{7.16a}$$

and for m odd we have

$$\mathbf{T}_m^{odd} = \begin{pmatrix} \mathbf{H}_m^{odd} & \mathbf{V}^{odd} \\ \mathbf{1} & \mathbf{0} \end{pmatrix} \tag{7.16b}$$

From Figure 7.7, $\mathbf{H}^{even}$ has a 2×4 block-diagonal form, with the blocks

$$\mathbf{H}_m^{even} = \begin{pmatrix} \dots & -\gamma & \alpha_{m,i} & \beta_{m,i+1} & \delta & \dots \\ \dots & \delta & \beta_{m,i} & \alpha_{m,i+1} & -\gamma & \dots \end{pmatrix}$$

where the $\alpha_{m,i}$ is on the diagonal at an even row/column i.

To employ periodic boundary conditions in the transverse direction we require the lattice to be an even width. This gives $H_{N+i,N+j} = H_{ij}$, where N is even.

The matrix on the odd slices also has the same form, except the blocks are now written

$$\mathbf{H}_m^{odd} = \begin{pmatrix} \dots & -\gamma & \alpha_{m,i} & \beta_{m,i+1} & \delta & \dots \\ \dots & \delta & \beta_{m,i} & \alpha_{m,i+1} & -\gamma & \dots \end{pmatrix}$$

where the $\alpha_{m,i}$ is on the diagonal at an odd row/column i. Similarly, the matrices $\mathbf{V}$ have a 2×4 block-diagonal form, where

$$\mathbf{V}^{even} = \begin{pmatrix} \dots & -\delta & -\gamma & \delta & \zeta & \dots \\ \dots & \zeta & \delta & -\gamma & -\delta & \dots \end{pmatrix}$$

with the $-\gamma$ of the top row on the diagonal at an even row/column, and

$$\mathbf{V}^{odd} = \begin{pmatrix} \dots & -\delta & -\gamma & \delta & \zeta & \dots \\ \dots & \zeta & \delta & -\gamma & -\delta & \dots \end{pmatrix}$$

with the $-\gamma$ of the top row on the diagonal at an odd row/column.

We now define the matrix

$$Q_L = \prod_{m=1,3,5,\dots}^{L-1} T_{m+1}^{even}\, T_m^{odd}$$

and calculate Lyapunov exponents $\gamma_j(W, \sigma)$ from Oseledec's Theorem, Eq. (7.7), using the protocol of Section 7.4.2.

7.6 Numerical Results

As a preliminary check on the accuracy of the transfer matrix method, we display results obtained at $W = 0$ for a system of $N = 10$ at $\sigma = 0.01$. We display results as a function of E in Figure 7.8. These are identical to results of Figure (7.5) which were obtained by diagonalising the Hamiltonian.

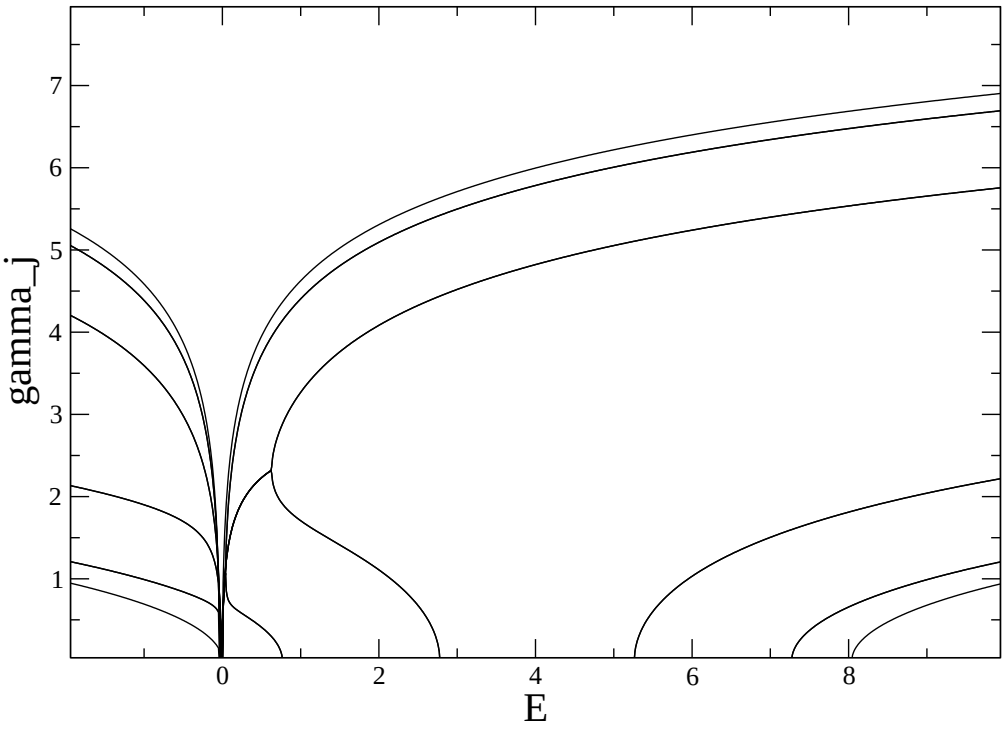

Figure 7.8: Simulation results for a system of width 10 for $\sigma = 0.01$, using $L = 10^6$. x-axis is E and y-axis is $\gamma_j = \lambda_j^{-1}$.

After this check, we now aim to collect results from the regime described by Eq. (7.13). A first task is to discover how the limits work out in practice. Eventually we will take the limit of $W \to 0$ while holding the ratio $W/\sigma \gg 1$ constant. One of the tasks in this section will be to find how large W/σ should be in order to approach the limit numerically.

For the remainder of this chapter, we set $t = 2$.

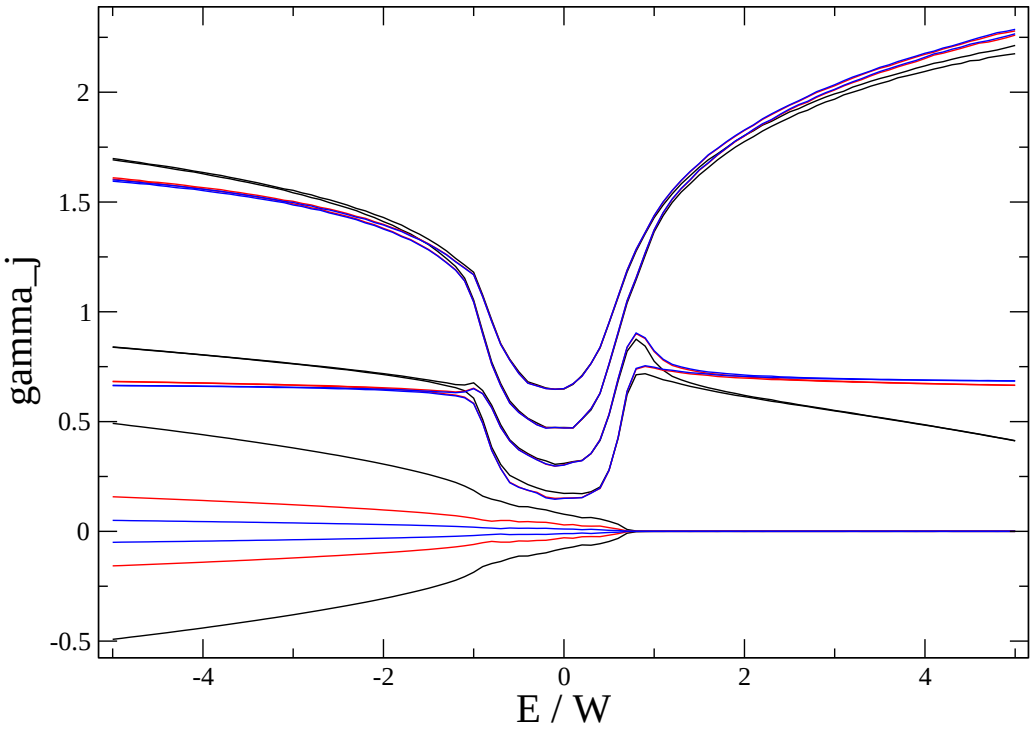

Figure 7.9: A plot of γ_j $(j = 0, 1, \ldots, 4)$ against E/W for a system of width 10. All data has $W/\sigma = 10$. We display the five smallest positive Lyapunov exponents for $W = 0.1$ (in black); $W = 0.01$ (red); $W = 0.001$ (blue). Note that this Figure also displays the smallest negative exponent, which forms a $\pm$ pair with γ_0.

7.6.1 Dependence of Eigenstates on Energy

We begin with a general study of the smallest $N/2$ exponents for a small system of width $N = 10$. Figure 7.9 displays the five smallest γ_j as a function of E/W for various values of W. In this Figure, we hold the ratio $W/\sigma = 10$.

Remarks on Figures 7.9 and 7.10

1. Most strikingly, none of the Lyapunov exponents vanish at $E = 0$.

2. For energies $|E| < \mathcal{O}(W)$ there is a trough for all Lyapunov exponents other than the smallest $j = 0$ exponent.

3. Exponents $j \neq 0$ are largely disorder-independent at $E = 0$. Only $\gamma_{j=0}$ exhibits a strong

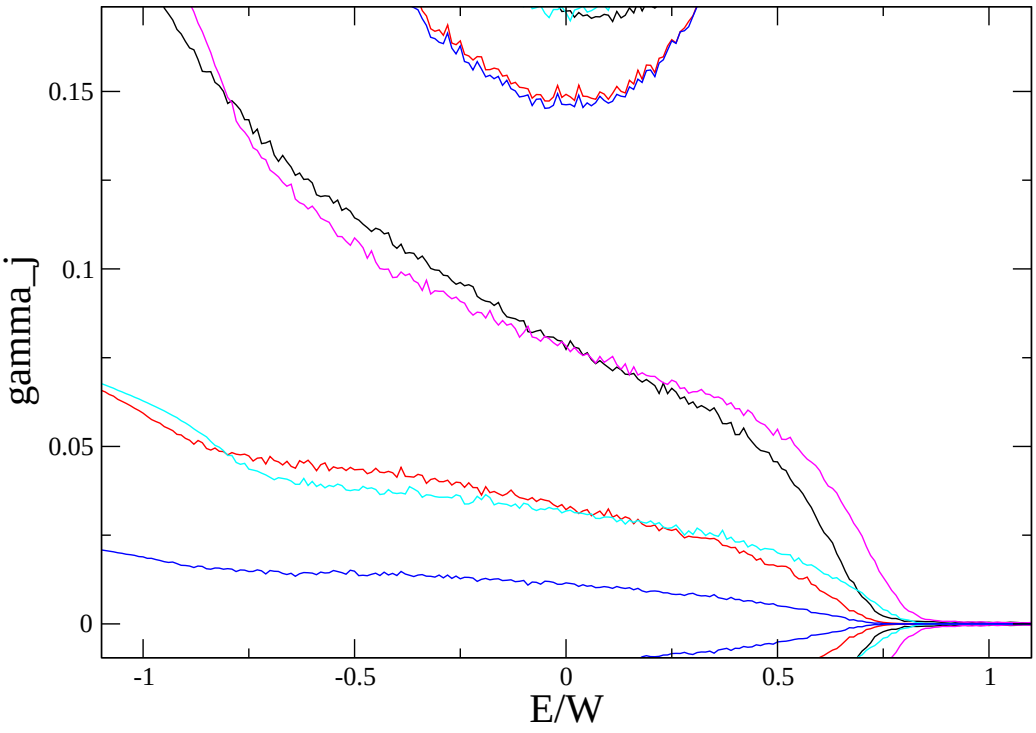

Figure 7.10: A plot of γ_j $(j = 0, 1)$ against E/W for a system of width 10. At $W = 0.1$: $W/\sigma = 10$ (black), $W/\sigma = 100$ (magenta). At $W = 0.01$: $W/\sigma = 10$ (red), $W/\sigma = 100$ (cyan). $W = 0.001$: $W/\sigma = 10$ (blue).

dependence on disorder, as evidenced by the separation between the black, red and blue curves for $\gamma_0(E = 0)$.

4. In Figure 7.10, we present a high-precision calculation of γ_0 for various values of W and σ, as a function of E/W. Here we have clear evidence that $\gamma_0(E/W;\, W, \sigma) = \gamma_0(E/W; W)$, provided $\sigma \ll W$, and that the exact value of σ is unimportant. The value of γ_0 is set by W, the strength of the disorder.

7.6.2 Dependence of Eigenstates on Disorder Strength

For $W = 0$ and $\sigma = 0$, the flat band is located at energy $E = 0$. We therefore set $E = 0$ and vary W and σ. One of the aims of this section is to find an upper bound on the value of κ.

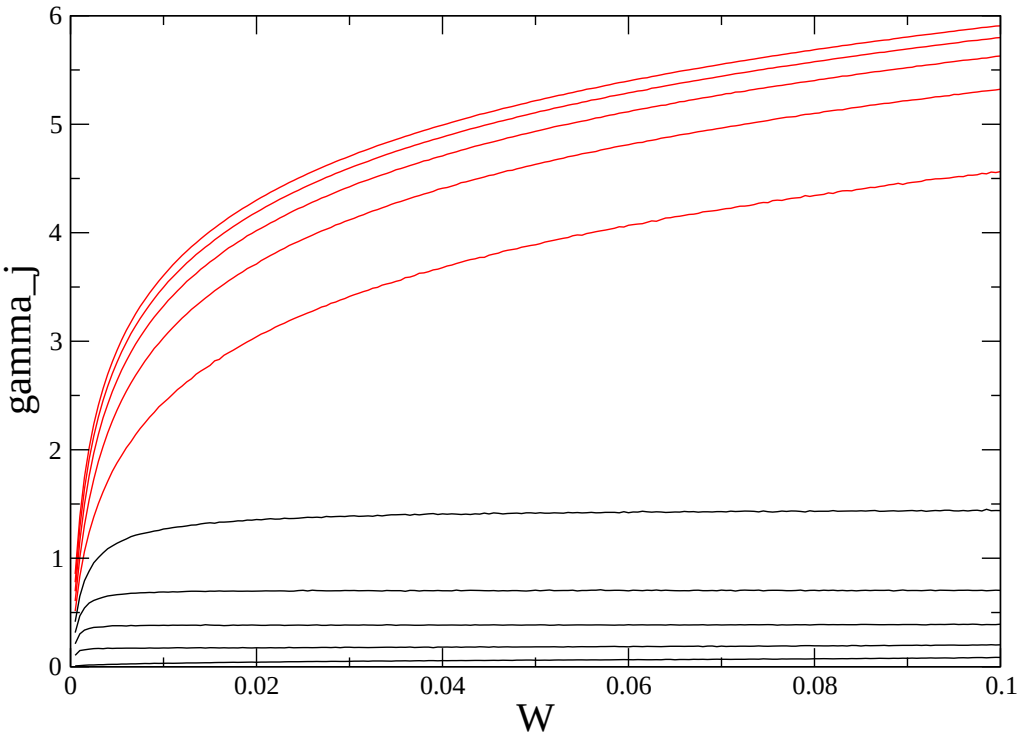

Figure 7.11: Constant $\sigma = 10^{-4}$. Simulation results for a system of width $N = 10$ and $L = 10^6$. Largest $N/2$ positive exponents are coloured in red, and smallest $N/2$ in black.

Remarks on Figures 7.11 and 7.12 In Figure 7.11 we hold σ constant and plot the smallest five exponents: these appear to plateau in the range $0.005 \lesssim W < 0.1$, and tend to zero for $W < 0.005$. In Figure 7.12, where $W/\sigma = 10$, there is no evidence that the exponents $\gamma_1 - \gamma_4$ tend to zero below some value of W. In fact, they appear to tend to finite values as $W \to 0$. Figure 7.11 suggests that, to be in the correct regime for Equation (7.13) to hold, we should keep $W/\sigma > 0.005/10^{-4} = 50$.

1. In Figure 7.11 the largest five Lyapunov exponents are well separated from the smallest five, whereas in Figure 7.12 there is no evidence of this. This is a consequence of the largest $N/2$ Lyapunov exponents appearing to scale as $\mathcal{O}(-\log\sigma)$ whilst the $N/2$ smallest are roughly independent of σ.

2. In both Figures 7.11 and 7.12, $\gamma_0(W) \to 0$ as $W \to 0$. This suggests that this vanishing of

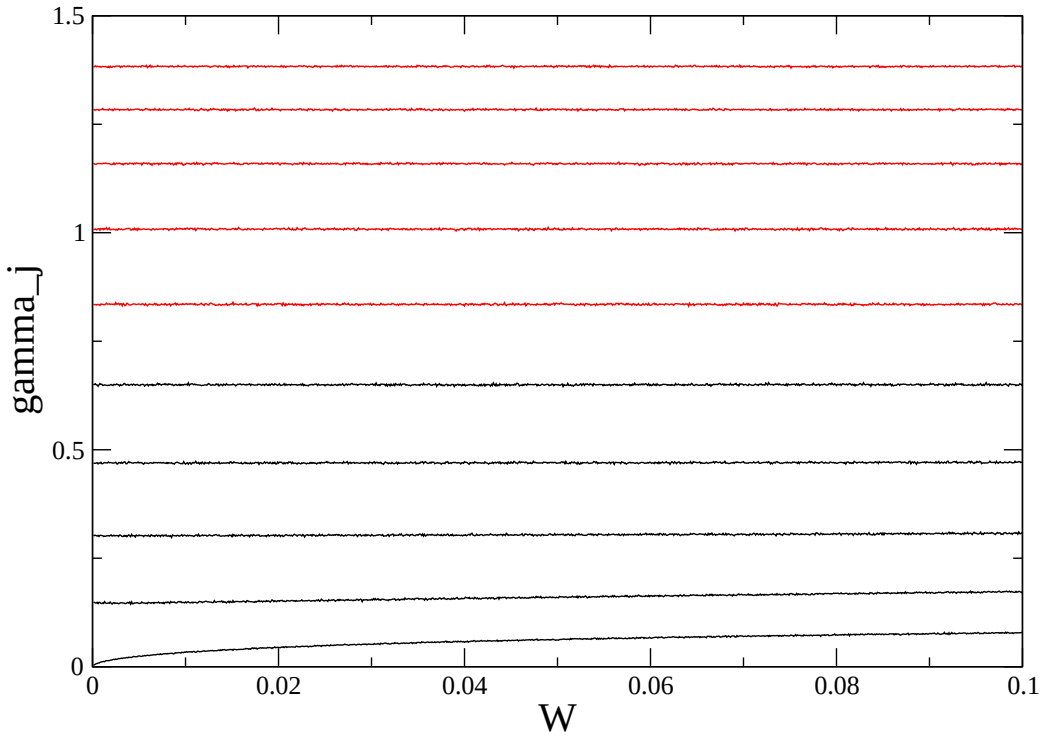

Figure 7.12: $W/\sigma = 10$. Simulation results for a system of width $N = 10$ and $L = 10^6$. Largest $N/2$ positive exponents are coloured in red, and smallest $N/2$ in black.

$\gamma_0(W = 0)$ will occur irrespective of the value of σ. However, for a realistic probe of the behaviour, we should use the message of Item 2, and hold $W/\sigma > 50$ in taking this limit.

From Figure 7.13 we observe that we enter the region of strong disorder when $W > 0.1$. Thus, to be in the regime of weak disorder, we must take $W < 0.1$.

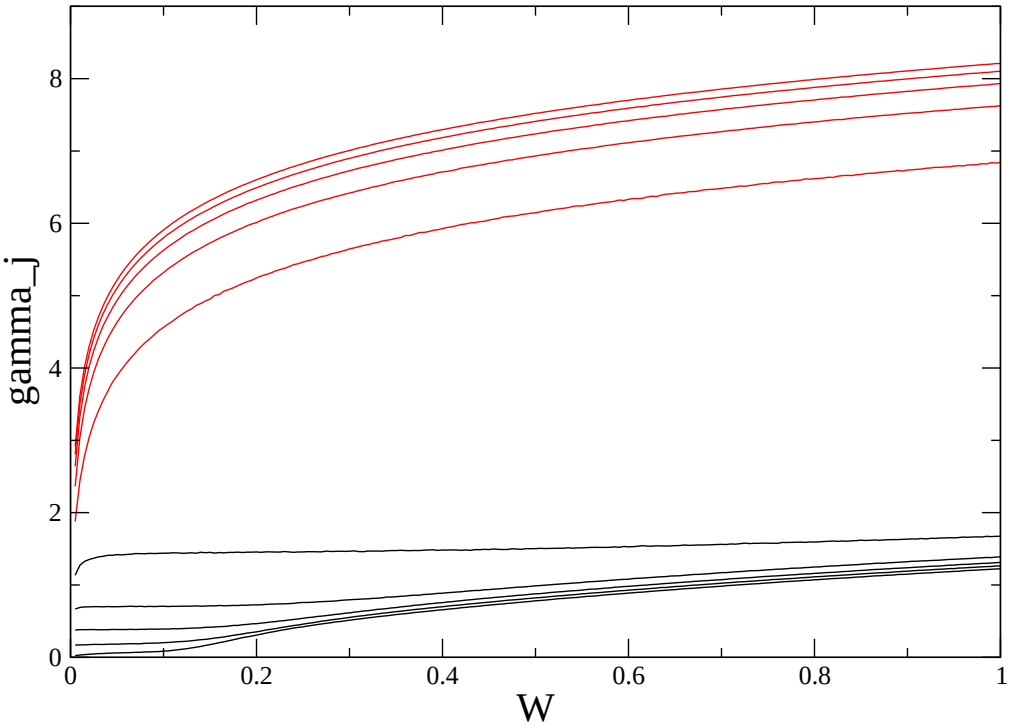

Figure 7.13: $\sigma = 10^{-4}$. Simulation results for a system of width $N = 10$ and $L = 10^6$. Largest $N/2$ positive exponents are coloured in red, and smallest $N/2$ in black.

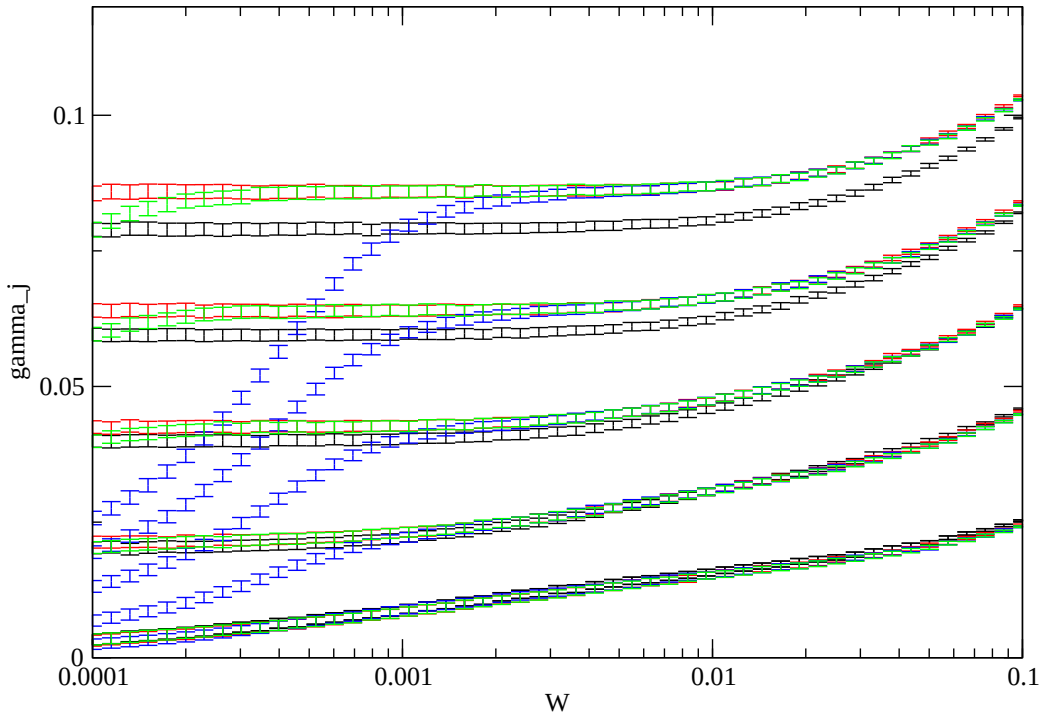

Figure 7.14: High-precision ($L = 3 \times 10^6$) simulation of exponents $j = 0, 1, \ldots, 4$ for width $N = 60$. Constant W/σ: black ($W/\sigma = 10$), red ($W/\sigma = 100$); constant σ: blue ($\sigma = 10^{-4}$), green ($\sigma = 10^{-5}$).

Figure 7.14 summarises most of the information in Section 7.6. For a system of width $N = 60$, as $W \to 0$ we find $\gamma_0 \to 0$ and other $\gamma_{j\neq 0} \not\to 0$, independent of W for small enough W. Deviations from W-independent behaviour for $j \neq 0$ are due to a breakdown of either $W \not\ll 1$ or $\sigma/W \not\ll 1$. Therefore, in the next section, we attempt to answer two questions: for a given N, what is the form of $\gamma_0(W)$ at small W; and for W small enough that $\gamma_{i\neq 0}$ are W-independent, what is the scaling behaviour as a function of N?

In the following sections, when making quantitative statements about the behaviour of γ_i, we must ensure the inequalities $W < 0.1$ and $W/\sigma > 50$ are satisfied.

In principle we should like to study γ_j for a system of infinite spatial extent. However, since the numerical procedure for calculating a full set of exponents scales as $N^3 L$ for a system of width N and length L, it is time-consuming to accurately study systems with widths $N > 100$.

We therefore use finite-size scaling ideas, introduced in Section 7.4.3, to extrapolate to infinite-sized lattices.

7.6.2.1 Smallest Exponent

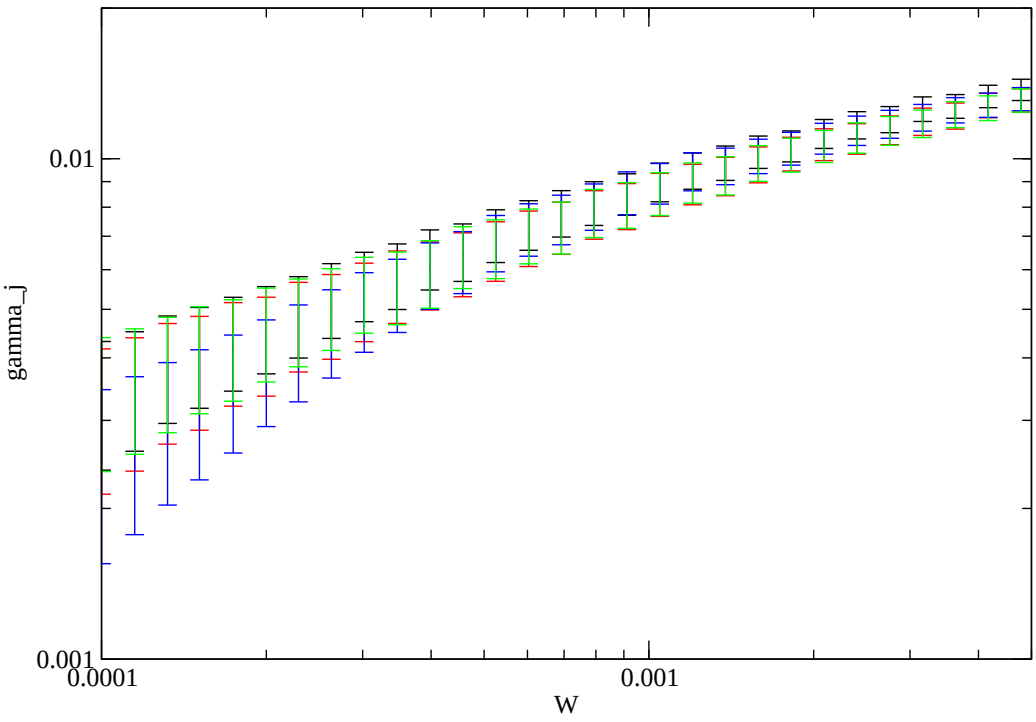

Figure 7.15: System of width $N = 60$. High-precision ($L = 3 \times 10^6$) simulation of exponent $j = 0$ for width $N = 60$. Constant W/σ: black ($W/\sigma = 10$), red ($W/\sigma = 100$); constant σ: blue ($\sigma = 10^{-4}$), green ($\sigma = 10^{-5}$).

We first focus attention on the lowest Lyapunov exponent, γ_0, which in Figure 7.14 appeared to approach zero as $W \to 0$. In Figure 7.15 we replot the data of Fig. 7.14, as a log-log plot. The large error bars make an precise estimate of the small W behaviour difficult. We use the parameter $\sigma/W = 0.01$, corresponding to the red data points of Fig. 7.15, and find the relationship

$$\gamma_0 \sim W^\eta \tag{7.17}$$

where, for $E = 0,\ N = 60$, the exponent is between the limits $0.3 < \eta < 0.5$.

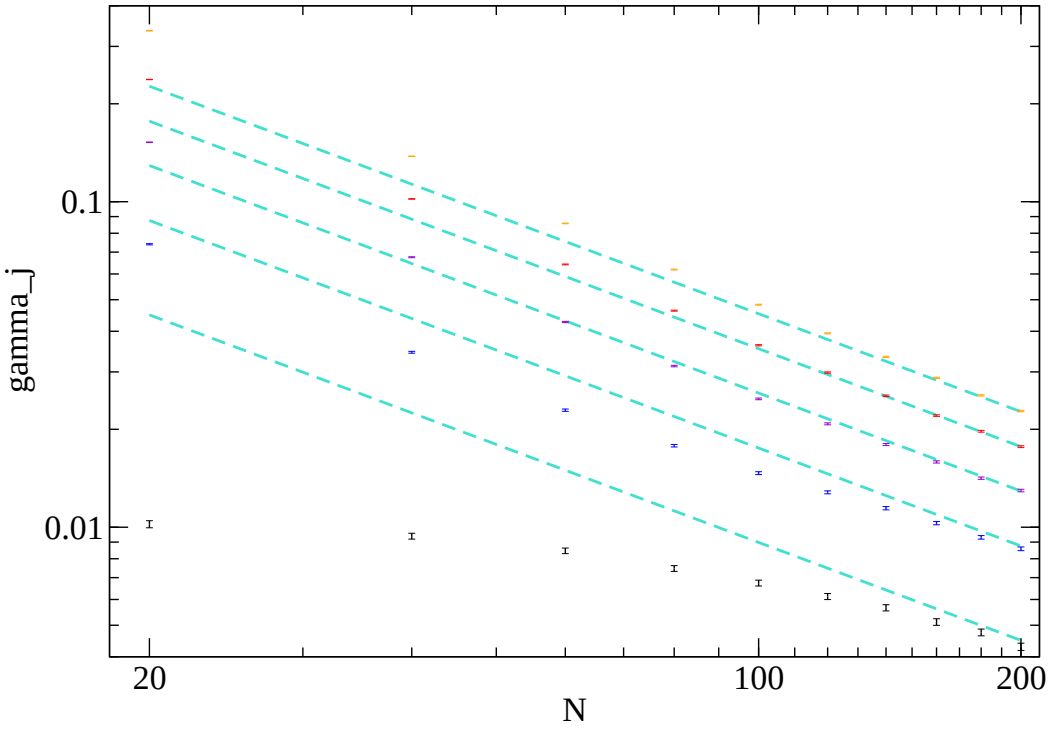

Figure 7.16: Exponents $j = 0, 1, \ldots, 4$ plotted as a function of N, at $E = 0$ for $W = 10^{-3}$ and $\sigma = 10^{-5}$. $L = 2 \times 10^6$. The dashed lines provide guidance for the eye, and are of the form $\gamma_j = K_j N^{-1}$, where K_j is some constant.

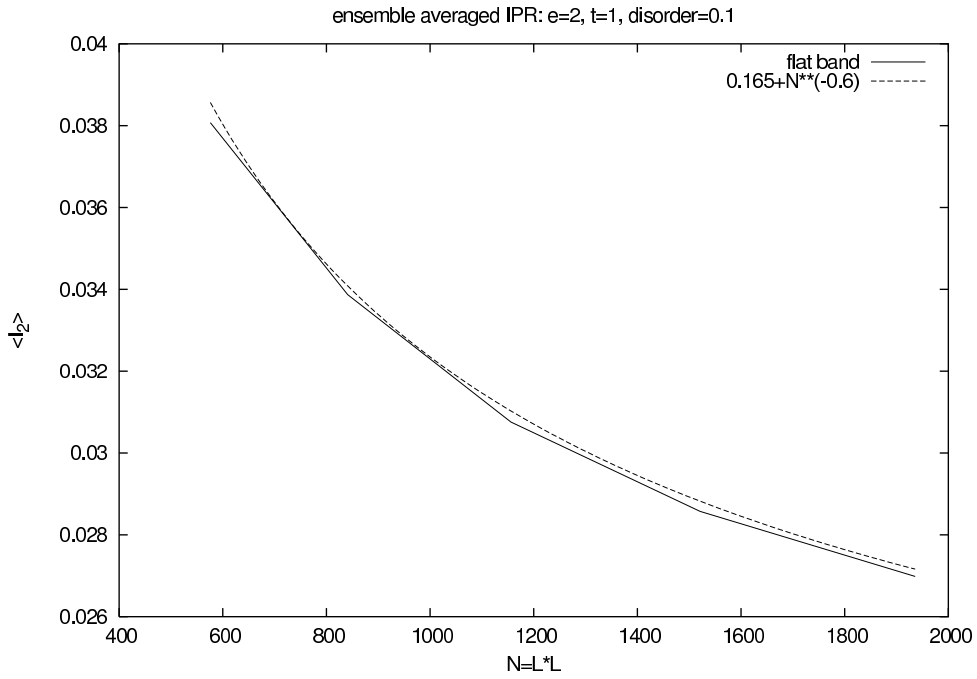

Figure 7.17: A plot of $L^2\langle|\psi(\mathbf{r})|^4\rangle$ against L^2 for a $d = 2$ pyrochlore lattice with $W = 0.1$.

7.6.3 Dependence of Eigenstates on System Width in the Limit of $W \to 0$

Figure 7.16 provides the most detailed characterisation of $\gamma_j(N)$ that we have produced. Taking $W = 10^{-3}$ and $\sigma = 10^{-5}$ we show data for $\gamma_0(N) - \gamma_4(N)$. Equation (7.17) suggests that modifying the value of W will change the absolute position of γ_0; that is, the position of the curve will move up or down relative to the curves for the other γ_j, which would remain fixed.

In conclusion, this scaling behaviour observed in this section are consistent with the finite-size scaling predictions of Section 7.4.3. For N large, the data would seem to asymptote towards the lines with gradient -1, indicative of the results $\gamma_j \sim N^{-1}$, and consistent with either extended or critical states.

7.7 Other evidence

Since the details of these single-particle eigenstates are still inconclusive, to get a clearer understanding of these states, we present numerical results of the inverse participation ratio $\langle|\psi(\mathbf{r})|^4\rangle$, described in Section 7.4.3.1. These results are displayed in Fig. 7.17 and taken from work done by P. Shukla.

From these data displayed in this Figure 7.17, $L^2\langle|\psi(\mathbf{r})|^4\rangle \propto (L^2)^{-0.6}$, indicating that $\langle|\psi(\mathbf{r})|^4\rangle \sim L^{-3.2}$. From the discussion in Section 7.4.3.1, in $d = 2$ this is consistent only with critical states.

7.8 Summary and Discussion

To summarise, in this Chapter we have investigated the effect of introducing disorder into a frustrated system. Projecting on-site disorder onto the flat bands of a frustrated results in disorder appearing in the quasi-long-range hopping terms. Since hopping terms are power-law with form $\sim r^{-\alpha}$ with α equal to the dimensionality d, states are expected to be critical, in essence somewhere between the extended and localised states of $\alpha < d$ and $\alpha > d$ respectively.

In order to study this, we have used a transfer matrix method on a two-dimensional frustrated lattice with on-site disorder. However, in the presence of frustration the transfer matrix T has singular elements, and so it was necessary to impose the $t_2 \to t_1$ limit and the weak disorder limit carefully to ensure that the results were in the correct parameter regime. Our

results indicate that states are indeed critical. Interestingly, the lowest Lyapunov exponent scales to zero with some characteristic power of the disorder $\gamma_0(W) \sim W^\eta$, although the error on η is still large. Other exponents attain a finite, limiting value as $W \to 0$, and as system width N increases, these exponents scale as N^{-1}, consistent with critical states.

Clearly the results of this chapter do not yet give a conclusive picture of these critical states. In particular, more theoretical work would be needed to understand the value of exponent η, and more simulations to investigate the critical wavefunctions would be necessary to fill in some of the gaps. We discuss a potential future avenue of investigation in the final chapter.

Chapter 8

Summary and Further Work

In this Thesis we have utilised, and built upon, concepts and topics from the field of frustrated systems. Within the subject of condensed matter physics, interacting systems that have degenerate ground states have demonstrated unusual behaviour due to strong thermal fluctuations, even at low temperatures. In this spirit, we have selected some archetypal frustrated systems – lattice spin and tight-binding models – and investigated the influence of ground-state degeneracy on their physical properties.

We now briefly summarise the content of this thesis. Chapters 1 – 3 were primarily a survey of the theoretical background that is utilised in later chapters. In detail, this was treated as follows. In Chapter 1 we introduced a conventional ferromagnetic–paramagnetic phase transition, and discussed that the symmetries of the underlying Hamiltonian are crucial for understanding the critical behaviour. We outlined a mean-field theory, and showed when this type of theory could be applied. Finally, we discussed unusual disordered phases, concentrating on the Coulomb phase, in which the *algebraic* correlations are of the same functional form as a dipole field. In Chapter 2 we discussed frustration in magnets, and concentrated particularly on those where the frustration arises due to the geometry of the lattice. Picking a lattice of corner-sharing octahedra as a convenient example, and using ideas due to Henley[28] and Huse *et al.*[30], we illustrated explicitly that a Coulomb phase could be supported when the interaction strength J became large. In Chapter 3 we outlined some mathematical tools for analysing the behaviour of interacting systems. We provided an overview of some key ideas from field theory, and then looked in detail at n-component vector field model in the limit of

$n \to \infty$. We used this limit to study the thermodynamics of the ferromagnetic–paramagnetic phase transition that was first encountered Chapter 1.

Having laid the ground in Chapters 1 – 3, in Chapter 4 we presented an analysis of an ordering transition out of the Coulomb phase. By introducing weak, additional interactions between spins on a lattice of corner-sharing octahedra, an ordered phase was realised. Using n-component classical spins, we imposed the $n \to \infty$ limit to make a saddle-point evaluation of the free energy. We studied spin-spin correlation functions for across the full range of temperature. In this chapter we argued that the transition falls into the same universality class as a ferromagnetic–paramagnetic transition with long-range, unixial dipolar interactions. In Chapter 5 we provided a continuum description of the transition, in which we constructed an effective Hamilton. We showed that the natural degrees of freedom for characterising the system are fluctuations of n solenoidal fields, and that the ordering transition corresponds to a condensation within this space of fields, and a breaking of the $\mathcal{O}(n)$-symmetry. Building on Chapters 4 and 5, in Chapter 6 we investigated the transition using an expansion in powers of $1/n$. In order to probe the behaviour away from $n = \infty$, we found that for any finite n, the ordering transition should be discontinuous.

We made a departure from ordering transitions in Chapter 7, and instead looked at the influence of disorder on frustrated systems. Working with a tight-binding model on the frustrated two-dimensional pyrochlore lattice, we used the method of transfer matrices to probe single-particle eigenstates of the Hamiltonian. We showed that these states are critical in the limit of very weak, on-site disorder.

The material in this thesis has been a mixture of analytical and numerical work. Much of the analytical work of Chapters 2 – 6 has been presented elsewhere[59], and in this reference, the results are supported by explicit numerical simulations. Whilst a number of the calculations have been performed on the corner-sharing octahedral lattice, of which there is no known realisation in nature, it must be emphasised that many of the results are more general than this one lattice. Chapter 7 is predominantly numerical work. It is intended that parts of Chapter 7 will be presented elsewhere[62].

8.1 Future Research Directions

One outstanding problem that has been highlighted in this thesis is the question of when is a transition out of the Coulomb phase continuous, and when is it first order? Our analytic results at $n = \infty$ in the spin model showed a continuous transition, whilst $n = 3$ simulations showed first-order behaviour. In Chapter 6 we made some preliminary analytical attempts to move beyond the $n = \infty$ result, though this work served to highlight how non-generic these transitions could be. Two future pieces of work are clear: first, we should perform a full RG calculation on the effective Hamiltonian of Eq. (5.15) to fully understand the long-distance behaviour of this effective theory. In a second piece of work, this time numerical, we should perform Monte Carlo simulations on a general n-component spin model, to see whether transitions are always first order, as is the case for Heisenberg spins.

Taking the work in another direction, one could ask the question of what form do excitations of the spin model take? Harmonic spin-wave theory can be performed about the ordered Néel state, and allow us to see how quantum fluctuations are influenced by the flat bands. Frustrated results in low excitation frequencies, so excitations are effective in reducing the ordered moment, and are thermally populated even at low temperatures. It would be interesting to see whether these spin-wave excitations could destabilise Néel order entirely.

The simulations of transitions in frustrated spin systems have so far assumed a static lattice. One extension to this work would be to include lattice degrees of freedom within the Hamiltonian, and allow for coupling between lattice phonons and the spin degrees of freedom. In the pyrochlore material $ZnCr_2O_4$, magnetic ordering transitions are accompanied by a structural distortion. It would be interesting to investigate, through simulation and analytical work, whether we always get a combined structural and magnetic transition when including a coupling to the lattice.

The localisation work of Chapter 7 was exclusively numerical. In the future, we would hope to develop a better understanding of the theory behind these results by looking at the effect of projection onto the flat band. In such a way we hope to develop a more analytical approach to this work. Such an approach would require mapping the system onto a non-linear sigma model, such as in Reference [48], and discussed in a book by Efetov[18].

Appendix A

A Compendium of Integrals for Thermodynamics in the Limit of $n \longrightarrow \infty$

In the body of the text, we quote a number results for the evaluation of non-trivial integrals: we display the detail of their evaluation here. Where possible, these are evaluated exactly; otherwise we state the asymptotic behaviour in the limit of a small parameter.

A.1 Integrals used in Calculations involving a Conventional Ferromagnet

For a conventional ferromagnet, the Green's function $G^{(\mathrm{F})}(\mathbf{q}) = (q^2 + \mu^2)^{-1}$ was identified in Eq. (3.22). In the analysis of the thermodynamics of a ferromagnet in Chapter 3, we use the following integrals:

$$\begin{aligned} D_n^{(\mathrm{F})}(\mu^2, \Lambda) &= \int^{\Lambda} \frac{d^3\mathbf{q}}{(2\pi)^3} \frac{1}{(q^2+\mu^2)^n} \\ I_n^{(\mathrm{F})}(\mathbf{k}, \mu^2, \Lambda) &= \int^{\Lambda} \frac{d^3\mathbf{q}}{(2\pi)^3} \frac{1}{(q^2+\mu^2)^{n-1}[(\mathbf{k}-\mathbf{q})^2+\mu^2]}. \end{aligned}$$

We begin with the following remarks:

1. We wish to study these integrals in the limit of $\mu \to 0$ and $k \ll \Lambda$.

2. For $k = 0$, $I_n^{(\mathrm{F})}(k = 0, \mu^2, \Lambda)$ reduces to $D_n^{(\mathrm{F})}(\mu^2, \Lambda)$.

3. The integral $D_1^{(\mathrm{F})}(\mu^2 \to 0, \Lambda \to \infty)$ is convergent at the lower limit and divergent at the upper limit (UV divergent). The integrals $D_{n>1}^{(\mathrm{F})}(\mu^2 \to 0, \Lambda \to \infty)$ are convergent at the upper limit and divergent at the lower limit (IR divergent). UV-divergent integrals are regularised with the upper cutoff $\Lambda \sim 1/a$, where a is the lattice spacing.

4. By symmetry, $I_n^{(\mathrm{F})}(\mathbf{k}, \mu^2, \Lambda) = I_n^{(\mathrm{F})}(k, \mu^2, \Lambda)$.

5. We identify the recursion relation

$$D_{n+1}^{(\mathrm{F})}(\mu^2, \Lambda) = -\frac{1}{n}\frac{\partial}{\partial \mu^2} D_n^{(\mathrm{F})}(\mu^2, \Lambda) \qquad n \geq 1$$

and hence can generate the whole family of integrals $D_{n>i}^{(\mathrm{F})}(\mu^2, \Lambda)$ from the evaluation of any the integral $D_i^{(\mathrm{F})}(\mu^2, \Lambda)$.

A.1.1 $D_{n\geq 2}^{(F)}(\mu^2, \Lambda)$

We postulate that, as $\mu \to 0$, $D_2^{(\mathrm{F})}(\mu^2, \Lambda)$ diverges $\sim K\mu^{-1}$. Hence $K = \lim_{\mu\to 0}\{\mu D_2^{(\mathrm{F})}(\mu^2, \Lambda)\}$.

On making the substitution $\mathbf{q} = \mu\mathbf{Q}$, we obtain

$$K = \lim_{\mu\to 0}\left\{\mu D_2^{(\mathrm{F})}(\mu^2, \Lambda)\right\} \;=\; \lim_{\mu\to 0}\left\{\frac{4\pi}{(2\pi)^3}\int_0^{\Lambda/\mu} dQ \frac{Q^2}{(Q^2+1)^2}\right\}.$$

For Q large, the integrand decays as Q^{-2}, and so we are justified in taking the upper cutoff $\to \infty$. We thus find

$$\begin{aligned} K &= \frac{1}{2\pi^2}\int_0^\infty dQ \left(\frac{1}{Q^2+1} - \frac{1}{(Q^2+1)^2}\right) \\ &= \frac{1}{2\pi^2}\left(\frac{\pi}{2} - \frac{\pi}{4}\right) = \frac{1}{8\pi}. \end{aligned}$$

Hence

$$D_2^{(F)}(\mu^2, \Lambda) \sim \frac{1}{8\pi}\,\mu^{-1} \quad \text{as} \quad \mu \to 0. \tag{A.1}$$

From the recursion relation, we generate the result for $n > 2$:

$$D_n^{(\mathrm{F})}(\mu^2, \Lambda) \sim \frac{1}{4\pi}\frac{(2n-5)!!}{(2n-2)!!}\,\mu^{3-2n} \quad \text{as} \quad \mu \to 0. \tag{A.2}$$

A.1.2 $I_2^{(F)}(k,\mu^2,\Lambda)$

To evaluate $I_2^{(\mathrm{F})}(k,\mu^2,\Lambda)$ we first set $\mu=0$ and look for the asymptotic behaviour of $I_2^{(\mathrm{F})}(k,\mu^2=0,\Lambda)$ for small k. We make the substitution $\mathbf{q}=k\boldsymbol{\tau}$ and postulate that, in the limit of $k\ll\Lambda$, $I_2^{(\mathrm{F})}(k,\mu^2=0,\Lambda)\sim Kk^{-1}$. Hence

$$K=\lim_{k/\Lambda\to 0}\{kI_2^{(\mathrm{F})}(k,\mu^2=0,\Lambda)\}=\lim_{k/\Lambda\to 0}\left\{\int^{\Lambda/k}\frac{d^3\boldsymbol{\tau}}{(2\pi)^3}\frac{1}{\tau^2|\hat{\mathbf{k}}-\boldsymbol{\tau}|^2}\right\}$$

where $\hat{\mathbf{k}}$ is a unit vector in the direction of $\mathbf{k}$. The integrand decays as τ^{-4} for τ large, and so we may take the upper cutoff $\to\infty$. Introducing the solid angle Ω, and taking $\hat{\mathbf{k}}$ to define the polar axis, we have

$$\begin{aligned}
K &= \frac{1}{(2\pi)^3}\int_0^\infty d\tau\int \mathrm{d}\Omega\frac{1}{|\hat{\mathbf{k}}-\boldsymbol{\tau}|^2}\\
&= \frac{1}{(2\pi)^2}\int_0^\infty d\tau\int_0^\pi d\theta\frac{\sin\theta}{\tau^2+1-2\tau\cos\theta}\\
&= \frac{1}{(2\pi)^2}\int_0^\infty d\tau\left[\frac{1}{2\tau}\ln(\tau^2+1-2\tau\cos\theta)\right]_0^\pi\\
&= \frac{1}{(2\pi)^2}\int_0^\infty d\tau\frac{1}{\tau}\ln\left|\frac{1+\tau}{1-\tau}\right|\\
&= \frac{1}{(2\pi)^2}\times\frac{\pi^2}{2}=\frac{1}{8},
\end{aligned}$$

so that

$$I_2^{(\mathrm{F})}(k,\mu^2=0,\Lambda)\sim\frac{1}{8k}\quad\text{for}\quad k\ll\Lambda. \tag{A.3}$$

Putting these results together gives

$$I_2^{(\mathrm{F})}(k,\mu^2,\Lambda)\sim\begin{cases}\dfrac{1}{8\pi\mu}, & \text{as } \mu\to 0 \text{ for } k=0\\[2ex] \dfrac{1}{8k}, & \text{for } k\ll\Lambda \text{ when } \mu=0.\end{cases} \tag{A.4}$$

A.2 Integrals used in Calculations involving a Highly-Constrained Antiferromagnet

In Chapter 4 we encounter the Green's function for the constrained antiferromagnet. This non-analytic function has the form

$$G^{(\mathrm{GFAFM})}(\mathbf{q}) = \left(3\,\frac{(\hat{\mathbf{n}}\cdot\mathbf{q})^2}{q^2} + q^2 + s\right)^{-1}. \tag{A.5}$$

For the remainder of this section, we drop the (GFAFM) superscript. Integrals involving this Green's function are

$$\begin{aligned} D_n(s,\Lambda) &= \int^{\Lambda} \frac{d^3\mathbf{q}}{(2\pi)^3}\,[G(\mathbf{q})]^n \\ I_n(\mathbf{k},s,\Lambda) &= \int^{\Lambda} \frac{d^3\mathbf{q}}{(2\pi)^3}\,[G(\mathbf{q})]^{n-1}\,G(\mathbf{k}-\mathbf{q}). \end{aligned}$$

Again, we make a number of initial remarks:

1. We wish to study these integrals in the limit of $s \to 0$ and, for the I_n, have the further condition $k \ll \Lambda$.

2. For $k = 0$, $I_n(k=0,s,\Lambda)$ reduces to $D_n(s,\Lambda)$.

3. For $s = 0$, $D_1(0,\Lambda)$ is dependent on the UV-cutoff Λ. $D_{n>1}(0,\Lambda)$ are divergent in the UV, and therefore strongly dependent on the value of s. We aim to extract this divergence as $s \to 0$.

4. We identify the recursion relation

$$D_{n+1}(s,\Lambda) = -\frac{1}{n}\frac{\partial}{\partial s}D_n(s,\Lambda) \qquad n \geq 1$$

   and hence can generate the whole family of integrals $D_{n>i}(s,\Lambda)$ from the evaluation of any the integral $D_i(s,\Lambda)$.

5. Due to the lack of rotational symmetry in $G(\mathbf{q})$, $I_n(\mathbf{k},s,\Lambda) \neq I_n(k,s,\Lambda)$.

A.2.1 $D_2(s^2, \Lambda)$

We choose to study $D_2(s, \Lambda)$ as $s \to 0$, since this is the least strongly IR-divergent integral. We postulate its asymptotic behaviour as a logarithmic divergence of the form $D_2(s, \Lambda) \sim A \ln(1/s)$ as $s \to 0$. In order to evaluate A, we have

$$A = \lim_{s \to 0} \left\{ -s \frac{\partial}{\partial s} D_2(s, \Lambda) \right\},$$

which, on using the recursion relation for $\partial D_2(s)/\partial s$, becomes

$$A = \lim_{s \to 0} \left\{ 2s D_3(s, \Lambda) \right\}.$$

We now employ the rescalings $q_\parallel = sQ_\parallel$ and $q_\perp = s^{1/2} Q_\perp$ to obtain

$$A = \lim_{s \to 0} \left\{ 2 \frac{2}{(2\pi)^3} \int_0^{\Lambda/s} dQ_\parallel \int_0^{\Lambda/s^{1/2}} dQ_\perp (2\pi Q_\perp) \frac{1}{\left(3 \frac{Q_\parallel^2}{Q_\perp^2 + sQ_\parallel^2} + (Q_\perp^2 + sQ_\parallel^2) + 1 \right)^3} \right\},$$

where the factor of 2 has come from restricting the range of $Q_\parallel$ integration to be positive. For $Q_\parallel \gg Q_\perp$, the integrand decays as $Q_\perp (Q_\parallel/Q_\perp)^{-6}$, and for $Q_\parallel \ll Q_\perp$ the integrand decays as $Q_\perp^{-5}$. We are again justified in taking the upper limits on the $Q_\parallel$ and $Q_\perp$ integrals $\to \infty$. Hence

$$A = \frac{4}{(2\pi)^2} \int_0^\infty dQ_\parallel \int_0^\infty dQ_\perp \frac{Q_\perp}{\left(3 \frac{Q_\parallel^2}{Q_\perp^2} + Q_\perp^2 + 1 \right)^3}.$$

To evaluate this integral we make the change of variables $Q_\parallel = (\rho^2 \sin\chi \cos\chi)/\sqrt{3}$ and $Q_\perp = \rho \sin\chi$. We require a Jacobian $\partial(Q_\parallel, Q_\perp)/\partial(\rho, \chi) = \rho^2 \sin\chi/\sqrt{3}$. Thus

$$\begin{aligned} A &= \frac{4}{(2\pi)^2 \sqrt{3}} \int_0^\infty d\rho \frac{\rho^3}{(\rho^2 + 1)^3} \int_0^{\pi/2} d\chi \sin^2\chi \\ &= \frac{4}{(2\pi)^2 \sqrt{3}} \times \frac{1}{4} \times \frac{\pi}{4} = \frac{1}{16\pi\sqrt{3}}. \end{aligned}$$

As a result, we can now identify the asymptotic behaviour of $D_2(s, \Lambda)$ as

$$D_2(s, \Lambda) \sim \frac{1}{16\pi\sqrt{3}} \ln(1/s) \quad \text{as} \quad s \to 0. \tag{A.6}$$

Using the recursion relation we generate the following result for $n > 2$:

$$D_n(s,\Lambda) \sim \frac{(n-3)!}{32\pi\sqrt{3}}\, s^{2-n} \quad \text{as} \quad s \to 0. \tag{A.7}$$

A.2.2 $I_2(\mathbf{k}, s, \Lambda)$

For $s = 0$, the integral $I_2(\mathbf{k}, s, \Lambda)$ simplifies to

$$I_2(\mathbf{k}, s=0, \Lambda) = \int^{\Lambda} \frac{d^3\mathbf{q}}{(2\pi)^3} \frac{1}{(3\, q_\parallel^2/q^2 + q^2)[3\,(k_\parallel - q_\parallel)^2/(\mathbf{k}-\mathbf{q})^2 + (\mathbf{k}-\mathbf{q})^2]}.$$

In the limit of $k \ll \Lambda$, the dominant contribution to the integral occurs where each term in the denominator is small. We thus require

$$\frac{q_\parallel}{q} \sim q \sim \frac{k_\parallel - q_\parallel}{|\mathbf{k}-\mathbf{q}|} \sim |\mathbf{k}-\mathbf{q}| \to 0.$$

In order to fulfil these conditions we require the following strong inequalities to hold: $q_\parallel \ll |\mathbf{q}_\perp|$ and $k \ll q \ll 1$.

We separately study the integral in two perpendicular $\mathbf{k}$-space directions, $k_\parallel$ and $k_\perp$.

For $\mathbf{k}$ in the direction of $k_\parallel$ we have

$$I_2(k_\parallel, s=0, \Lambda) = \int^{\Lambda} \frac{d^3\mathbf{q}}{(2\pi)^3} \frac{1}{\left(3\,\frac{q_\parallel^2}{q^2} + q^2\right)\left(3\,\frac{(k_\parallel - q_\parallel)^2}{(k_\parallel - q_\parallel)^2 + |\mathbf{q}_\perp|^2} + (k_\parallel - q_\parallel)^2 + |\mathbf{q}_\perp|^2\right)}.$$

Since $k_\parallel \ll q_\parallel$ we cut off the lower limit of the $q_\parallel$- integral at $k_\parallel$:

$$I_2(k_\parallel, s=0, \Lambda) = \frac{2}{(2\pi)^3} \int_{k_\parallel}^{\Lambda} dq_\parallel \int_0^{\Lambda} 2\pi q_\perp dq_\perp \frac{1}{\left(3\,\frac{q_\parallel^2}{q^2} + q^2\right)^2},$$

and make the rescalings $q_\parallel = k_\parallel Q_\parallel$, $q_\perp = k_\parallel^{1/2} Q_\perp$ to obtain

$$I_2(k_\parallel, s=0, \Lambda) = \frac{4\pi}{(2\pi)^3} \int_1^{\Lambda/k_\parallel} dQ_\parallel \int_0^{\Lambda/k_\parallel^{1/2}} dQ_\perp \frac{Q_\perp}{\left(3\,\frac{Q_\parallel^2}{k_\parallel Q_\parallel^2 + Q_\perp^2} + k_\parallel Q_\parallel^2 + Q_\perp^2\right)^2}.$$

Observing that the integrand falls off as $Q_\perp^{-3}$ for large $Q_\perp$, for small $k_\parallel$ we take the upper limit

on the integral to ∞ and have

$$I_2(k_\parallel, s=0, \Lambda) = \frac{4\pi}{(2\pi)^3} \int_1^{\Lambda/k_\parallel} dQ_\parallel \int_0^\infty dQ_\perp \frac{Q_\perp^5}{\left(3\,Q_\parallel^2 + Q_\perp^4\right)^2}.$$

The $Q_\perp$-integral is straightforward. Finally we are left with

$$I_2(k_\parallel, s=0, \Lambda) = \frac{4\pi}{(2\pi)^3}\ \frac{\pi}{24\sqrt{3}} \int_1^{\Lambda/k_\parallel} dQ_\parallel\ \frac{1}{Q_\parallel},$$

which provides the asymptotic form

$$I_2(k_\parallel, s=0, \Lambda) \sim \frac{1}{48\pi\sqrt{3}}\ \ln\left(\frac{\Lambda}{k_\parallel}\right). \tag{A.8}$$

Secondly, we study $I_2(\mathbf{k}, s=0, \Lambda)$ for $\mathbf{k}$ in the direction of $k_\perp$, where $k_\perp$ defines a plane of directions that have $\mathbf{k}\cdot\hat{\mathbf{n}} = k_\parallel = 0$.

$$I_2(\mathbf{k}_\perp, s=0, \Lambda) = \int^\Lambda \frac{d^3\mathbf{q}}{(2\pi)^3} \frac{1}{\left(3\,\frac{q_\parallel^2}{q^2} + q^2\right)\left(3\,\frac{q_\parallel^2}{q_\parallel^2 + |\mathbf{k}_\perp - \mathbf{q}_\perp|^2} + q_\parallel^2 + |\mathbf{k}_\perp - \mathbf{q}_\perp|^2\right)}.$$

From this expression we note the integral is dependent only on the magnitude of $\mathbf{k}_\perp$. We rescale $q_\parallel = k_\perp^2 Q_\parallel$, $\mathbf{q}_\perp = k_\perp \mathbf{Q}_\perp$ and obtain

$$I_2(k_\perp, s=0, \Lambda) = \frac{2}{(2\pi)^3} \int_0^{\Lambda/k_\perp} d^2\mathbf{Q}_\perp \int_0^{\Lambda/k_\perp^2} dQ_\parallel \frac{1}{\left(3\,\frac{Q_\parallel^2}{k_\perp^2 Q_\parallel + Q_\perp^2} + k_\perp^2 Q_\parallel + Q_\perp^2\right)} \times \frac{1}{\left(3\,\frac{Q_\parallel^2}{k_\perp^2 Q_\parallel^2 + |\hat{\mathbf{e}} - \mathbf{Q}_\perp|^2} + k_\perp^2 Q_\parallel^2 + |\hat{\mathbf{e}} - \mathbf{Q}_\perp|^2\right)}.$$

where $\hat{\mathbf{e}}$ is a unit vector in the direction of $\mathbf{k}_\perp$. Taking $k_\perp \ll 1$, and noting that the integrand decays as $Q_\parallel^{-4}$ we extend the upper limit of the $Q_\parallel$-integral to ∞. We have

$$\begin{aligned} I_2(k_\perp, s=0, \Lambda) &= \frac{2}{(2\pi)^3} \int_0^{\Lambda/k_\perp} d^2\mathbf{Q}_\perp \int_0^\infty dQ_\parallel \frac{1}{\left(3\,\frac{Q_\parallel^2}{Q_\perp^2} + Q_\perp^2\right)\left(3\,\frac{Q_\parallel^2}{|\hat{\mathbf{e}} - \mathbf{Q}_\perp|^2} + |\hat{\mathbf{e}} - \mathbf{Q}_\perp|^2\right)} \\ &= \frac{2}{(2\pi)^3} \int_0^{\Lambda/k_\perp} d^2\mathbf{Q}_\perp\ Q_\perp^2\ |\hat{\mathbf{e}} - \mathbf{Q}_\perp|^2 \int_0^\infty dQ_\parallel \frac{1}{\left(3\,Q_\parallel^2 + Q_\perp^4\right)\left(3\,Q_\parallel^2 + |\hat{\mathbf{e}} - \mathbf{Q}_\perp|^4\right)}. \end{aligned}$$

The definite integral on $Q_\parallel$ may be done directly. We have remaining

$$\begin{aligned} I_2(k_\perp, s=0, \Lambda) &= \frac{\pi}{(2\pi)^3\sqrt{3}} \int_0^{\Lambda/k_\perp} d^2\mathbf{Q}_\perp \, \frac{1}{Q_\perp^2 + |\hat{\mathbf{e}} - \mathbf{Q}_\perp|^2} \\ &= \frac{\pi}{(2\pi)^3\sqrt{3}} \int_0^{\Lambda/k_\perp} dQ_\perp \int_0^{2\pi} d\theta \, \frac{Q_\perp}{1 - 2Q_\perp \cos\theta + 2Q_\perp^2} \end{aligned}$$

The definite integral on θ may also be done directly, and leaves a $Q_\perp$ integral that is evaluated through a hyperbolic trigonometric substitution:

$$\begin{aligned} I_2(k_\perp, s=0, \Lambda) &= \frac{\pi}{(2\pi)^3\sqrt{3}} \int_0^{\Lambda/k_\perp} dQ_\perp \, \frac{2\pi Q_\perp}{\sqrt{1 + 4Q_\perp^4}} \\ &= \frac{1}{16\pi\sqrt{3}} \, \mathrm{Arsinh}\left(\frac{\Lambda}{k_\perp}\right). \end{aligned}$$

Finally, for large argument x, the function $\mathrm{arsinh}(x) \sim \ln(2x + \ldots)$, giving us

$$I_2(k_\perp, s=0, \Lambda) \sim \frac{1}{16\pi\sqrt{3}} \, \ln\left(2\frac{\Lambda}{k_\perp}\right). \tag{A.9}$$

Combining results (A.8) and (A.9), we obtain the asymptotic form:

$$I_2(\mathbf{k}, \Lambda) \sim F(\hat{\mathbf{k}} \cdot \hat{\mathbf{n}}) \, \ln\left(\frac{\Lambda}{k}\right), \tag{A.10}$$

where $F(\hat{\mathbf{k}} \cdot \hat{\mathbf{n}}) > 0$ is a numerical factor that depends only on the direction of $\mathbf{k}$.

A.2.3 $K(\mathbf{q})$

In Chapter 6 we encounter the function

$$K(\mathbf{p}) = [u(0)] \underbrace{\int \frac{d^3\mathbf{q}}{(2\pi)^3} \, [G(\mathbf{q})]^2 \, G(\mathbf{p} - \mathbf{q})}_{I_3(\mathbf{p})},$$

where $G(\mathbf{q})$ is of the form of Eq. (A.5), and $u(\mathbf{q})$ is taken from Eq. (3.14)

For $p = 0$, the asymptotic form of $I_3(p = 0) = D_3$ can be got from Eq. (A.7): it is simply $D_3(s, \Lambda) \sim \frac{1}{32\pi\sqrt{3}} \, s^{-1}$. For a general $\mathbf{p}$, for now we just note that, within the domain of integration, there are three distinct regions. These are illustrated in Figure A.1.

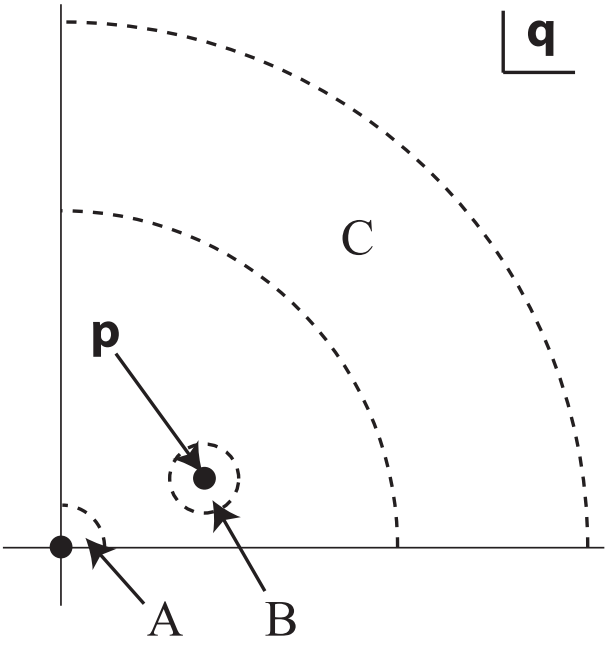

Figure A.1: Domain of integration in $\mathbf{q}$-space. $q_\parallel$ is in the horizonal direction, and $q_\perp$ in the vertical direction. The outermost arc represents the lattice cutoff $\Lambda \sim 1/a$.

Within any one of these regions, the integrand may be approximated

$$\begin{array}{lll|l} \text{Region A}: & q \ll p & & I_3^{(A)}(\mathbf{p}) = G(\mathbf{p}) \int_0^p \frac{d^3\mathbf{q}}{(2\pi)^3} [G(\mathbf{q})]^2 \\ \text{Region B}: & |\mathbf{p}-\mathbf{q}| \ll p & & I_3^{(B)}(\mathbf{p}) = [G(\mathbf{p})]^2 \int_0^p \frac{d^3\mathbf{q}}{(2\pi)^3} G(\mathbf{q}) \\ \text{Region C}: & p \ll q \ll \Lambda & & I_3^{(C)}(\mathbf{p}) = \int_p^\Lambda \frac{d^3\mathbf{q}}{(2\pi)^3} [G(\mathbf{q})]^3. \end{array}$$

To identify the principal contribution to the function $K(\mathbf{p}) \approx u(0)[I_3^{(A)}(\mathbf{p}) + I_3^{(B)}(\mathbf{p}) + I_3^{(C)}(\mathbf{p})]$, we investigate the divergences of $I_3^{(i)}(\mathbf{p})$. Rescaling $\mathbf{q}$ according to $q_\parallel = sQ_\parallel$ and $q_\perp = s^{1/2}Q_\perp$ we find

$$\begin{aligned} I_3^{(A)}(\mathbf{p}) &\sim G(\mathbf{p})\, s^{-1} \int_0^{p/s^{1/2}} d^3\mathbf{Q} \frac{1}{\left(\frac{Q_\parallel^2}{Q_\perp^2} + Q_\perp^2 + 1\right)^2} \\ I_3^{(B)}(\mathbf{p}) &\sim [G(\mathbf{p})]^2 \int_0^{p/s^{1/2}} d^3\mathbf{Q} \frac{1}{\frac{Q_\parallel^2}{Q_\perp^2} + Q_\perp^2 + 1} \\ I_3^{(C)}(\mathbf{p}) &\sim s^{-2} \int_{p/s^{1/2}}^{\Lambda/s^{1/2}} d^3\mathbf{Q} \frac{1}{\left(\frac{Q_\parallel^2}{Q_\perp^2} + Q_\perp^2 + 1\right)^3}. \end{aligned}$$

The integral in $I_3^{(A)}(\mathbf{p})$ is convergent at both limits, and is independent of p, since as $s \to 0$

we may take the upper limit to ∞. The integral in $I_3^{(B)}(\mathbf{p})$ is convergent at the lower limit, and diverges logarithmically at the upper cutoff. The integrand in $I_3^{(C)}(\mathbf{p})$ decays as Q^{-4} for large Q, and so the integral is proportional to $s^{3/2}$. Therefore, the leading contribution to $K(\mathbf{p}) = u(0)I_3(\mathbf{p})$ is from Region A in Figure A.1.

Now recalling that, from Eq. (3.14),

$$u(0) = \frac{u_0}{1 + u_0 \int_0^\Lambda \frac{d^3\mathbf{q}}{(2\pi)^3} [G(\mathbf{q})]^2}$$

and that, for small s, $u_0 \int_0^\Lambda \frac{d^3\mathbf{q}}{(2\pi)^3} [G(\mathbf{q})]^2 \gg 1$, then we can calculate $K(\mathbf{p})$ by inserting the explicit form of $I_3^{(A)}(\mathbf{p})$ in place of $I_3(\mathbf{p})$. We obtain

$$\begin{aligned} K(\mathbf{p}) &= [u(0)]\, I_3^{(A)}(\mathbf{p}) \\ &\longrightarrow G(\mathbf{p}) \frac{\int_0^p \frac{d^3\mathbf{q}}{(2\pi)^3} [G(\mathbf{q})]^2}{\int_0^\Lambda \frac{d^3\mathbf{q}}{(2\pi)^3} [G(\mathbf{q})]^2} \,. \end{aligned}$$

Finally, making the same rescalings as before, the ratio of the two integrals tends to unity as $s \to 0$ (for any finite p), since the upper limits may both be taken to ∞.

Thus we have

$$\lim_{s\to 0} K(\mathbf{p}) = \lim_{s\to 0} \left\{ [u(0)] \int \frac{d^3\mathbf{q}}{(2\pi)^3} [G(\mathbf{q})]^2 G(\mathbf{p}-\mathbf{q}) \right\} = G(\mathbf{p}, s=0).$$

A.2.4 $F_n(s,\Lambda)$

We define the family of functions

$$F_n(s,\Lambda) = \int^\Lambda \frac{d^3\mathbf{q}}{(2\pi)^3} \frac{1}{\left(3\frac{q_\parallel^2}{q_\perp^2} + q_\perp^2 + s\right)^2} \left(\ln\frac{1}{q}\right)^{-n}.$$

The parameter $s \ll 1$, and $n = 1$ or 2.

For the denominator to be small, each term within the parentheses must separately be small. This requires $q_\parallel \ll q_\perp$, and specifically we require $q_\parallel \sim s$ and $q_\perp \sim s^{1/2}$. In the limit of $s \ll 1$,

asymptotically the integral simplifies to

$$F_n(s,\Lambda) = \frac{2}{(2\pi)^3}\int_s^\Lambda dq_\parallel \int_{s^{1/2}}^\Lambda dq_\perp (2\pi q_\perp)\frac{q_\perp^4}{\left(3q_\parallel^2+q_\perp^4\right)^2}\left(\frac{1}{2}\ln\frac{1}{q^2}\right)^{-n}.$$

The dominant contribution to this integral is at the lower cutoff to the integrals. We rescale the integral using $q_\parallel = sQ_\parallel$ and $\mathbf{q}_\perp = s^{1/2}Q_\perp$ to obtain

$$F_n(s,\Lambda) = \frac{4\pi\, 2^n}{(2\pi)^3}\int_1^{\Lambda/s^{1/2}} dQ_\perp\; Q_\perp^5\;\left(\ln\frac{1}{sQ_\perp^2}\right)^{-n}\int_1^{\Lambda/s} dQ_\parallel \frac{1}{\left(3Q_\parallel^2+Q_\perp^4\right)^2}.$$

Since the integrand of the $Q_\parallel$- integral decays as $Q_\parallel^{-4}$, we use the result

$$\int_1^\infty dQ_\parallel\;\frac{1}{(3Q_\parallel^2+Q_\perp^4)^2} \sim \begin{cases} \frac{1}{27} - \frac{2}{175}Q_\perp^4 + \ldots & Q_\perp \ll 1 \\ \frac{\pi\sqrt{3}}{12Q_\perp^6} - \frac{1}{Q_\perp^8} + \ldots & Q_\perp \gg 1. \end{cases}$$

Inserting this result into the previous expression for $F_n(s,\Lambda)$, we see that the divergence, or convergence, of $F_n(s\to 0,\Lambda)$ is set by the upper cutoff of the $Q_\perp$ integral. We have

$$F_n(s,\Lambda) = \frac{1}{8\pi\sqrt{3}}\int_1^{\Lambda/s^{1/2}} dQ_\perp\;\frac{1}{Q_\perp}\;\left(\ln\frac{1}{s^{1/2}Q_\perp}\right)^{-n}.$$

Making the substitution $x = -\ln(s^{1/2}Q_\perp)$ we obtain

$$F_n(s,\Lambda) = \frac{1}{8\pi\sqrt{3}}\int_{\ln(1/\Lambda)}^{\frac{1}{2}\ln(1/s)} dx\; x^{-n}.$$

For $n=1$ we find that $F_1(s,\Lambda)$ diverges as $s\to 0$:

$$F_1(s,\Lambda) = \frac{1}{8\pi\sqrt{3}}\Big[\ln|x|\Big]_{\ln 1/\Lambda}^{(1/2)\ln(1/s)} \sim \frac{1}{8\pi\sqrt{3}}\ln\Big|\ln\frac{1}{s}\Big| \qquad s\ll 1. \tag{A.11}$$

For $n=2$ the quantity $F_2(s,\Lambda)$ converges to a finite quantity as $s\to 0$:

$$F_2(s,\Lambda) = \frac{1}{8\pi\sqrt{3}}\left[-\frac{1}{x}\right]_{\ln 1/\Lambda}^{(1/2)\ln(1/s)} \sim \frac{1}{8\pi\sqrt{3}}\left(\ln\frac{1}{\Lambda}\right)^{-1} \qquad s\ll 1. \tag{A.12}$$

Appendix B

Useful Results for Correlation Functions in the Highly-Constrained Antiferromagnet

Calculating correlation functions involve a number of awkward integrals. In this appendix we show some results for the distorted octahedral lattice.

B.1 Correlations in the high-T phase

We begin from the definition of the function

$$\mathcal{J} \equiv \int \frac{d^3\mathbf{q}}{(2\pi)^3} \frac{e^{i\mathbf{q}\cdot\mathbf{r}}}{(a^2+b^2+c^2)+\epsilon[(a+b+c)^2-2(a^2+b^2+c^2)]}.$$

We start by writing its denominator as an integral over an auxiliary variable t,

$$\mathcal{J} \equiv \int \frac{d^3\mathbf{q}}{(2\pi)^3} e^{i\mathbf{q}\cdot\mathbf{r}} \int_0^\infty dt \exp -t\{(a^2+b^2+c^2)+\epsilon[(a+b+c)^2-2(a^2+b^2+c^2)]\}$$

and then first doing the integral over the $\mathbf{q}$. Here we make the long-distance approximation and say that since we are only interested in the long-range behaviour of $\mathcal{J}$, only long-wavelength fluctuations will be important. On this approximation the exponent in the integrand becomes

quadratic; it is written

$$-\frac{1}{2}Q^T G^{-1} Q + h^T Q$$

with

$$Q^T = \begin{pmatrix} q_x & q_y & q_z \end{pmatrix}, \qquad G^{-1} = 2t \begin{pmatrix} 1-\epsilon & \epsilon & \epsilon \\ \epsilon & 1-\epsilon & \epsilon \\ \epsilon & \epsilon & 1-\epsilon \end{pmatrix}, \qquad h^T = i \begin{pmatrix} x & y & z \end{pmatrix}.$$

We take the range of integration to infinity and integrate on $\mathbf{q}$ to obtain

$$\mathcal{J} = \frac{1}{(2\pi)^3} \int_0^\infty dt \det(2\pi G)^{1/2} \exp\{\frac{1}{2} h^T \; G \; h\}.$$

Using the form for G we have

$$\det G^{-1} = 8t^3(1-2\epsilon)(1-\epsilon-2\epsilon^2) = 8t^3(1-2\epsilon)^2(1+\epsilon)$$

and

$$G = \frac{1}{2t(1-2\epsilon)(1+\epsilon)} \begin{pmatrix} 1 & -\epsilon & -\epsilon \\ -\epsilon & 1 & -\epsilon \\ -\epsilon & -\epsilon & 1 \end{pmatrix}$$

giving

$$\mathcal{J} = \frac{1}{(2\pi)^{3/2}} [8(1-2\epsilon)^2(1+\epsilon)]^{-1/2} \int_0^\infty dt \; t^{-3/2} \exp\left\{ -\frac{1}{4t(1-2\epsilon)(1+\epsilon)} [r^2(1+\epsilon) - 3\epsilon(\mathbf{r}\cdot\hat{n})^2] \right\}.$$

where $\hat{n}$ is a unit vector in the direction of the strain.

The integral is straightforward upon changing variables to

$$\frac{r^2(1+\epsilon) - 3\epsilon(\mathbf{r}\cdot\hat{n})^2}{4(1-2\epsilon)(1+\epsilon)} \tau = t,$$

giving

$$\mathcal{J} = \frac{1}{(2\pi)^{3/2}} [8(1-2\epsilon)^2(1+\epsilon)]^{-1/2} \left[\frac{r^2(1+\epsilon) - 3\epsilon(\mathbf{r}\cdot\hat{n})^2}{4(1-2\epsilon)(1+\epsilon)} \right]^{-1/2} \int_0^\infty d\tau \; \tau^{-3/2} \exp\left\{ -\frac{1}{\tau} \right\}.$$

The remaining integral can be done exactly: it yields $\sqrt{\pi}$. We finally obtain the result

$$\mathcal{J} = \frac{1}{4\pi\sqrt{1-2\epsilon}} \left[r^2(1+\epsilon) - 3\epsilon(\mathbf{r}\cdot\hat{n})^2 \right]^{-1/2}. \tag{B.1}$$

B.2 Correlations at the critical point

B.2.1 Parallel to the strain

We consider correlation functions in the direction $\mathbf{r} = r_\parallel \hat{r}_\parallel$. The q-space volume element $\mathrm{d}^3\mathbf{q}$ is written in spherical polar coordinates and we write $\chi = \cos\theta = q_\parallel/q$, where θ is the polar angle measured from $\mathbf{q}\cdot\widehat{r}_\parallel = \cos\theta$. With the range $\theta : [0,\pi]$, $q : [0,\Lambda]$, we have

$$I_c(r_\parallel) = \frac{2\pi}{(2\pi)^3} \int_0^\Lambda \mathrm{d}q\, q^2 \int_{-1}^1 \mathrm{d}\chi\, e^{i\chi q r_\parallel} \frac{1}{q^2+\chi^2}. \tag{B.2}$$

We now rescale the integral using $Q = q\sqrt{r_\parallel}$, $\quad X = \chi\sqrt{r_\parallel}$ and send $r_\parallel \to \infty$:

$$I_c(r_\parallel) = \frac{1}{4\pi^2\, r_\parallel} \int_0^\infty \mathrm{d}Q\, Q^2 \int_{-\infty}^\infty \mathrm{d}X\, e^{iXQ}\, \frac{1}{Q^2+X^2}. \tag{B.3}$$

Closing the X-contour in the upper half-plane encircles one pole at $X = iQ$. Taking $2\pi i$ times the residue from this pole gives

$$I_c(r_\parallel) = \frac{1}{4\pi\, r_\parallel} \int_0^\infty \mathrm{d}Q\, Q\, e^{-Q^2} = \frac{1}{8\pi\, r_\parallel}. \tag{B.4}$$

B.2.2 Perpendicular to the strain

For $\mathbf{r} = r_\perp \hat{r}_\perp$, it is more convenient to evaluate the integral in Cartesian coordinates. We chose the q_z-axis to lie along the direction of the strain, and the q_x-axis to be in the direction of $r_\perp$. Introducing a large-q cutoff with a factor e^{-q^2}, we have

$$I_c(r_\perp) = \frac{1}{(2\pi)^3} \int_{-\infty}^\infty \mathrm{d}q_x \mathrm{d}q_y \mathrm{d}q_z\, e^{iq_x r_\perp} e^{-q^2} \frac{q^2}{q_z^2+q^4} \tag{B.5}$$

$$= \frac{1}{(2\pi)^3} \int_{-\infty}^\infty \mathrm{d}q_x \mathrm{d}q_y \mathrm{d}q_z\, e^{iq_x r_\perp} e^{-q^2} \int_0^\infty \mathrm{d}\lambda\, \frac{1}{2} \left(e^{-\lambda(q^2+iq_z)} + e^{-\lambda(q^2-iq_z)} \right). \tag{B.6}$$

The q_y-integration follows immediately, and the q_x- and q_z integrals follow on completing the square in the exponent, and shifting the integration variable. We have

$$I_c(r_\perp) = \frac{1}{8\pi^3}\int_0^\infty \mathrm{d}\lambda\,\left(\frac{\pi}{1+\lambda}\right)\,e^{-(r_\perp^2+\lambda^2)/4(1+\lambda)} \tag{B.7}$$

$$= \frac{1}{8\pi^{3/2}}\int_0^\infty \mathrm{d}\lambda\,e^{-\phi(\lambda)}, \tag{B.8}$$

which defines the function

$$\phi(\lambda) = \frac{3}{2}\ln(1+\lambda) + \frac{1}{4}\frac{r_\perp^2}{1+\lambda} + \frac{1}{4}\frac{\lambda^2}{1+\lambda}.$$

For $r_\perp$ large, $\phi(\lambda)$ has a minimum (to $\mathcal{O}(r_\perp^{-1})$) at $\lambda_0 = r_\perp - 4$, around which it has the Taylor expansion in $\tilde{\lambda} = \lambda - \lambda_0$ of

$$\phi(\tilde{\lambda}) = \frac{1}{2}r_\perp + \frac{3}{2}\ln r_\perp + \frac{1}{4}r_\perp^{-1}\tilde{\lambda}^2 + \ldots$$

Since the integral in Eq. (B.8) is approximately a Gaussian centred at $r_\perp$ and with characteristic width $r_\perp^{1/2}$, the range of λ can be extended to ∞ in both directions, and the integral evaluated within a steepest-descents framework: we obtain

$$I_c(r_\perp) = \frac{1}{8\pi^{3/2}}\,r_\perp^{-3/2}\,e^{-r_\perp/2}\int_{-\infty}^{\infty}\mathrm{d}\tilde{\lambda}\,e^{-\tilde{\lambda}^2/4r_\perp} \tag{B.9}$$

$$= \frac{1}{4\pi r_\perp}\,e^{-r_\perp/2}. \tag{B.10}$$

References

[1] Ryuzo Abe. Expansion of a critical exponent in inverse powers of spin dimensionality. *Progress of Theoretical Physics*, 48(4):1414–1415, 1972.

[2] E. Abrahams, P. W. Anderson, D. C. Licciardello, and T. V. Ramakrishnan. Scaling theory of localization: Absence of quantum diffusion in two dimensions. *Phys. Rev. Lett.*, 42(10):673–676, Mar 1979.

[3] Amnon Aharony. Critical behavior of magnets with dipolar interactions. v. uniaxial magnets in d dimensions. *Phys. Rev. B*, 8(7):3363–3370, Oct 1973.

[4] Fabien Alet, Grégoire Misguich, Vincent Pasquier, Roderich Moessner, and Jesper Lykke Jacobsen. Unconventional continuous phase transition in a three-dimensional dimer model. *Physical Review Letters*, 97(3):030403, 2006.

[5] P. W. Anderson. Ordering and antiferromagnetism in ferrites. *Phys. Rev.*, 102(4):1008–1013, May 1956.

[6] P. W. Anderson. Absence of diffusion in certain random lattices. *Phys. Rev.*, 109(5):1492–1505, Mar 1958.

[7] A. Auerbach. *Interacting electrons and quantum magnetism*. Springer-Verlag: New York, 1994.

[8] G. Benettin, L. Galgani, A. Giorgilli, and J-M. Strelcyn. Lyapunov characteristic exponents for smooth dynamical systems and for hamiltonian systems; a method for computing all of them. part 1: Theory. *Meccanica*, 15(1):9 –20, March 1980.

[9] G. Benettin, L. Galgani, A. Giorgilli, and J-M. Strelcyn. Lyapunov characteristic exponents for smooth dynamical systems and for hamiltonian systems; a method for computing all of them. part 2: Numerical application. *Meccanica*, 15(1):21 –30, March 1980.

[10] Doron L. Bergman, Gregory A. Fiete, and Leon Balents. Ordering in a frustrated pyrochlore antiferromagnet proximate to a spin liquid. *Physical Review B (Condensed Matter and Materials Physics)*, 73(13):134402, 2006.

[11] Doron L. Bergman, Ryuichi Shindou, Gregory A. Fiete, and Leon Balents. Quantum effects in a half-polarized pyrochlore antiferromagnet. *Physical Review Letters*, 96(9):097207, 2006.

[12] T. H. Berlin and M. Kac. The spherical model of a ferromagnet. *Phys. Rev.*, 86(6):821–835, Jun 1952.

[13] J. Cardy. *Scaling and Renormalization in Statistical Physics*. Cambridge University Press, 1996.

[14] P. Chandra and B. Doucot. Possible spin-liquid state at large S for the frustrated square heisenberg lattice. *Phys. Rev. B*, 38(13):9335–9338, Nov 1988.

[15] Gang Chen, Jan Gukelberger, Simon Trebst, Fabien Alet, and Leon Balents. Coulomb gas transitions in three-dimensional classical dimer models. *Physical Review B (Condensed Matter and Materials Physics)*, 80(4):045112, 2009.

[16] O. N. Dorokhov. On the coexistence of localized and extended electronic states in the metallic phase. *Solid State Communications*, 51(6):381 – 384, 1984.

[17] J T Edwards and D J Thouless. Numerical studies of localization in disordered systems. *Journal of Physics C: Solid State Physics*, 5(8):807–820, 1972.

[18] K. Efetov. *Supersymmetry in Disorder and Chaos*. Cambridge University Press, 1997.

[19] M Enjalran, M J P Gingras, Y-J Kao, A Del Maestro, and H R Molavian. The spin liquid state of the $Tb_2Ti_2O_7$ pyrochlore antiferromagnet: a puzzling state of affairs. *Journal of Physics: Condensed Matter*, 16(11):S673–S678, 2004.

[20] F. Evers and A. D. Mirlin. Fluctuations of the inverse participation ratio at the anderson transition. *Phys. Rev. Lett.*, 84(16):3690–3693, Apr 2000.

[21] Ferdinand Evers and Alexander D. Mirlin. Anderson transitions. *Reviews of Modern Physics*, 80(4):1355, 2008.

[22] Tom Fennell, P. P. Deen, A. R. Wildes, K. Schmalzl, D. Prabhakaran, A. T. Boothroyd, R. J. Aldus, D. F. McMorrow, and S. T. Bramwell. Experimental proof of a magnetic coulomb phase, 2009.

[23] R. H. Fowler and G. S. Rushbrooke. An attempt to extend the statistical theory of perfect solutions. *Trans. Faraday Soc.*, 33:1272 – 1294, 1937.

[24] D. A. Garanin and Benjamin Canals. Classical spin liquid: Exact solution for the infinite-component antiferromagnetic model on the kagomé lattice. *Phys. Rev. B*, 59(1):443–456, Jan 1999.

[25] V. L. Ginzburg. *Sov. Phys.- Solid State*, 2:1824, 1937.

[26] Masaki Goda, Shinya Nishino, and Hiroki Matsuda. Inverse anderson transition caused by flatbands. *Physical Review Letters*, 96(12):126401, 2006.

[27] W. Heisenberg. *Z. Physik*, 31:253, 1925.

[28] C. L. Henley. Power-law spin correlations in pyrochlore antiferromagnets. *Phys. Rev. B*, 71(1):014424, Jan 2005.

[29] T. Holstein and H. Primakoff. Field dependence of the intrinsic domain magnetization of a ferromagnet. *Phys. Rev.*, 58(12):1098–1113, Dec 1940.

[30] David A. Huse, Werner Krauth, R. Moessner, and S. L. Sondhi. Coulomb and liquid dimer models in three dimensions. *Phys. Rev. Lett.*, 91(16):167004, Oct 2003.

[31] S. V. Isakov, K. Gregor, R. Moessner, and S. L. Sondhi. Dipolar spin correlations in classical pyrochlore magnets. *Phys. Rev. Lett.*, 93(16):167204, Oct 2004.

[32] S. V. Isakov, R. Moessner, and S. L. Sondhi. Why spin ice obeys the ice rules. *Phys. Rev. Lett.*, 95(21):217201, Nov 2005.

[33] John B. Kogut. An introduction to lattice gauge theory and spin systems. *Rev. Mod. Phys.*, 51(4):659–713, Oct 1979.

[34] B Kramer and A MacKinnon. Localization: theory and experiment. *Reports on Progress in Physics*, 56(12):1469–1564, 1993.

[35] M. A. Krivoglaz. *Sov. Phys.- Solid State*, 5:2526, 1964.

[36] L. D. Landau. *Phys. Z. Sowejetunion*, 11:26, 1937.

[37] A. I. Larkin and D. E. Khmel'nitskii. Phase transition in uniaxial ferroelectrics. *Sov. Phys.-JETP*, 29(6):1123 – 1128, 1969.

[38] S.-H. Lee, C. Broholm, T. H. Kim, W. Ratcliff, and S-W. Cheong. Local spin resonance and spin-peierls-like phase transition in a geometrically frustrated antiferromagnet. *Phys. Rev. Lett.*, 84(16):3718–3721, Apr 2000.

[39] L. S. Levitov. Delocalization of vibrational modes caused by electric dipole interaction. *Phys. Rev. Lett.*, 64(5):547–550, Jan 1990.

[40] D. C. Licciardello and D. J. Thouless. Constancy of minimum metallic conductivity in two dimensions. *Phys. Rev. Lett.*, 35(21):1475–1478, Nov 1975.

[41] I. M. Lifshitz. Energy spectrum structure and quantum states of disordered condensed systems. *Soviet Physics Uspekhi*, 7(4):549 – 573, 1965.

[42] Shang-Keng Ma. Critical exponents for charged and neutral bose gases above λ points. *Phys. Rev. Lett.*, 29(19):1311–1314, Nov 1972.

[43] A. MacKinnon and B. Kramer. One-parameter scaling of localization length and conductance in disordered systems. *Phys. Rev. Lett.*, 47(21):1546–1549, Nov 1981.

[44] P. A. Mello, P. Pereyra, and N. Kumar. Macroscopic approach to multichannel disordered conductors. *Annals of Physics*, 181(2):290 – 317, 1988.

[45] I. Mirebeau, P. Cadavez-Peres, S. T. Bramwell, M. J. P. Gingras, and J. S. Gardner. Pressure-induced crystallization of a spin liquid. *Nature*, 420:54, 2002.

[46] I. Mirebeau, I. N. Goncharenko, G. Dhalenne, and A. Revcolevschi. Pressure and field induced magnetic order in the spin liquid $Tb_2Ti_2O_7$ as studied by single crystal neutron diffraction. *Phys. Rev. Lett.*, 93(18):187204, Oct 2004.

[47] A. D. Mirlin and F. Evers. Multifractality and critical fluctuations at the anderson transition. *Phys. Rev. B*, 62(12):7920–7933, Sep 2000.

[48] Alexander D. Mirlin, Yan V. Fyodorov, Frank-Michael Dittes, Javier Quezada, and Thomas H. Seligman. Transition from localized to extended eigenstates in the ensemble of power-law random banded matrices. *Phys. Rev. E*, 54(4):3221–3230, Oct 1996.

[49] Grégoire Misguich, Vincent Pasquier, and Fabien Alet. Correlations and order parameter at a coulomb-crystal phase transition in a three-dimensional dimer model. *Physical Review B (Condensed Matter and Materials Physics)*, 78(10):100402, 2008.

[50] R. Moessner and J. T. Chalker. Low-temperature properties of classical geometrically frustrated antiferromagnets. *Phys. Rev. B*, 58(18):12049–12062, Nov 1998.

[51] R. Moessner and J. T. Chalker. Properties of a classical spin liquid: The heisenberg pyrochlore antiferromagnet. *Phys. Rev. Lett.*, 80(13):2929–2932, Mar 1998.

[52] N. F. Mott and W. D. Twose. The theory of impurity conduction. *Adnvances In Physics*, 10(38):107 – 163, April 1961.

[53] N.F. Mott. Conduction in glasses containing transition metal ions. *Journal of Non-Crystalline Solids*, 1(1):1 – 17, 1968.

[54] L. Neel. Magnetic properties of ferrites: ferrimagnetism and antiferromagnetism. *Ann. Phys. (Paris)*, 3:137, 1948.

[55] Shinya Nishino, Hiroki Matsuda, and Masaki Goda. Flat-band localization in weakly disordered system. *Journal of the Physical Society of Japan*, 76(2):024709, 2007.

[56] V. I. Oseledec. A multiplicative ergodic theorem. the lyapunov characteristic numbers of dynamical systems. *Trans. Moscow Math. Soc.*, 19:179, 1968.

[57] M. E. Peskin and D. V. Schroeder. *An introduction to quantum field theory.* Reading, Mass: Addison-Wesley, 1995.

[58] J L Pichard and G Sarma. Finite size scaling approach to anderson localisation. *Journal of Physics C: Solid State Physics*, 14(6):L127–L132, 1981.

[59] T. S. Pickles, T. E. Saunders, and J. T. Chalker. Critical phenomena in a highly constrained classical spin system: Néel ordering from the coulomb phase. *EPL (Europhysics Letters)*, 84(3):36002 (5pp), 2008.

[60] A P Ramirez. Strongly geometrically frustrated magnets. *Annual Review of Materials Science*, 24(1):453–480, 1994.

[61] L. H. Ryder. *Quantum field theory*. Cambridge University Press, 1996.

[62] P. Shukla, T. S. Pickles, and J. T. Chalker. To be published.

[63] A.M.C. Souza and H. J. Herrmann. Flatband localization in the anderson-falicov-kimball model. *arXiv*, 0810:3585:4, 2008.

[64] H. E. Stanley. Spherical model as the limit of infinite spin dimensionality. *Phys. Rev.*, 176(2):718–722, Dec 1968.

[65] J. Villain, R. Bidaux, J.-P. Carton, and R. Conte. Order as an effect of disorder. *Journal de Physique*, 41(11):1263–1272, 1980.

[66] F. Wegner. Inverse participation ratio in $2 + \epsilon$ dimensions. *Zeitschrift für Physik B Condensed Matter*, 36(3):209 –214, September 1980.

[67] F. J. Wegner. Electrons in disordered systems. scaling near the mobility edge. *Zeitschrift für Physik B: Condensed Matter*, 25(4):327 – 337, December 1976.

[68] G. C. Wick. On the general theory of collisions for particles with spin. *Ann. Physics (New York)*, 7:404 – 428, June 1959.

[69] Kenneth G. Wilson. Quantum field theory models in less than 4 dimensions. *Phys. Rev. D*, 7(10):2911–2926, May 1973.

[70] R. Youngblood, J. D. Axe, and B. M. McCoy. Correlations in ice-rule ferroelectrics. *Phys. Rev. B*, 21(11):5212–5220, Jun 1980.

[71] R. W. Youngblood and J. D. Axe. Polarization fluctuations in ferroelectric models. *Phys. Rev. B*, 23(1):232–238, Jan 1981.